Interferometric array imaging in clutter

Liliana Borcea† and George Papanicolaou‡ and Chrysoula Tsogka⋆

† Computational and Applied Mathematics, MS 134, Rice University, 6100 Main Street, Houston, TX 77005-1892.(borcea@caam.rice.edu)

‡ Department of Mathematics, Stanford University, Stanford, CA 94305. (papanico@math.stanford.edu)

⋆ Department of Mathematics, University of Chicago, Chicago, IL 60637. (tsogka@math.uchicago.edu)

Abstract. We introduce a space-time interferometric array imaging functional that provides statistically stable images in cluttered environments. We also present a resolution theory for this imaging functional that relates the space-time coherence of the data to the range and cross-range resolution of the image. Extensive numerical simulations illustrate the theory and address some implementation issues.

PACS numbers: 43.60.Gk, 43.60.Cg, 43.60.Rw, 43.60 Tj

1. Introduction

Broadband array imaging of acoustic sources in a known, homogeneous or slowly varying background is done efficiently with Kirchhoff migration

$$\mathcal{I}^{\rm KM}(\vec{\mathbf{y}}^s) = \sum_{\vec{\mathbf{x}}_r \in A} P(\vec{\mathbf{x}}_r, \tau(\vec{\mathbf{x}}_r, \vec{\mathbf{y}}^s)) \tag{1.1}$$

where $P(\vec{\mathbf{x}}_r, t)$ are time traces of the signals emanating from the sources and recorded by a passive array A with receivers located at $\vec{\mathbf{x}}_r$. The imaging functional $\mathcal{I}^{\rm KM}(\vec{\mathbf{y}}^s)$ is evaluated at a search point $\vec{\mathbf{y}}^s$ in the domain of the object to be imaged, and $\tau(\vec{\mathbf{x}}_r, \vec{\mathbf{y}}^s)$ is the travel time from $\vec{\mathbf{x}}_r$ to $\vec{\mathbf{y}}^s$. In a homogeneous medium it is distance over the propagation speed c_0, $\tau(\vec{\mathbf{x}}_r, \vec{\mathbf{y}}^s) = |\vec{\mathbf{x}}_r - \vec{\mathbf{y}}^s|/c_0$. If a localized source around $\vec{\mathbf{y}}$ emits a short pulse then the functional $\mathcal{I}^{\rm KM}(\vec{\mathbf{y}}^s)$ will have a sharp peak when the search point $\vec{\mathbf{y}}^s$ is near $\vec{\mathbf{y}}$. From the location of this peak we get an estimate of the unknown source location $\vec{\mathbf{y}}$, which is why $\mathcal{I}^{\rm KM}(\vec{\mathbf{y}}^s)$ is an imaging functional. When the array is active then the reflectors to be imaged will produce echoes that are recorded at the array as time traces $P(\vec{\mathbf{x}}_s, \vec{\mathbf{x}}_r, t)$, where $\vec{\mathbf{x}}_s$ denotes the probing signal source location in the array and $\vec{\mathbf{x}}_r$ are the recorder locations. Kirchhoff migration is now done with the functional

$$\mathcal{I}^{\rm KM}(\vec{\mathbf{y}}^s) = \sum_{\vec{\mathbf{x}}_s, \vec{\mathbf{x}}_r \in A} P(\vec{\mathbf{x}}_s, \vec{\mathbf{x}}_r, \tau(\vec{\mathbf{x}}_s, \vec{\mathbf{y}}^s) + \tau(\vec{\mathbf{x}}_r, \vec{\mathbf{y}}^s)), \tag{1.2}$$

which will have a peak when $\vec{\mathbf{y}}^s$ is near a reflector, thereby providing an estimate of its location.

The Kirchhoff migration functionals and their numerous variants have been used successfully in many applications in seismic imaging [9, 21], in non-destructive testing [17, 38], in radar [29, 15, 39] and elsewhere. Some of the variants that have been considered are (a) special array configurations such as zero-offset or synthetic aperture arrays in which $\vec{\mathbf{x}}_s = \vec{\mathbf{x}}_r$ [24, 9], (b) selective scatterer illumination using the singular value decomposition [32], (c) iterated application of Kirchhoff (or full wave) migration to capture nonlinear effects in the inversion, usually in homogeneous media and with monochromatic data [23], and many others. While many studies consider imaging in homogeneous media, migration applies also to smooth, variable velocity backgrounds. In this case a velocity estimation process must be carried out [21, 19, 48, 47]. The mathematical analysis of the imaging functionals (1.1) and (1.2), for large arrays and broadband data, is carried out in [9, 8, 49]. We review briefly the resolution theory for (1.1) in this paper, in Appendix A.

It has been known for a long time that if the objects to be imaged are in a richly scattering environment then Kirchhoff migration does not work well. This is because the echo from a reflector does not appear as a clean peak in the signals recorded at the array but has instead a lot of delay spread, or coda, that is generated by the inhomogeneous medium (as in Figure 6 below). Consequently, Kirchhoff migration leads to unreliable images that change unpredictably with the detailed features of the clutter. The purpose of this paper is to address this problem of imaging in inhomogeneous or cluttered media.

1.1. Matched field imaging

One way to deal with the delay spread that clutter introduces is to compute the cross correlations of the time traces at the array and to migrate them, instead of migrating the traces themselves as in (1.1) and (1.2). This idea is the basis for imaging with matched field functionals [18, 1, 35]. There are many variants for this method depending on what is known or can be estimated about the background from the data by techniques similar, for example, to the ones used for velocity estimation in Kirchhoff migration. Here, we suppose that we know the smooth part of the background velocity, which we take as constant for simplicity, but we do not know the rapidly fluctuating part (the clutter). If we knew the rapid fluctuations of the velocity, then we would effectively know the Green's function of the clutter and we could migrate the data with it, rather than with travel times in a homogeneous medium. This is the same as doing physical time reversal [30, 31, 25, 32, 44, 37], which is known to have focusing properties that are much better than the ones in homogeneous media, and provides, therefore, better resolution when used for imaging in clutter than what Kirchhoff migration gives in the corresponding homogeneous medium. The catch is, of course, that we do not know

the Green's function of the cluttered medium, and it does not help if we know it only approximately because the effective removal of the delay spread in the data requires that we reconstruct accurately with migration the multiple scattering that produced it. The essential point in migrating cross correlations of the data is that they tend to reduce the delay spread and to enhance the peaks from the reflectors that we want to image, without knowing anything about the clutter itself. The underlying assumption here is that what we want to image has some regular structure that is encoded in the array data while the clutter is irregular so that the delay spread in the data looks random. It is therefore natural that when modeling the data and the imaging process, we use wave propagation in random media in order to capture clutter effects.

Enhanced spatial focusing in physical time reversal in random media [26, 27, 25] and the realization that it is **statistically stable** [10] in broadband regimes motivated us to carry out a theoretical study of the imaging resolution of matched field functionals in random media [11]. Statistical stability means that the physical time reversal process is self-averaging with respect to the random fluctuations in the medium properties, the clutter. This is not true in narrowband regimes because the interference patterns that form near the point of focusing, the speckle patterns, do not average out as they do in broadband regimes. Enhanced focusing in time reversal means that the cross range resolution is $\lambda_0 L/a_e$ where λ_0 is the central wavelength, L is the range and $a_e(L)$ is the **effective aperture** of the array that is typically larger than the physical aperture a and depends on the random medium as well as the range [10, 11]. The focal spot size $\lambda_0 L/a_e$ in time reversal is therefore smaller in random media than in homogeneous ones where it is given by the Rayleigh formula $\lambda_0 L/a$ [16].

We showed in [11] that when we do not know the random medium, so that we cannot image with time reversal and image instead with a matched field functional, which is also called interferometry, the cross-range resolution is equal to $a_e(L)$. This is much worse than in time reversal but it is the best that can be done when the random medium is not known. We have thus two imaging functionals with extreme cross-range resolutions: time reversal that uses full knowledge of the actual realization of the random medium and matched field that uses no knowledge at all. Both time reversal and matched field imaging are statistically stable, which is a key property for successful imaging, while Kirchhoff migration is not.

1.2. Coherent interferometry

While interferometric or matched field imaging provides the best statistically stable cross-range resolution that is possible with no knowledge of the random medium, it provides no range resolution at all. To get range resolution with it we must either have large arrays or several arrays widely separated from each other, so that we can use what is essentially geometric triangulation [11]. The main result of this paper is to introduce

a more general class of imaging functionals, the coherent interferometric functionals, and to give a resolution theory for them that is a natural extension of the one in [11]. The main idea is to compute the cross correlations of the traces locally in time, and not over the whole time interval, and to migrate them. By segmenting the traces into time intervals and calculating the correlations locally in each interval we get range resolution that is of the order of the time intervals multiplied by the propagation speed c_0. The shorter the time intervals the better the range resolution. In a homogeneous medium they can be as short as the width T_p of the probing pulse. Depending on the shape of the pulse and the way its width is defined, T_p is equal to a constant multiplied by the reciprocal bandwidth B^{-1}, which we denote by $T_p \sim B^{-1}$. This way we see that the range resolution in a homogeneous medium is $c_0 B^{-1}$. We do not consider here the issue of how to choose optimally the shape of the pulse beyond fixing its bandwidth appropriately.

How large should the time segments be when there is delay spread? They should be of the order of the delay spread T_d. They should not be smaller because then the correlations will not capture the delay spread and compress it, leading therefore to unstable images. And they should not be larger because then we will lose range resolution. If the local cross correlations of the traces are computed correctly, the range resolution in coherent interferometric imaging will be $c_0 T_d$. We show in Section 3 that the reciprocal of T_d is proportional to the decoherence frequency of the traces, Ω_d. Since $T_d > T_p$ we have that $\Omega_d < B$, so range resolution in random media is proportional to $c_0 \Omega_d^{-1}$ and is worse than $c_0 B^{-1}$, the resolution in homogeneous media. We show in Section 5 that expression $c_0 \Omega_d^{-1}$ for the range resolution can be derived from first principles for a large class of random media.

What about the cross-range resolution? By analogy to Ω_d we introduce the decoherence length X_d which is the distance between traces on the array over which they become uncorrelated. We show in Section 3 that the cross-range resolution in coherent interferometry is $\lambda_0 L/X_d$. This is worse than the Rayleigh resolution in a homogeneous medium $\lambda_0 L/a$, because $X_d \leq a$, in general. We will also see in Section 3 that the decoherence length X_d is comparable to the focal spot size in time reversal, so that $X_d = \lambda_0 L/a_e$. If we use this expression for X_d in the cross-range resolution formula $\lambda_0 L/X_d$ we see that it equals a_e, which is the matched field cross-range resolution that was derived in [11]. We show in Section 5 that this cross-range resolution can be derived from first principles for a large class of random media.

This resolution theory for coherent interferometry in random media is the main result of this paper.

1.3. Outline of the paper

In Section 2 we state more precisely the imaging problem for passive and active arrays. All of the analytical results in this paper are carried out only for passive array imaging. The active array analysis is in principle very similar but does not follow directly from the passive one and will be presented elsewhere. In Section 3 we introduce the coherent interferometric functional, discuss its properties and compare it to other imaging functionals. Our extensive numerical simulations, for both active and passive arrays, are presented in Section 4. The resolution analysis is given in Sections 5 and 6, and it is followed by a brief Section 7 summarizing the results. In Appendix A we review briefly the well known resolution analysis of the Kirchhoff migration functional (1.1) and in Appendix B we give for completeness the derivation of the two-frequency moment formula that we use in the resolution analysis of Sections 5 and 6.

2. The array imaging problem

In Section 2.1 we introduce the forward model for imaging a point or a distributed source with a passive array of receivers in a cluttered environment. We also state the inverse problem of imaging the source location or the source density. In Section 2.2 we give the Born approximation model for imaging with an active array a point reflector or reflectors with distributed reflectivity. We also state the inverse problem of imaging the reflector location or the distributed reflectivity.

We use the term array imaging throughout because we assume that the transducer locations $\vec{\mathbf{x}}_r$ are close enough, less than half a central wavelength apart, so that the radiation field of the array is essentially that of an aperture whose size is determined by the number of transducers.

2.1. Imaging in clutter with a passive array

In the schematic in Figure 1 a point source at $\vec{\mathbf{y}}_\star$ emits a signal that is recorded by an array of receivers located at $\vec{\mathbf{x}}_r$. The signal is an initially spherical wave convolved with the pulse function

$$f(t) = e^{-i\omega_0 t} f_B(t), \tag{2.3}$$

where ω_0 is the carrier frequency and $2B$ is the bandwidth of

$$\widehat{f}(\omega) = \int_{-\infty}^{\infty} e^{i(\omega-\omega_0)t} f_B(t) dt = \widehat{f}_B(\omega - \omega_0). \tag{2.4}$$

The Fourier transform of the baseband pulse $\widehat{f}_B$ is assumed to have support in the interval $[-B, B]$. We will refer to B, rather than to $2B$, as the bandwidth. The wave

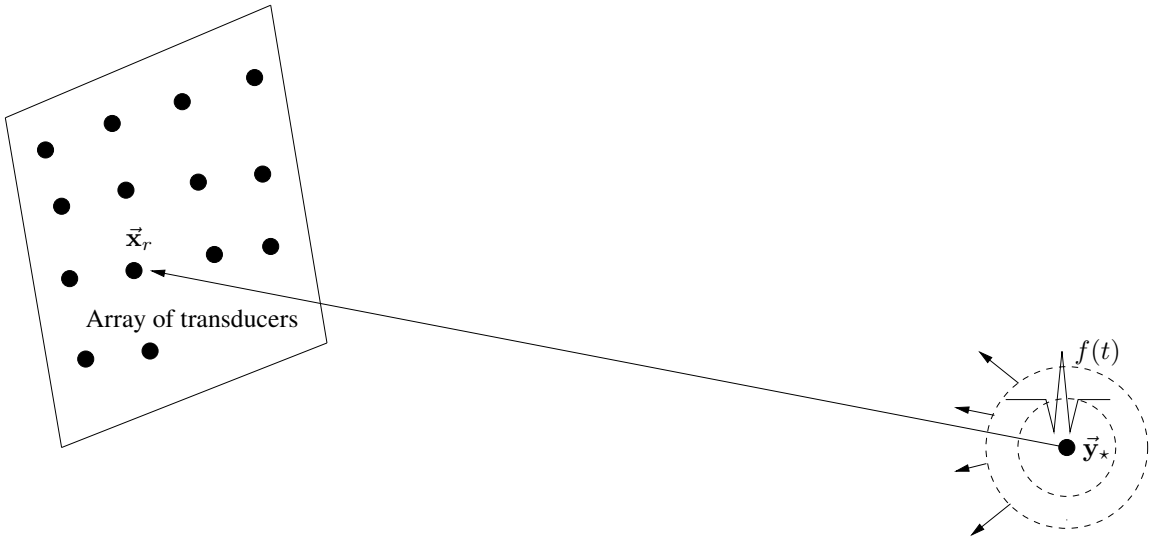

Figure 1. Schematic for the data acquisition by a passive array of receivers

propagates through a random medium and its amplitude at $\vec{\mathbf{x}}_r$ is given by the time convolution of the pulse with the Green's function

$$P(\vec{\mathbf{x}}_r, t) = e^{-i\omega_0 t} f_B(t) \star G(\vec{\mathbf{x}}_r, \vec{\mathbf{y}}_\star, t). \tag{2.5}$$

In the frequency domain we have

$$\widehat{P}(\vec{\mathbf{x}}_r, \omega) = \widehat{f}_B(\omega - \omega_0)\widehat{G}(\vec{\mathbf{x}}_r, \vec{\mathbf{y}}_\star, \omega). \tag{2.6}$$

Here $\widehat{G}$ is the outgoing Green's function of the reduced wave equation

$$\Delta\widehat{G}(\vec{\mathbf{x}}, \vec{\mathbf{y}}_\star, \omega) + k^2 n^2(\vec{\mathbf{x}})\widehat{G}(\vec{\mathbf{x}}, \vec{\mathbf{y}}_\star, \omega) = \delta(\vec{\mathbf{x}} - \vec{\mathbf{y}}_\star) \tag{2.7}$$

in the random medium, where $k = \omega/c_0$ is the wavenumber. The index of refraction $n(\vec{\mathbf{x}}) = c_0/c(\vec{\mathbf{x}})$ is assumed to be a statistically homogeneous random process so that

$$n^2(\vec{\mathbf{x}}) = 1 + \sigma_0 \mu\left(\frac{\vec{\mathbf{x}}}{l}\right). \tag{2.8}$$

The mean of $n^2(\vec{\mathbf{x}})$ is one and the normalized fluctuation process μ is a stationary and isotropic random field that is bounded and has rapidly decaying covariance

$$R(\vec{\mathbf{x}}) = R(|\vec{\mathbf{x}}|) = \langle \mu(\vec{\mathbf{x}} + \vec{\mathbf{x}}')\mu(\vec{\mathbf{x}}')\rangle\,. \tag{2.9}$$

Normalization here means that $R(0) = 1$ and

$$\int_{R^3} \langle \mu(\vec{\mathbf{x}})\mu(\mathbf{0})\rangle\, d\vec{\mathbf{x}} = 1$$

so that l is the correlation length and σ_0 the standard deviation of the fluctuations of $n^2(\vec{\mathbf{x}})$. This is a simple, mono-scale model for the random medium fluctuations that allows for a relatively simple theoretical discussion. Imaging in a random medium is influenced significantly by the properties of the fluctuation process, but we will not consider this issue here. We will also not consider slowly varying backgrounds or random

fluctuations that are statistically inhomogeneous. As we explain in Section 3.4, when we use the coherent interferometric functional (3.21) and can determine adaptively the smoothing or decoherence parameters X_d and Ω_d in a stable way, then we can image in the random medium which produced the noisy array data even though we do not know anything about this random medium and how to model it. It is only when we want to have a resolution theory in which the smoothing parameters are determined from first principles that a detailed model for the fluctuations is needed.

Equation (2.5) relates the field amplitude recorded at the array to the source location $\vec{\mathbf{y}}_\star$, so it is the forward model equation. The inverse problem for a point source is to find the location $\vec{\mathbf{y}}_\star$ of the point source given measurements $P(\vec{\mathbf{x}}_r, t)$ at points $\vec{\mathbf{x}}_r$ on the array.

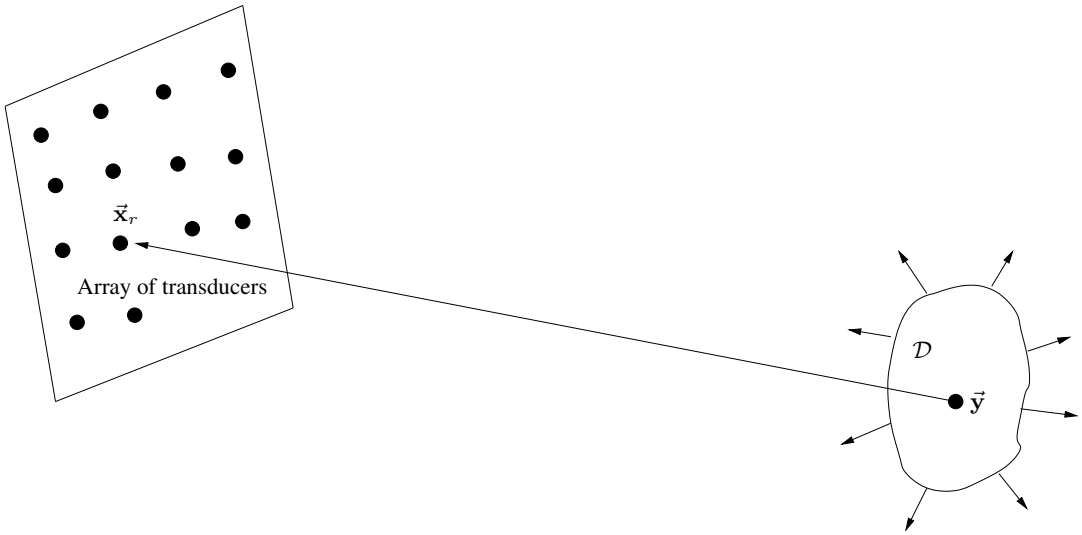

Figure 2. Schematic for passive array data from a distributed source in $\mathcal{D}$.

For a continuous distribution of sources in $\mathcal{D}$ (see figure 2) that emit the same signal simultaneously, the recorded data at the array are modeled by

$$P(\vec{\mathbf{x}}_r, t) = \int_{\mathcal{D}} \rho(\vec{\mathbf{y}}) e^{-i\omega_0 t} f_B(t) \star G(\vec{\mathbf{x}}_r, \vec{\mathbf{y}}, t) d\vec{\mathbf{y}}, \tag{2.10}$$

where $\rho(\vec{\mathbf{y}})$ is the source density in $\mathcal{D}$. The inverse problem for the distributed source is to find $\rho(\vec{\mathbf{y}})$, and its support $\mathcal{D}$ in particular, from the data $P(\vec{\mathbf{x}}_r, t)$ at the array.

2.2. Imaging with an active array

In Figure 3 we show a schematic for imaging with an active array, distributed reflectors of reflectivity $\rho(\vec{\mathbf{y}})$, occupying a region $\mathcal{D}$. The array is active because it emits pulses (2.3) from transducers at $\vec{\mathbf{x}}_s \in A$ and records the echoes with receivers at $\vec{\mathbf{x}}_r \in A$. We model the recorded field amplitudes using the Born approximation for scattering

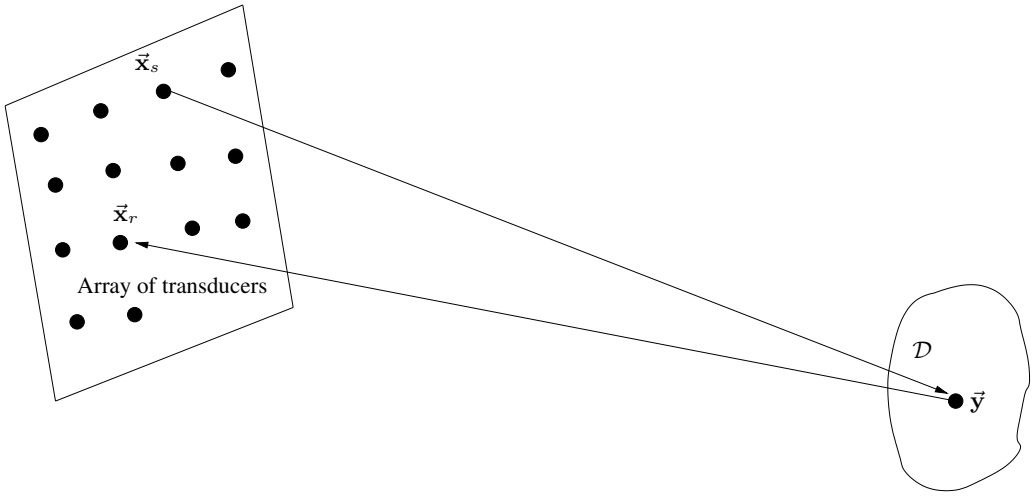

Figure 3. Schematic for imaging with an active array distributed reflectors in $\mathcal{D}$.

between reflectors, but allow for full multiple scattering by the random medium. In the frequency domain the model amplitudes are given by

$$\widehat{P}(\vec{\mathbf{x}}_s, \vec{\mathbf{x}}_r, \omega) = k^2 \widehat{f}_B(\omega - \omega_0) \int_{\mathcal{D}} d\vec{\mathbf{y}} \rho(\vec{\mathbf{y}}) \widehat{G}(\vec{\mathbf{y}}, \vec{\mathbf{x}}_s, \omega) \widehat{G}(\vec{\mathbf{x}}_r, \vec{\mathbf{y}}, \omega). \tag{2.11}$$

The forward model for the array data is thus a random linear transformation of the reflectivity $\rho(\vec{\mathbf{y}})$. It is random because the Green's functions are the ones for the random medium (2.7). The inverse problem is to estimate the reflectivity $\rho(\vec{\mathbf{y}})$, and its support $\mathcal{D}$ in particular, from data recorded at the array.

In the numerical simulations that we show in Section 4 we use only one illuminating transducer for computational simplicity.

It is important to explain why when imaging in a cluttered environment the Born approximation model (2.11) is quite sufficient. This is because when the random inhomogeneities have a strong enough effect, the information from multiple scattering between reflectors is completely lost in the delay spread in the data. This is very clearly seen in Figure 6. The top right plot shows the recorded traces, with central illumination, from three small reflectors. In addition to the three prominent hyperbolas that come from the direct reflections, there are several fainter hyperbolas that come from multiple scattering between the three reflectors. The bottom right plot in Figure 6 shows what happens when there is clutter. The delay spread in the data obliterates the fainter hyperbolas. Whatever image we do get will come only from the direct reflections, which is what the model (2.11) contains.

3. Statistically stable imaging in clutter

The reason that the Kirchhoff migration functionals (1.1),(1.2) do not image well when there is clutter, which we model with a random medium, is because we back propagate

the recorded data in a deterministic, homogeneous or slowly varying medium. Ideally, we would like to back propagate in the real medium, as in time reversal. However, we do not know the randomly fluctuating background. We may know its statistical properties, but we do not know its actual realization, which is what is needed if we are to back propagate in it.

For a point source located at $\vec{\mathbf{y}}_\star$ the signal received by the array at $\vec{\mathbf{x}}_r$ is modeled in the frequency domain by

$$\widehat{P}(\vec{\mathbf{x}}_r, \omega) = \widehat{f}_B(\omega - \omega_0)\widehat{G}(\vec{\mathbf{x}}_r, \vec{\mathbf{y}}_\star, \omega), \tag{3.12}$$

where $\widehat{G}(\vec{\mathbf{x}}, \vec{\mathbf{y}}, \omega)$ is the Green's function in the random medium, that is, the solution of the random Helmholtz equation (2.7). The Kirchhoff migration functional (1.1), which we write again with the full deterministic Green's function for the back propagation, has the form

$$\mathcal{I}^{\text{KM}}(\vec{\mathbf{y}}^s) = \sum_{\vec{\mathbf{x}}_r \in A} \int_{|\omega-\omega_0|\le B} d\omega\, \widehat{P}(\vec{\mathbf{x}}_r, \omega)\overline{\widehat{G}_0(\vec{\mathbf{x}}_r, \vec{\mathbf{y}}^s, \omega)}, \tag{3.13}$$

When we substitute the expression (3.12) for $\widehat{P}(\vec{\mathbf{x}}_r, \omega)$ in (3.13) we get

$$\mathcal{I}^{\text{KM}}(\vec{\mathbf{y}}^s) = \sum_{\vec{\mathbf{x}}_r \in A} \int_{|\omega-\omega_0|\le B} d\omega\, \widehat{f}_B(\omega - \omega_0)\widehat{G}(\vec{\mathbf{x}}_r, \vec{\mathbf{y}}_\star, \omega)\overline{\widehat{G}_0(\vec{\mathbf{x}}_r, \vec{\mathbf{y}}^s, \omega)}, \tag{3.14}$$

The main difference between this expression and Kirchhoff migration in a homogeneous medium (A.7), as reviewed in Appendix A, is that the phase cancellation that occurs in the deterministic case when $\vec{\mathbf{y}}^s$ is close to the unknown source location $\vec{\mathbf{y}}_\star$, does not occur in (3.14). The random phase of $\widehat{G}(\vec{\mathbf{x}}_r, \vec{\mathbf{y}}_\star, \omega)$ cannot be canceled with the deterministic phase of $\widehat{G}_0(\vec{\mathbf{x}}_r, \vec{\mathbf{y}}^s, \omega)$ so as to produce a peak in the Kirchhoff migration functional from which the source location $\vec{\mathbf{y}}_\star$ can be estimated. This is seen clearly in the numerical simulations described in Section 4 and in Figure 8 in particular. What is also seen in that figure is that for different realizations of the same random medium the Kirchhoff migration functional produces very different images when the random fluctuations are significant. This is the phenomenon of **statistical instability** that comes from the random phase of $\widehat{G}(\vec{\mathbf{x}}_r, \vec{\mathbf{y}}_\star, \omega)$ in (3.14). The Kirchhoff migration functional (3.14) is therefore unsuitable for imaging in clutter.

Can we find an imaging functional that can, when there is clutter, produce an estimate of the unknown source location $\vec{\mathbf{y}}_\star$ from the array data $\{P(\vec{\mathbf{x}}_r, t)\}$ in a statistically stable way? The image will, of course, be blurred by the clutter. However, we want this blurred image to be statistically stable, that is, the sought after imaging functional must be **self-averaging** with respect to the realizations of the random medium. The image that is formed by a self averaging imaging functional can then be processed further by deblurring methods, as we show in a companion paper [12]. In the next sections, we consider three different types of self-averaging functionals. They are: time reversal functionals, incoherent interferometric or matched field functionals, and coherent interferometric functionals.

3.1. Imaging and time reversal in random media

If we know the random medium between the array and the vicinity of the unknown source, that is, if we know the random Green's functions $\widehat{G}(\vec{\mathbf{x}}_r, \vec{\mathbf{y}}, \omega)$ for $\vec{\mathbf{x}}_r \in A$ and $\vec{\mathbf{y}}$ near $\vec{\mathbf{y}}_\star$, then we can image with the **time reversal functional**

$$\mathcal{I}^{\text{TR}}(\vec{\mathbf{y}}^s) = \sum_{\vec{\mathbf{x}}_r \in A} \int_{|\omega-\omega_0|\le B} d\omega\, \widehat{P}(\vec{\mathbf{x}}_r, \omega)\overline{\widehat{G}(\vec{\mathbf{x}}_r, \vec{\mathbf{y}}^s, \omega)}. \tag{3.15}$$

It is called the time reversal functional because it also represents the field near the source $\vec{\mathbf{y}}_\star$, when the array time-reverses the signals received and re-emits them into the (random) medium from which they came. This is **physical time reversal** [30, 31, 32]. It becomes an imaging functional **if we know** the random Green's functions, because then (3.15) can be computed numerically from the array data. The time reversal functional $\mathcal{I}^{\text{TR}}(\vec{\mathbf{y}}^s)$ is usually self-averaging, especially in broadband regimes [10], and has better focusing properties in random media than in homogeneous media. Note that $\mathcal{I}^{\text{TR}}$ in homogeneous media is identical to the Kirchhoff migration functional $\mathcal{I}^{\text{KM}}$. The enhanced focusing of time reversal in random media is called super resolution [26, 27, 25], and it has been analyzed in detail in [10]. The super resolution phenomenon is due to scattering that enhances the angular diversity of the back propagated waves near the source, making the focal spot tighter than in a homogeneous medium. Statistical stability is the result of good phase cancellation when the random Green's function is used for back propagation, as can be seen from the theoretical expression of the time reversal functional

$$\mathcal{I}^{\text{TR}}(\vec{\mathbf{y}}^s) = \sum_{\vec{\mathbf{x}}_r \in A} \int_{|\omega-\omega_0|\le B} d\omega\, \widehat{f}_B(\omega-\omega_0)\widehat{G}(\vec{\mathbf{x}}_r, \vec{\mathbf{y}}_\star, \omega)\overline{\widehat{G}(\vec{\mathbf{x}}_r, \vec{\mathbf{y}}^s, \omega)}. \tag{3.16}$$

In both deterministic and random media the range resolution of $\mathcal{I}^{\text{TR}}$ is c_0/B, which is the width of the pulse times the homogeneous propagation speed. The cross-range resolution in deterministic media is $L/(k_0 a)$ in narroband cases, as is well known [16], and $c_0 L/(Ba)$ (see Appendix A.1) in broadband regimes. In random media it can be much better because the **effective aperture** a_e of the array, a quantity that depends on the random medium, can be much larger than the physical aperture a [25]. The cross-range resolution for $\mathcal{I}^{\text{TR}}$ in random media is $L/(k_0 a_e)$ in relatively narrowband regimes, [10]. The dependence of the cross-range resolution on the bandwidth is discussed in [11].

The problem with $\mathcal{I}^{\text{TR}}$ as an imaging functional is, of course, that we do not know the clutter. It is because we do not know it that we model it as a random medium. We emphasize that knowing the random medium means knowing its particular realization that generated the data recorded by the array. Knowing this realization roughly, or knowing only its statistical properties, does not help and using such information for imaging can have a negative effect on statistical stability and on image resolution.

3.2. The matched field functional and incoherent interferometry

Even though we cannot use time reversal for imaging in clutter we would still like to exploit the remarkable properties of $\mathcal{I}^{\rm TR}$, its statistical stability and super-resolution in order to image. One way to exploit statistical stability is with the matched field or incoherent interferometric functional which we now introduce.

We want to avoid the random phase problems in Kirchhoff migration imaging so we mimic physical time reversal by computing cross-correlations of data traces, the interferograms

$$P(\vec{\mathbf{x}}_r,\cdot)*_t P(\vec{\mathbf{x}}_{r'},-\cdot)(t)=\int_{-\infty}^{\infty}P(\vec{\mathbf{x}}_r,s)P(\vec{\mathbf{x}}_{r'},s-t)ds. \tag{3.17}$$

We back propagate the interferograms in the homogeneous medium and then, we sum over the array

$$\mathcal{I}^{\rm INT}(\vec{\mathbf{y}}^s)=\sum_{\vec{\mathbf{x}}_r,\vec{\mathbf{x}}_{r'}} P(\vec{\mathbf{x}}_r,\cdot)*_t P(\vec{\mathbf{x}}_{r'},-\cdot)|_{\tau(\vec{\mathbf{x}}_r,\vec{\mathbf{y}}^s)-\tau(\vec{\mathbf{x}}_{r'},\vec{\mathbf{y}}^s)}. \tag{3.18}$$

Interferometric methods for imaging are considered in the recent work of Schuster et al [46], which contains many references to the seismic imaging literature, as well as in [42]. Interferometric functionals for imaging in clutter are used in [20].

The interferograms are self-averaging and in (3.18) we are doing what amounts to differential Kirchhoff migration on the lag of the interferograms, which is the back propagation of correlations of traces. In the frequency domain, $\mathcal{I}^{\rm INT}$ has the form

$$\mathcal{I}^{\rm INT}(\vec{\mathbf{y}}^s)=\int d\omega\left|\sum_{\vec{\mathbf{x}}_r}\widehat{P}(\vec{\mathbf{x}}_r,\omega)e^{-i\omega\tau(\vec{\mathbf{x}}_r,\vec{\mathbf{y}}^s)}\right|^2 \tag{3.19}$$

This is the form of a matched field functional [18, 1, 35, 28], especially when the exponential of the travel time is replaced by the deterministic Green's function

$$\mathcal{I}^{\rm INT}(\vec{\mathbf{y}}^s)=\int d\omega\left|\sum_{\vec{\mathbf{x}}_r}\widehat{P}(\vec{\mathbf{x}}_r,\omega)\overline{\widehat{G}_0(\vec{\mathbf{x}}_r,\vec{\mathbf{y}}^s,\omega)}\right|^2 \tag{3.20}$$

Since we take absolute values in (3.20) we can achieve some random phase cancellation for $\widehat{P}$, and because we integrate over the bandwidth we can expect statistical stability. We discuss this further in the next section.

The imaging properties of the interferometric functional $\mathcal{I}^{\rm INT}$ were analyzed in detail in [11] along with the presentation of the results of numerical simulations. The main shortcoming of $\mathcal{I}^{\rm INT}$ is that it provides essentially no range resolution at all, except by geometric triangulation if the array is large enough or when more than one array is used. The loss of range information can be seen clearly from (3.18) because the correlations are taken over all time so that information about absolute arrival times is lost. It can also be seen from (3.19) where an overall phase is lost, which accounts for the loss of range information. Cross correlations of traces are done over the whole array in (3.18), even

though they may be negligible when there is clutter unless the distance between $\vec{\mathbf{x}}_r$ and $\vec{\mathbf{x}}_{r'}$ is small. The way to avoid this difficulty is to consider interferometric functionals in which the time-trace correlations are constructed over specific time segments that correspond to information arriving from specific ranges. This is an intuitively appealing idea but it is not easy to implement because the time segmentation of the data must be done properly or else the results will not be much better than when no segmentation is used. There is a delicate trade off between segmentations with relatively short segments, which provide good range resolution, while they are also long enough so that the local correlations are statistically stable. We consider this basic issue in the next section.

There is another way to recover range resolution from broadband, active array data when the targets to be imaged are in a cluttered environment but sufficiently well separated. This is done with the singular value decomposition, matched field functionals and an arrival times analysis. It is described in detail in [13, 14].

3.3. The coherent interferometric functional

We see from the frequency domain form of $\mathcal{I}^{\text{INT}}$ in (3.19) that data at only one frequency are used in constructing the functional, before doing the integration over the bandwidth. If there are correlations between $\widehat{P}(\vec{\mathbf{x}}_r, \omega_1)$ and $\widehat{P}(\vec{\mathbf{x}}_{r'}, \omega_2)$ for two different frequencies ω_1 and ω_2, they are not used in $\mathcal{I}^{\text{INT}}$. This is another way of saying that correlations are taken over all time in (3.18), rather than over time segments, as we will see later in this Section. We will first consider the imaging functionals in the frequency domain because this is the form we use in the analysis and numerical simulations. Then, we shall rewrite them in the time domain as stacked, migrated trace correlations.

The key idea in constructing good imaging functionals in random media is to realize that there are two intrinsic, and characteristic, parameters in the data $\widehat{P}(\vec{\mathbf{x}}_r, \omega)$ that determine in a decisive way the quality of the image that is formed. One is the **decoherence frequency** Ω_d, and the other is the **decoherence length** X_d. They can be estimated in principle from the data $\widehat{P}(\vec{\mathbf{x}}_r, \omega)$. The decoherence frequency is the difference in frequencies ω_1 and ω_2 over which $\widehat{P}(\vec{\mathbf{x}}_r, \omega_1)$ and $\widehat{P}(\vec{\mathbf{x}}_r, \omega_2)$ become uncorrelated. The decoherence length is the difference in transducer locations $\vec{\mathbf{x}}_r$ and $\vec{\mathbf{x}}_{r'}$ over which $\widehat{P}(\vec{\mathbf{x}}_r, \omega)$ and $\widehat{P}(\vec{\mathbf{x}}_{r'}, \omega)$ become uncorrelated. While the estimation of Ω_d and X_d is possible, it is by no means a simple task and it is best done adaptively, as the image is formed. We will not discuss adaptive estimation techniques here, as this is the subject of a forthcoming paper [12]. We will discuss however the effect of Ω_d and X_d on image formation and resolution.

The decoherence length X_d can be related simply to the cross-range focusing resolution in time reversal, which as noted above is given by $L/(k_0 a_e)$. This is because of the reciprocity of the random Green's functions which allow us to identify cross correlations of the data $\widehat{P}(\vec{\mathbf{x}}_r, \omega)$ and $\widehat{P}(\vec{\mathbf{x}}_{r'}, \omega)$ with focusing in time reversal, as in

(3.16). We may, in fact, set $X_d = L/(k_0 a_e)$. This is an interesting expression because it relates two important length scales, X_d and a_e, that can be estimated, in principle, from different data sets.

We now introduce the coherent interferometric functional

$$\mathcal{I}^{\rm CINT}(\vec{\mathbf{y}}^s;\Omega_d,X_d) = \int\int_{|\omega_1-\omega_2|\le\Omega_d} d\omega_1 d\omega_2 \sum\sum_{|\vec{\mathbf{x}}_r-\vec{\mathbf{x}}_{r'}|\le X_d} \widehat{P}(\vec{\mathbf{x}}_r,\omega_1)\overline{\widehat{P}(\vec{\mathbf{x}}_{r'},\omega_2)} \\ e^{-i(\omega_1\tau(\vec{\mathbf{x}}_r,\vec{\mathbf{y}}^s)-\omega_2\tau(\vec{\mathbf{x}}_{r'},\vec{\mathbf{y}}^s))} \tag{3.21}$$

This functional depends on the parameters Ω_d and X_d, which are not determined at first. $\mathcal{I}^{\rm CINT}$ is equal to the square of the Kirchoff migration functional $\mathcal{I}^{\rm KM}$ (3.13) when $\Omega_d = B$ and $X_d = a$, that is, when there is no smoothing to account for the reduced coherence in the data. In a deterministic medium this is appropriate because frequency coherence of the traces persists over the bandwidth, as does spatial coherence of the traces across the array. On the other hand, if the decoherence frequency is very short, $\Omega_d \approx 0$, then the coherent interferometric functional (3.21) reduces essentially to the incoherent one (3.19), the matched field functional. We see, therefore, that (3.21) is a smoothed or regularized version of the Kirchoff migration functional (3.13), in which the smoothing or (statistical) regularization parameters are related to the intrinsic coherence of the data. The interpretation of (3.21) as the back propagation of local trace correlations will become clear from its time domain version.

Let us introduce a notation that we also use in Section 5. If range is measured from a fixed point on the array, such as its center, then we write $\vec{\mathbf{x}}_r = (\mathbf{x}_r, 0)$. With this notation, we also introduce the midpoint (sum) and offset (difference) variables:

$$\mathbf{x}_r = \bar{\mathbf{x}} - \tilde{\mathbf{x}}/2,\ \mathbf{x}_{r'} = \bar{\mathbf{x}} + \tilde{\mathbf{x}}/2 \tag{3.22}$$

as well as the sum or center frequency and the difference frequency variables

$$\omega_1 = \bar{\omega} - \tilde{\omega}/2,\ \omega_2 = \bar{\omega} + \tilde{\omega}/2 \tag{3.23}$$

Here, the midpoint variable $\bar{\mathbf{x}}$ runs over all the recorder locations in the array A and the offset variable runs over points for which $\mathbf{x}_r$ and $\mathbf{x}_{r'}$ remain in the array. The center frequency variable $\bar{\omega}$ runs over the bandwidth and the difference variable $\tilde{\omega}$ is such that ω_1 and ω_2 are inside the bandwidth.

Using the notation (3.22) and (3.23), we rewrite the coherent interferometric functional (3.21) in the form

$$\mathcal{I}^{\rm CINT}(\vec{\mathbf{y}}^s;\Omega_d,X_d) = \int_{|\bar{\omega}-\omega_0|\le B} d\bar{\omega} \sum_{\bar{\mathbf{x}}\in A} \int_{|\tilde{\omega}|\le\Omega_d} \sum_{|\tilde{\mathbf{x}}|\le X_d} \widehat{P}(\bar{\mathbf{x}}-\frac{\tilde{\mathbf{x}}}{2},\bar{\omega}-\frac{\tilde{\omega}}{2})\overline{\widehat{P}(\bar{\mathbf{x}}+\frac{\tilde{\mathbf{x}}}{2},\bar{\omega}+\frac{\tilde{\omega}}{2})} \\ e^{i\bar{\omega}[\tau(\bar{\mathbf{x}}+\frac{\tilde{\mathbf{x}}}{2},\vec{\mathbf{y}}^s)-\tau(\bar{\mathbf{x}}-\frac{\tilde{\mathbf{x}}}{2},\vec{\mathbf{y}}^s)]} e^{\frac{i\tilde{\omega}}{2}[\tau(\bar{\mathbf{x}}-\frac{\tilde{\mathbf{x}}}{2},\vec{\mathbf{y}}^s)+\tau(\bar{\mathbf{x}}+\frac{\tilde{\mathbf{x}}}{2},\vec{\mathbf{y}}^s)]} \tag{3.24}$$

where we do not show, for simplicity, edge restrictions in the range of the difference variables $\tilde{\mathbf{x}}$ and $\tilde{\omega}$. Let us assume that the difference variables are small. We can then

simplify the exponents in (3.24) to get

$$\tau(\bar{\mathbf{x}}+\frac{\tilde{\mathbf{x}}}{2},\vec{\mathbf{y}}^s)-\tau(\bar{\mathbf{x}}-\frac{\tilde{\mathbf{x}}}{2},\vec{\mathbf{y}}^s)\approx\nabla_{\bar{\mathbf{x}}}\tau(\bar{\mathbf{x}},\vec{\mathbf{y}}^s)\cdot\tilde{\mathbf{x}} \tag{3.25}$$

and

$$\frac{1}{2}[\tau(\bar{\mathbf{x}}-\frac{\tilde{\mathbf{x}}}{2},\vec{\mathbf{y}}^s)+\tau(\bar{\mathbf{x}}+\frac{\tilde{\mathbf{x}}}{2},\vec{\mathbf{y}}^s)]\approx\tau(\bar{\mathbf{x}},\vec{\mathbf{y}}^s). \tag{3.26}$$

If we now define the time-frequency and space-wavenumber, smoothed Wigner function of the data

$$W_D(\bar{\mathbf{x}},\mathbf{p},\bar{t},\bar{\omega};\Omega_d,X_d)=\int_{|\tilde{\omega}|\le\Omega_d}d\tilde{\omega}\sum_{|\tilde{\mathbf{x}}|\le X_d}\widehat{P}(\bar{\mathbf{x}}-\frac{\tilde{\mathbf{x}}}{2},\bar{\omega}-\frac{\tilde{\omega}}{2})\overline{\widehat{P}(\bar{\mathbf{x}}+\frac{\tilde{\mathbf{x}}}{2},\bar{\omega}+\frac{\tilde{\omega}}{2})}e^{i(\mathbf{p}\cdot\tilde{\mathbf{x}}+\bar{t}\tilde{\omega})} \tag{3.27}$$

we can write the coherent interferometric functional (3.21) in the simplified form

$$\mathcal{I}^{\text{CINT}}(\vec{\mathbf{y}}^s;\Omega_d,X_d)=\int_{|\bar{\omega}-\omega_0|\le B}d\bar{\omega}\sum_{\bar{\mathbf{x}}}W_D(\bar{\mathbf{x}},\ \bar{\omega}\nabla_{\bar{\mathbf{x}}}\tau(\bar{\mathbf{x}},\vec{\mathbf{y}}^s),\ \tau(\bar{\mathbf{x}},\vec{\mathbf{y}}^s),\ \bar{\omega};\Omega_d,X_d) \tag{3.28}$$

It is important to note here that the smoothed Wigner function of the data (3.27) is not statistically stable. Summing over the array and especially over the bandwidth is what makes the coherent interferometric functional (3.28) statistically stable.

It is interesting to write the analog of the coherent interferometric functional (3.28) in the time domain. This is easily done by inverting the Fourier transforms and then doing the smoothing or regularization in the time domain. The result is

$$\mathcal{I}^{\text{TCINT}}(\vec{\mathbf{y}}^s;T_d,X_d)=\sum_{\tilde{\mathbf{x}}\in A}\sum_{|\tilde{\mathbf{x}}|\le X_d}\int_{|\bar{t}-\tau(\bar{\mathbf{x}},\vec{\mathbf{y}}^s)|\le T_d}d\bar{t}\int_{|\tilde{t}-\nabla_{\tilde{\mathbf{x}}}\tau(\bar{\mathbf{x}},\vec{\mathbf{y}}^s)\cdot\tilde{\mathbf{x}}|\le T_p}d\tilde{t}$$
$$P(\bar{\mathbf{x}}-\frac{\tilde{\mathbf{x}}}{2},\bar{t}-\frac{\tilde{t}}{2})P(\bar{\mathbf{x}}+\frac{\tilde{\mathbf{x}}}{2},\bar{t}+\frac{\tilde{t}}{2}) \tag{3.29}$$

where $T_d=\pi/\Omega_d$ is the decoherence time and $T_p=\pi/B$ is the pulse width. Note that $\mathcal{I}^{\text{TCINT}}$ is not the exact transformation of (3.28), but rather its time domain analog. This is because cutoffs in frequency become sinc kernels in the time domain. We have used cutoffs in the time domain to underscore the parallel form that $\mathcal{I}^{\text{CINT}}$ and $\mathcal{I}^{\text{TCINT}}$ have. In the analysis and in the numerical computations of Section 4, we use the frequency domain version of the coherent interferometric functional.

We can now compare the coherent interferometric functional (3.29) to the matched field functional (3.18). First, in (3.17), we have to integrate the variable $\bar{t}$ over all time, as in (3.29). Then, (in 3.18), we have to evaluate the variable $\tilde{t}$ at $\nabla_{\tilde{\mathbf{x}}}\tau(\bar{\mathbf{x}},\vec{\mathbf{y}}^s)\cdot\tilde{\mathbf{x}}$, omitting the integration. This evaluation of $\tilde{t}$ corresponds to the differential migration in (3.18), that is, the evaluation of the cross correlation at the difference of the travel times. The integration over $\tilde{t}$ in (3.29) has no analog in (3.18). Finally in (3.18), we have to integrate over all $\tilde{\mathbf{x}}$, without restricting its length to be less than X_d, as is done in (3.29). However, the main feature of the coherent interferometric functional (3.29) is that trace correlations are computed locally in time. This affects the range resolution in an essential way as we discuss next.

3.4. Model independent resolution limits for coherent interferometry

The time domain version (3.29) of the coherent interferometric functional is particularly well structured for doing a rough but basic resolution estimation. If the search point $\vec{\mathbf{y}}^s$ is close to the source $\vec{\mathbf{y}}_\star$ then the uncertainty in range will come from the width of the time interval used for calculating the correlations, $|\bar{t} - \tau(\bar{\mathbf{x}}, \vec{\mathbf{y}}^s)| \leq T_d$. This means a rough estimate of the range resolution σ_R^R in a random medium is

$$\sigma_R^R = c_0 T_d = \frac{\pi c_0}{\Omega_d} \tag{3.30}$$

where we have used the relation $T_d = \pi/\Omega_d$ that relates the decoherence time to the decoherence frequency and the fact that travel time is range over propagation speed. In the deterministic case, $\Omega_d = B$, the full bandwidth, so the range resolution is given by $\sigma_R^D = \pi c_0/B$. This agrees with the results of the Kirchhoff migration functional in Appendix A.1.

We can get a rough estimate of the direction of arrival resolution σ_{DOA}^R from the range of integration of the time lag $\tilde{t}$ in (3.29). Since $\tilde{\mathbf{x}}$ is bounded in length by X_d, the direction of arrival $c_0|\nabla_{\bar{\mathbf{x}}}\tau(\bar{\mathbf{x}}, \vec{\mathbf{y}}^s)|$ is bounded by $\pi c_0/(BX_d)$ so that

$$\sigma_{DOA}^R = \frac{\pi c_0}{BX_d} \tag{3.31}$$

The cross-range resolution σ_{CR}^R is then given by $L\sigma_{DOA}^R$

$$\sigma_{CR}^R = \frac{\pi c_0 L}{BX_d} \tag{3.32}$$

When there is no randomness and $X_d = a$, the full array size, then the cross-range resolution is the same as the one we obtain from the analysis of the Kirchhoff migration functional in Appendix A, $\sigma_{CR}^D = \frac{\pi c_0 L}{Ba}$.

In Section 5 we will analyze in detail, and from first principles, the coherent interferometric functional (3.28) for a particular class of random media and in a particular scaling regime. The result of this analysis is that the rough range and cross-range resolution estimates (3.30) and (3.32) are, in fact, correct. We also show in Section 5 how the decoherence frequency and length, Ω_d and X_d, respectively, are related to the statistical properties of the fluctuations in the random medium. What, however, is especially interesting for imaging is that the rough range and cross-range resolution estimates (3.30) and (3.32) are **universal** in the class of array data for which the decoherence frequency and length Ω_d and X_d are well defined. The resolution estimates do not depend on any particular model or scaling regime for the random wave propagation. They do depend, however, on being able to estimate from the data, in a robust way, the coherence parameters Ω_d and X_d. We have, therefore, a self consistent way to assess when the resolution estimates (3.30) and (3.32) are expected to hold. This new insight into the relationship between image resolution and array data coherence plays an important role in the design of adaptive algorithms for stable image formation [12].

4. Numerical simulations

We present in this section the results of numerical simulations for imaging with the coherent interferometric functional (3.21), for both the passive and the active array configurations (cf. Sections 2.1 and 2.2).

4.1. The setup for the numerical simulations

The setup for the numerical experiments is shown in Figure 4 where the dimensions of the problem are given in terms of the central wavelength λ_0. We use an array of 185 transducers at a distance $h = \lambda_0/2$ from each other. The object to be imaged is at range $L = 90\lambda_0$ and at zero cross-range, measured with respect to the center of the array. In the passive array simulations the object is a configuration of three point sources emitting the same pulse $f(t)$ simultaneously and the distance between these points is $d = 6\lambda_0$. In the active array simulations the three sources are replaced by three disks of radius λ_0 whose centers are located at the same points. The disks are non penetrable scatterers modeled with homogeneous Dirichlet boundary conditions (acoustic soft scatterers). A probing pulse is emitted by the central array element. The pulse $f(t)$ is the time derivative of a Gaussian with central frequency $\omega_0/(2\pi) = 1$kHz and bandwidth $0.6 - 1.3$kHz (measured at 6dB). With a propagation speed of 3km/s the central wavelength is then $\lambda_0 = 3$m.

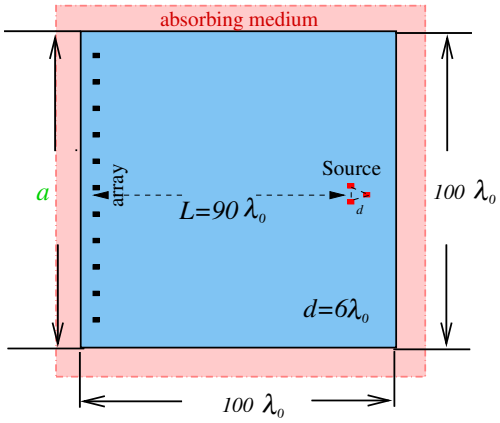

Figure 4. The computational setup. The dimensions of the problem are given in terms of the central wavelength λ_0.

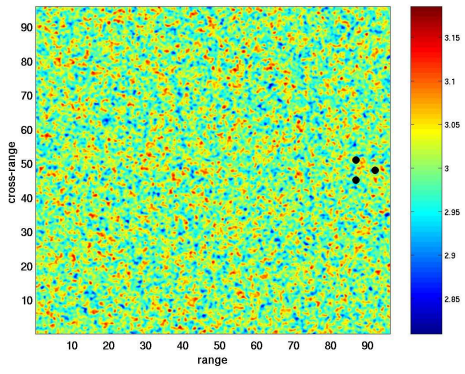

Figure 5. A typical realization of the random sound speed $c(\mathbf{x})$. The location of the objects to be imaged is shown as three black dots. The horizontal axis is range (in wavelenghts) and the vertical is cross-range (in wavelenghts).

To simulate imaging in a cluttered medium, the objects to be imaged (sources or scatterers) are embedded in a heterogeneous background medium with an index of refraction $n(\vec{\mathbf{x}}) = c_0/c(\vec{\mathbf{x}})$ given by (2.8). The fluctuations in the sound speed $c(\vec{\mathbf{x}})$ are modeled using a random Fourier series with mean $c_0 = 3.0$km/s and a Gaussian

correlation function. The correlation length is $l = 1.5$m and the standard deviation is $s = 3\%$. A typical realization of the random medium is shown in Figure 5 where the units in the horizontal and vertical axes are given in terms of the central wavelength and the scale of the color bar is in km/s.

To generate the array data we solve the acoustic wave equation, formulated as a first order in time velocity-pressure system, using a mixed finite element method [4, 5]. The propagation medium is considered to be infinite in all directions and in the numerical computations a perfectly matched absorbing layer (PML) surrounds the domain.

In Figure 6 we show numerically generated data recorded at the array. We show time traces in a homogeneous medium as well as in a random medium. It is clear from Figure 6 that in the active array case the effect of the random medium is a lot stronger as the waves travel twice the distance from the array to the scatterers. The coherent interferometry images obtained for these data, with the functional (3.21), are presented in the next section, where they are also compared with images obtained using Kirchhoff migration.

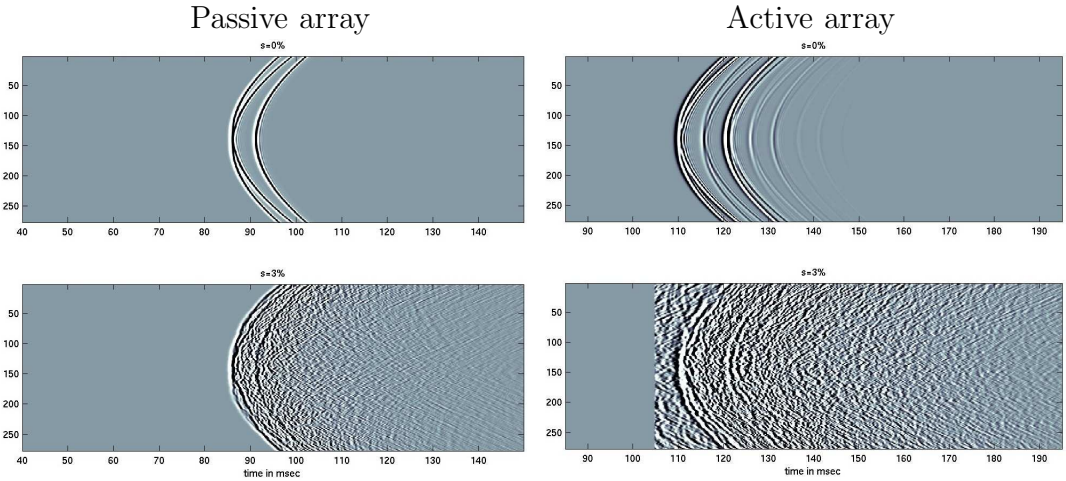

Figure 6. Time traces recorded on the array Top: homogeneous medium. Bottom: random medium with standard deviation $s = 3\%$. The horizontal axis is time (in msec) and the vertical is array transducer location (in m).

4.2. Imaging with coherent interferometry and with Kirchhoff migration

We show first in Figure 7 the images obtained with Kirchhoff migration in a homogeneous medium. We note that coherent interferometry (3.21) with no smoothing, so that $X_d = a$ and $\Omega_d = B$, is the same as the square of the Kirchhoff migration functional (1.1,1.2). For this reason, in the following, instead of showing the Kirchhoff migration images, we show their square.

The search domain, which is also the domain over which we show the image, is a

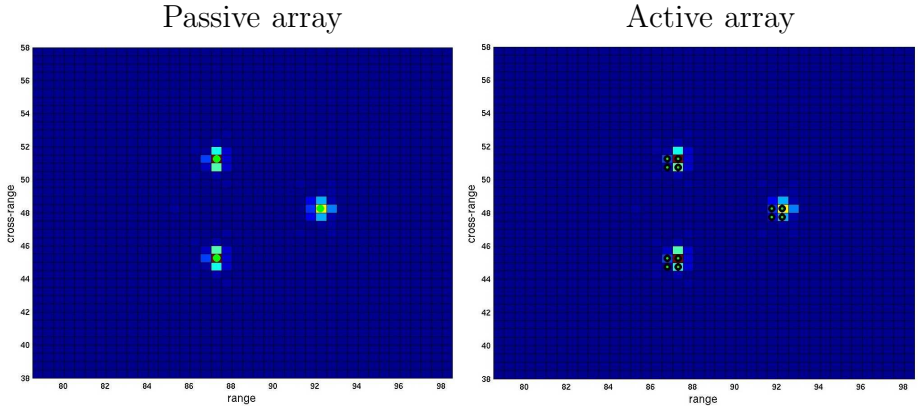

Figure 7. Kirchoff migration images in a homogeneous medium. The vertical axis is cross-range and the horizontal axis is range. The correct location of the objects is indicated with a star.

square of size $20\lambda_0 \times 20\lambda_0$, as in Figure 7. The vertical axis is the cross-range while the horizontal axis is range. The pixel size in the image is $\lambda_0/2$. In all the images that we show, the search domain, the domain of $\vec{\mathbf{y}}^s$, is fixed and equal to this one.

As expected, images with Kirchhoff migration are very good in homogeneous media and, more generally, in smooth deterministic media. When the background medium is randomly inhomogeneous, however, Kirchhoff migration images are no longer reliable because they are noisy and statistically unstable. That is, the images change from one realization of the random medium to another. This is clearly seen in Figure 8, especially in the active array case. The randomness in the images is inherited from the data recorded on the array and remains in them because there is no random phase cancellation in $\mathcal{I}^{\rm KM}$.

To obtain statistically stable images we use the coherent interferometric functional (3.21). This corresponds to migrating cross-correlations of the array data over the decoherence length X_d and frequency Ω_d. The images obtained for different values of X_d and Ω_d are shown in Figures 9-11.

The true decoherence parameters X_d and Ω_d are not known and depend on the random medium which is also assumed unknown. In principle, we can estimate these parameters directly from the data. However, this estimation can be rather delicate in practice, especially in inhomogeneous random media where X_d and Ω_d are not constant. Instead of estimating X_d and Ω_d directly from the data, we have introduced an algorithm that finds the decoherence parameters by looking at the image itself, as it is formed with (3.21). The essential idea is to minimize the spatial roughness of the image, as it is being formed, while controlling the smoothing. The main advantage of this approach is that the image that emerges is statistically stable while the data are not, and so the smoothing parameters X_d and Ω_d are easier to estimate from the image itself. The detailed description of the algorithm is presented in [12]. Here we demonstrate with

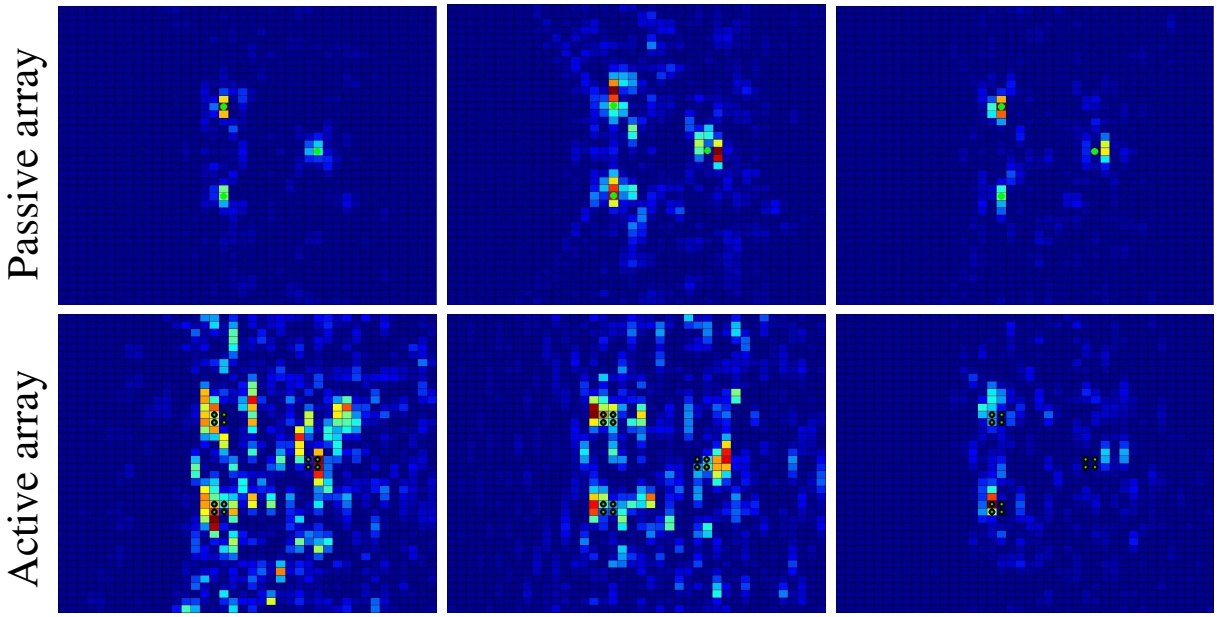

Figure 8. Kirchhoff migration images for three realizations of a random medium with standard deviation $s = 3\%$.

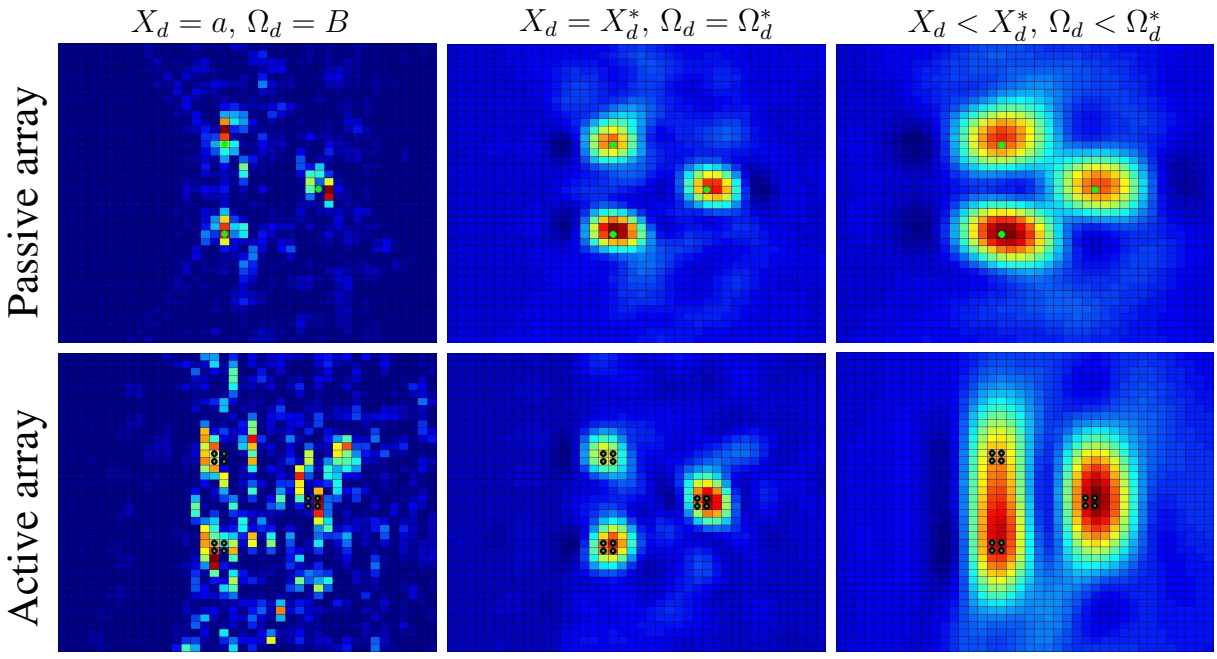

Figure 9. Coherent Interferometry images in random media with $s = 3\%$.

numerical simulations that optimal smoothing (decoherence) parameters $X_d^\star, \Omega_d^\star$ exist, by displaying in Figure 9 the images for X_d, Ω_d smaller, equal and larger than $X_d^\star, \Omega_d^\star$, respectively. When the X_d and Ω_d used in (3.21) are smaller than the optimal ones, the estimated image is over-smoothed, that is, blurrier than the optimal image. In the opposite direction, when X_d and Ω_d in $\mathcal{I}^{\text{CINT}}$ are over-estimated, then the image is noisy and statistically unstable. Note in particular that the decoherence frequency plays a crucial role in the statistical stability (see Figure 11).

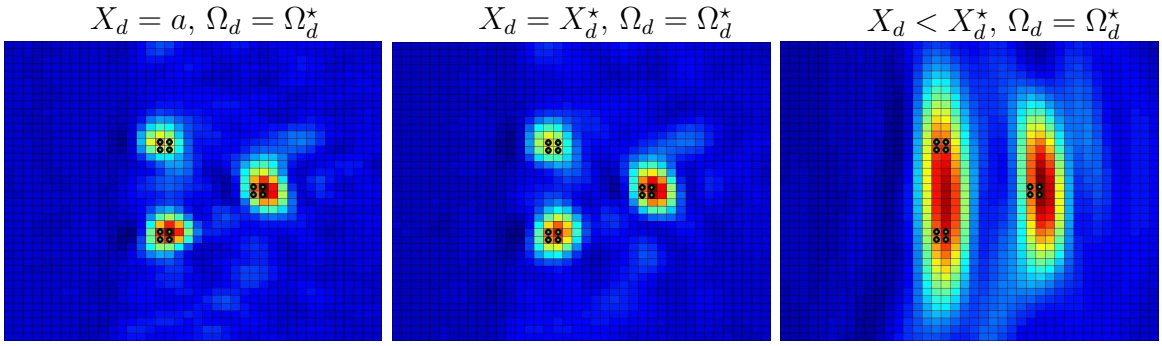

Figure 10. Coherent Interferometry: The effect of X_d on image resolution. The value of Ω_d is fixed and X_d decreases from left to right with the optimal in the middle.

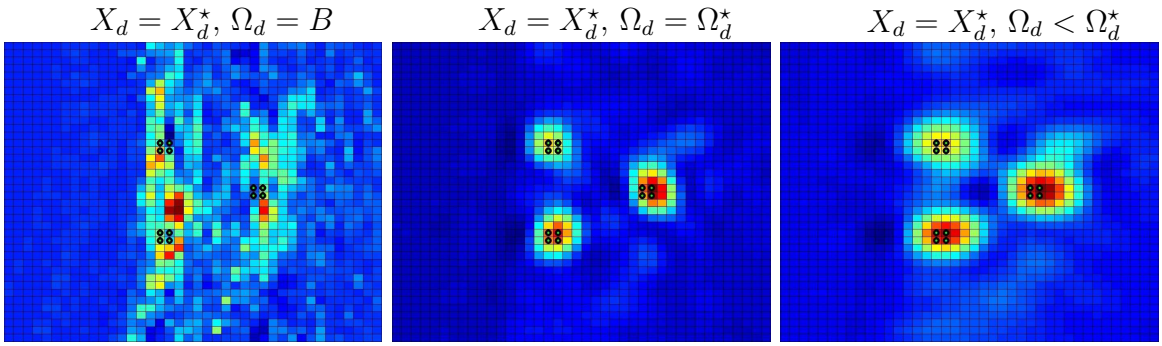

Figure 11. Coherent Interferometry: The effect of Ω_d on image resolution. The value of X_d is fixed and Ω_d decreases from left to right with the optimal in the middle.

As we know from the analysis of time reversal in random media [22, 10, 40, 2, 3, 43, 33] another parameter that plays an important role in the statistical stability is the bandwidth. In coherent interferometric imaging the bandwidth enters through the summation over $\overline{\omega}$ in (3.28). To illustrate how the average over frequency (sum over $\overline{\omega}$) affects the stability of $\mathcal{I}^{\text{CINT}}$, we show in Figure 12 images obtained with and without averaging over frequency.

The images shown in Figures 10-12 are for the active array case, with central illumination. They clearly illustrate the role of X_d and Ω_d in the resolution and the stability of the images. We note in particular that when imaging in clutter the resolution

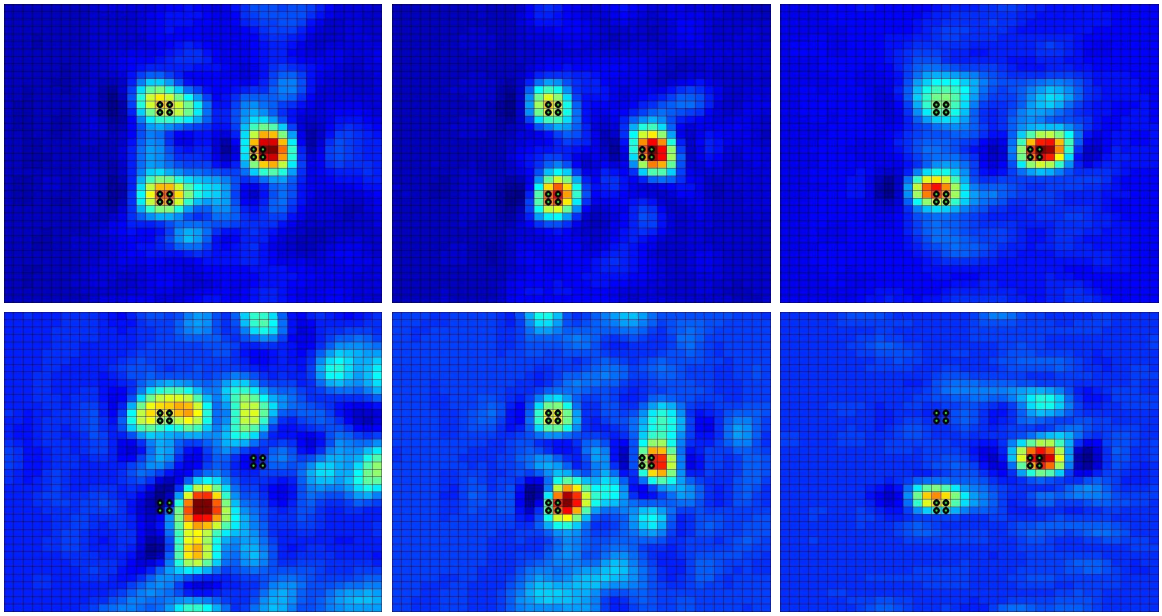

Figure 12. Coherent Interferometry: The effect of bandwidth on the stability of the images. The values of X_d and Ω_d are the optimal ones. Top: with averaging over frequency. Bottom: without averaging over frequency. Left to right: three different realizations of the random medium.

of the image is no longer determined by the array aperture and the bandwidth of the pulse, as is the case in deterministic media (compare Figure 11-middle with Figure 7-right). Instead, imaging resolution in random media depends on the decoherence length X_d and frequency Ω_d. In the following section, we present a theoretical analysis of coherent interferometry which gives resolution estimates, in the passive array case. As noted in Section 3.4, even though the analysis is done with a particular model in a particular asymptotic regime, the numerical results presented in this section are in qualitative agreement with the theoretical results. The numerical simulations are done in a realistic physical setting without any approximations like the ones used in the theoretical analysis.

5. Analysis of the coherent interferometric functional

In this section, we give a quantitative resolution analysis of the coherent interferometric imaging method introduced in Section 3, in a parabolic (forward scattering) high frequency asymptotic regime.

We assume that the size of the array is small in comparison with the range of the source and introduce a system of coordinates centered in the middle of the array, as shown in Figure 13. The array is taken, for simplicity, to be a square of aperture a in the plane orthogonal to the z axis, which connects the source with the origin. In this

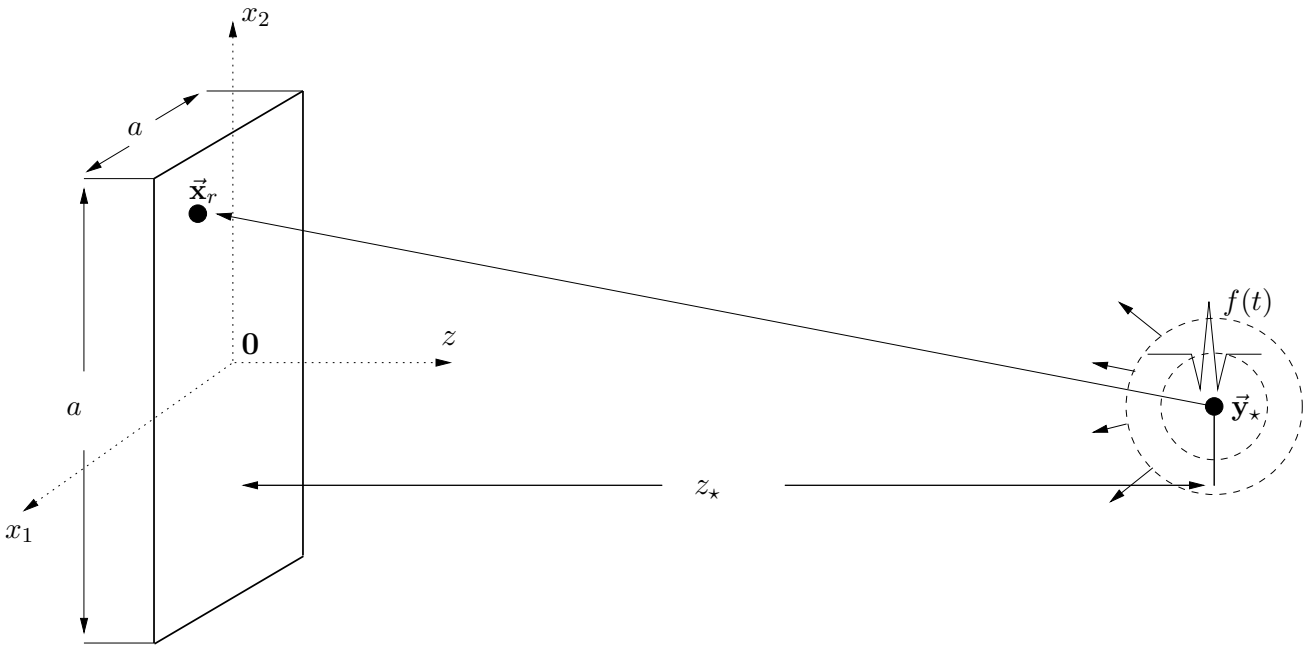

Figure 13. The array, assumed planar and with aperture a, is centered at the origin of the system of coordinates, at distance $z_\star$ from the source.

system of coordinates we introduce the notation

$$\vec{\mathbf{y}}_\star = (\mathbf{y}_\star = \mathbf{0}, z_\star), \quad \vec{\mathbf{x}}_r = (\mathbf{x}_r, 0), \tag{5.33}$$

where $z_\star$ and $\mathbf{y}_\star$ are the range and the cross-range of the source, respectively. The later is, by the choice of the coordinate system, the zero vector in $\mathbb{R}^2$. Similarly, $\mathbf{x}_r$ denotes the location of the r-th transducer in the planar array.

We will use the parabolic approximation of the Green's function and we write $\widehat{G}$ as

$$\widehat{G}(\vec{\mathbf{x}}, \vec{\mathbf{y}}_\star, \omega) = e^{ik|z-z_\star|}\psi(\vec{\mathbf{x}}, \vec{\mathbf{y}}_\star, \omega), \quad \text{for an arbitrary } \vec{\mathbf{x}} = (\mathbf{x}, z) \in \mathbb{R}^3, \tag{5.34}$$

where the amplitude ψ satisfies the parabolic equation

$$\begin{aligned} 2ik\psi_z + \Delta_{\mathbf{x}}\psi + k^2\sigma_0\mu\left(\frac{\mathbf{x}}{l}, \frac{z}{l}\right)\psi = 0, \quad & z < z_\star, \\ \psi \quad = \delta(\mathbf{x} - \mathbf{y}_\star), \quad & z = z_\star, \end{aligned} \tag{5.35}$$

and $\Delta_{\mathbf{x}}$ is the two-dimensional Laplace operator, with respect to the transverse coordinates $\mathbf{x}$. This approximation is valid when $k|\psi_z| \gg |\psi_{zz}|$ or, equivalently, when back scattering is negligible. This is usually the case with weak random inhomogeneities in remote sensing regimes, with $z_\star$ much larger than $L_{\mathbf{x}}$, a transverse length scale given, for example, by the aperture a of the array. Even though the random inhomogeneities are weak, we **do not** use a single scattering approximation. Since the waves travel over long distances from the source to the array, multiple scattering in the forward direction is significant and taken into account by the random parabolic equation (5.34).

When the fluctuations are zero, $\sigma_0 = 0$, the solution of (5.35) is

$$\psi_0(\vec{\mathbf{x}}, \vec{\mathbf{y}}_\star, \omega) \sim \frac{1}{|z - z_\star|} e^{\frac{ik|\mathbf{x}-\mathbf{y}_\star|^2}{2|z-z_\star|}}, \tag{5.36}$$

where the subscript 0 indicates that the medium is homogeneous and $\sim$ is used, throughout the paper, to denote equality up to a multiplicative constant. Thus, for $|z - z_\star| \gg |\mathbf{x} - \mathbf{y}_\star|$,

$$\widehat{G}_0(\vec{\mathbf{x}}, \vec{\mathbf{y}}_\star, \omega) = \frac{1}{4\pi|\vec{\mathbf{x}} - \vec{\mathbf{y}}_\star|} e^{ik|\vec{\mathbf{x}} - \vec{\mathbf{y}}_\star|} \sim \frac{1}{|z - z_\star|} e^{ik\left(|z-z_\star| + \frac{|\mathbf{x}-\mathbf{y}|^2}{2|z-z_\star|}\right)}, \tag{5.37}$$

which is the parabolic approximation of the Green's function in the homogeneous medium, as expected. Naturally, when the random fluctuations are present, $\widehat{G}$ and ψ are random functions.

5.1. Scaling

We scale variables with a horizontal scale $L_z \sim z_\star$ along the main direction of propagation of the waves, a transversal length $L_{\mathbf{x}}$, the carrier wavenumber $k_0 = \omega_0/c_0$ and the carrier frequency ω_0, respectively,

$$\mathbf{x} = L_{\mathbf{x}}\mathbf{x}', \quad z = L_z z', \quad k = k_0 k', \quad \omega = \omega_0 \omega', \quad B = \omega_0 B'. \tag{5.38}$$

The scaled range of the source is

$$z'_\star = \frac{z_\star}{L_z} \tag{5.39}$$

and, for a point $\vec{\mathbf{x}}_r = (\mathbf{x}_r, 0)$ in the array, the scaled distance to the source is

$$|\vec{\mathbf{x}}_r - \vec{\mathbf{y}}_\star|' = \frac{|\vec{\mathbf{x}}_r - \vec{\mathbf{y}}_\star|}{L_z} = \left[(z'_\star)^2 + \left(\frac{L_{\mathbf{x}}}{L_z}\right)^2 |\mathbf{x}'_r - \mathbf{y}'_\star|^2\right]^{\frac{1}{2}} \approx z'_\star + \left(\frac{L_{\mathbf{x}}}{L_z}\right)^2 \frac{|\mathbf{x}'_r - \mathbf{y}'_\star|^2}{2z'_\star}. \tag{5.40}$$

In the remainder of this Section, all variables are scaled and we simplify the notation by dropping the primes in (5.38)-(5.40).

Substituting (5.38) in (5.35) and neglecting the multiplicative constant in the initial condition, the scaled parabolic equation is

$$\begin{aligned} 2ik\psi_z + \theta\Delta_{\mathbf{x}}\psi + \frac{\sigma\delta}{\theta\sqrt{\epsilon}} k^2 \mu\left(\frac{\mathbf{x}}{\delta}, \frac{z}{\epsilon}\right)\psi = 0, \quad & z < z_\star, \\ \psi = \delta(\mathbf{x} - \mathbf{y}_\star), \quad & z = z_\star, \end{aligned} \tag{5.41}$$

with the dimensionless parameters

$$\epsilon = \frac{l}{L_z}, \quad \delta = \frac{l}{L_{\mathbf{x}}} \quad \text{and} \quad \sigma = \frac{\sigma_0\delta}{\epsilon^{3/2}} \tag{5.42}$$

depending on the random medium, and with the Fresnel number given by

$$\theta = \frac{L_z}{k_0 L_{\mathbf{x}}^2}. \tag{5.43}$$

Since we are interested in a remote sensing regime, with the source being a long distance away from the receivers, as compared with the aperture of the array and the correlation length, we order the length scales as

$$\text{Ł}_z \gg L_{\mathbf{x}} \gg l, \quad \text{or, equivalently,} \quad \epsilon \ll \delta \ll 1. \tag{5.44}$$

The particular choice $\sigma_0 = \sigma\epsilon^{3/2}/\delta$ of the strength of the fluctuations is made so that, in conjunction with ordering (5.44) of the length scales, we can take the *white noise* limit $\epsilon \to 0$ in (5.41). This asymptotic regime is used in Appendix B, together with the *high frequency* $\theta \ll 1$ approximation, to obtain simple expressions for the second moments of ψ. We discuss the moment formula in Section 5.2. We then use it in Section 5.4 to analyze the imaging functional for locating the source, given measurements (2.5) at the array.

5.2. The moment formula

To find the source location $\vec{\mathbf{y}}_\star$ we use a *coherent interferometric* functional (3.21) of the traces $P(\vec{\mathbf{x}}_r, t)$ and $P(\vec{\mathbf{x}}_{r'}, -t)$, at receivers‡ r and r'. In the random medium, the traces decorrelate rapidly, so we take receiver locations and frequencies, that are within a θ neighborhood of each other.

We analyze the imaging functional (3.21) in Section 5.4. This involves the random functions

$$\widehat{P}(\vec{\mathbf{x}}_r, \omega)\overline{\widehat{P}(\vec{\mathbf{x}}_{r'}, \omega')} = \widehat{f}_B(\omega - 1)\overline{\widehat{f}_B(\omega' - 1)}\widehat{G}(\vec{\mathbf{x}}_r, \vec{\mathbf{y}}_\star, \omega)\overline{\widehat{G}(\vec{\mathbf{x}}_{r'}, \vec{\mathbf{y}}_\star, \omega')}. \quad (5.45)$$

When the functional (3.21) is self-averaging we can analyze it using the expectation of (5.45). The self-averaging property comes primarily from the smoothing with the decoherence frequency Ω_d. We do not examine this property in detail here and refer to [40] for a systematic analysis of self-averaging issues for the random parabolic equation (5.41).

We first change variables by defining

$$\overline{\omega} = \frac{\omega + \omega'}{2}, \quad \widetilde{\omega} = \frac{\omega' - \omega}{\theta}, \quad (5.46)$$

$$\overline{\mathbf{x}} = \frac{\mathbf{x}_r + \mathbf{x}_{r'}}{2}, \quad \widetilde{\mathbf{x}} = \frac{\mathbf{x}_{r'} - \mathbf{x}_r}{\theta}, \quad (5.47)$$

where we omit subscripts on the midpoint and offset variables $\overline{\mathbf{x}}$ and $\widetilde{\mathbf{x}}$, respectively. We also note that because of (5.38) the scaled wavenumbers satisfy

$$\overline{k} = \overline{\omega}, \quad \widetilde{k} = \widetilde{\omega}. \quad (5.48)$$

In Appendix B we derive the moment formula

$$\left\langle \widehat{G}(\vec{\mathbf{x}}_r, \vec{\mathbf{y}}_\star, \omega)\overline{\widehat{G}(\vec{\mathbf{x}}_{r'}, \vec{\mathbf{y}}_\star, \omega')} \right\rangle \approx \widehat{G}_0(\vec{\mathbf{x}}_r, \vec{\mathbf{y}}_\star, \omega)\overline{\widehat{G}_0(\vec{\mathbf{x}}_{r'}, \vec{\mathbf{y}}_\star, \omega')} \phi_1(z_\star) e^{-\frac{\widetilde{k}^2 D_f z_\star}{2} - \phi_2(z_\star)\frac{\overline{k}^2 D_p z_\star |\widetilde{\mathbf{x}}|^2}{6}}, \quad (5.49)$$

where

$$\phi_1(z) = \cosh^{\frac{1}{2}}(z\sqrt{i\widetilde{k}D_p})\, \frac{z\sqrt{i\widetilde{k}D_p}}{\sinh(z\sqrt{i\widetilde{k}D_p})}, \quad (5.50)$$

‡ Here we use the prime to distinguish between different receiver locations or frequencies. The prime does not refer to the scaling as all our variables are now dimensionless.

$$\phi_2(z) = \frac{3}{i\widetilde{k}D_p z}\left(\frac{\sqrt{i\widetilde{k}D_p}}{\tanh(z\sqrt{i\widetilde{k}D_p})} - \frac{1}{z}\right), \tag{5.51}$$

and D_p, D_f are given in terms of the covariance (2.9) of the fluctuations by

$$D_p = -\frac{\sigma^2}{4}R_0''(0), \quad D_f = \frac{\sigma^2\delta^2}{4}R_0(0), \quad \text{for } R_0(|\mathbf{x}|) = \int_{-\infty}^{\infty} R(|\mathbf{x}|, z)dz. \tag{5.52}$$

When $\widetilde{k} = 0$ this formula is well known [34]. It is also known in some special cases with $\widetilde{k} \neq 0$, [45].

While one can do calculations with formula (5.49), we shall use the simplified version

$$\left\langle \widehat{G}(\vec{\mathbf{x}}_r, \vec{\mathbf{y}}_\star, \omega)\overline{\widehat{G}(\vec{\mathbf{x}}_{r'}, \vec{\mathbf{y}}_\star, \omega')}\right\rangle \approx \widehat{G}_0(\vec{\mathbf{x}}_r, \vec{\mathbf{y}}_\star, \omega)\overline{\widehat{G}_0(\vec{\mathbf{x}}_{r'}, \vec{\mathbf{y}}_\star, \omega')}e^{-\frac{\widetilde{k}^2 D_f z_\star}{2} - \frac{\overline{k}^2 D_p z_\star |\widetilde{\mathbf{x}}|^2}{6}}, \tag{5.53}$$

obtained from (5.49) by approximating $\phi_1(z_\star)$ and $\phi_2(z_\star)$ by one. This is a good approximation in the weak fluctuation regime with $\sigma \ll \delta$, where simple series expansions of (5.50)-(5.51) give

$$\phi_1(z) = 1 + O(\sigma^2) \quad \text{and} \quad (\phi_2(z) - 1)D_p = O\left(\frac{\sigma^2}{\delta^2}\right) D_f \ll D_f. \tag{5.54}$$

5.3. Space and frequency decoherence

¿From the moment formula (5.53) we can get a theoretical estimate of the space and frequency decoherence parameters of the array data. We can set them equal to the variance of the Gaussians in $\widetilde{k}$ and in $\widetilde{\mathbf{x}}$ in (5.53)

$$|\omega - \omega'| \leq \Omega_d = \frac{\theta}{\sqrt{D_f z_\star}} \tag{5.55}$$

and

$$|\mathbf{x}_r - \mathbf{x}_{r'}| \leq X_d(\overline{\omega}) = \frac{\theta}{\overline{k}}\sqrt{\frac{3}{D_p z_\star}} = \frac{\theta z_\star}{\overline{k} a_e}. \tag{5.56}$$

Here

$$a_e = \sqrt{\frac{D_p z_\star^3}{3}} \tag{5.57}$$

is the *effective aperture* in the random medium [40], scaled by $L_{\mathbf{x}}$. When we use (5.43) in (5.56) and rearrange terms we get

$$L_{\mathbf{x}} X_d(\overline{\omega}) = \frac{L_z z_\star}{k_0 \overline{k} L_{\mathbf{x}} a_e}, \tag{5.58}$$

which is, in dimensionless variables and scales, the equality of the decoherence length X_d to the *time reversal spot size* [10, 40]. We also use the notation $X_d(\overline{\omega})$ to indicate that the decoherence length depends on the central frequency.

5.4. The imaging functional

Let us take a search point $\vec{\mathbf{y}}^s = (\mathbf{y}_s, z_s)$ and define the imaging function

$$\mathcal{I}^{\text{CINT}}(\vec{\mathbf{y}}^s) = \sum_{\mathbf{x}_r \in A} \int_{|\omega-1|\le B} d\omega \int_{\substack{|\omega'-1|\le B \\ |\omega-\omega'|\le \Omega_d}} d\omega' \sum_{\substack{\mathbf{x}_{r'} \in A \\ |\mathbf{x}_r - \mathbf{x}_{r'}| \le X_d(\overline{\omega})}} \widehat{P}(\vec{\mathbf{x}}_r, \omega)\overline{\widehat{P}(\vec{\mathbf{x}}_{r'}, \omega')} \times \tag{5.59}$$

$$\overline{\widehat{G}_0(\vec{\mathbf{x}}_r, \vec{\mathbf{y}}^s, \omega)}\widehat{G}_0(\vec{\mathbf{x}}_{r'}, \vec{\mathbf{y}}^s, \omega'),$$

where A denotes the array. Here, we do a fictitious back propagation to $\vec{\mathbf{y}}^s$, by means of the homogeneous medium Green's function (5.37), that in scaling (5.38) becomes

$$\widehat{G}_0(\vec{\mathbf{x}}_r, \vec{\mathbf{y}}^s, \omega) \sim \frac{1}{z_s} e^{ik_0 L_z k z_s + i\frac{k|\mathbf{x}_r - \mathbf{y}_s|^2}{2\theta z_s}} = \frac{1}{z_s} e^{i\left(\frac{L_z}{L_{\mathbf{x}}}\right)^2 \frac{k}{\theta} z_s + \frac{k|\mathbf{x}_r - \mathbf{y}_s|^2}{2\theta z_s}}. \tag{5.60}$$

Of course, $\mathcal{I}^{\text{CINT}}(\vec{\mathbf{y}}^s)$ depends on the random Green's functions, so back propagating with G_0 cannot achieve perfect phase cancellation in (5.59), at $\vec{\mathbf{y}}^s = \vec{\mathbf{y}}_\star$, as desired. This leads to blurring of the image, as we now show.

We recall from Section 5.2 that $\mathcal{I}^{\text{CINT}}(\vec{\mathbf{y}}^s)$ is essentially deterministic (self-averaging), so we can replace the random part in (5.59) by its expectation using the moment formula (5.53). Let us assume small spacings between the receivers, so that we can approximate the sums in (5.60) by integrals

$$\sum_{\mathbf{x}_r \in A} \sum_{\substack{\mathbf{x}_{r'} \in A \\ |\mathbf{x}_r - \mathbf{x}_{r'}| \le X_d(\overline{\omega})}} \sim \int_{\overline{\mathbf{x}} \in A} d\overline{\mathbf{x}} \int_{\theta|\widetilde{\mathbf{x}}| \le X_d(\overline{\omega})} d\widetilde{\mathbf{x}}, \tag{5.61}$$

where discrete locations $\overline{\mathbf{x}}_r$ and $\widetilde{\mathbf{x}}_r$ have been replaced by the continuum varying $\overline{\mathbf{x}}$ and $\widetilde{\mathbf{x}}$, respectively. Equation (5.59) becomes, up to multiplicative constants,

$$\mathcal{I}^{\text{CINT}}(\vec{\mathbf{y}}^s) \sim \int_{\overline{\mathbf{x}} \in A} d\overline{\mathbf{x}} \int_{|\overline{\omega}-1|\in B} d\overline{\omega} \int_{\theta|\widetilde{\mathbf{x}}| \le X_d(\overline{\omega})} d\widetilde{\mathbf{x}} \int_{\theta|\widetilde{\omega}| \le \Omega_d} d\widetilde{\omega}\ \widehat{f}_B\left(\overline{\omega} - 1 - \frac{\theta\widetilde{\omega}}{2}\right) \overline{\widehat{f}_B\left(\overline{\omega} - 1 + \frac{\theta\widetilde{\omega}}{2}\right)}$$

$$\widehat{G}_0\left((\overline{\mathbf{x}} - \tfrac{\theta\widetilde{\mathbf{x}}}{2}, 0), \vec{\mathbf{y}}_\star, \overline{\omega} - \tfrac{\theta\widetilde{\omega}}{2}\right) \overline{\widehat{G}_0\left((\overline{\mathbf{x}} + \tfrac{\theta\widetilde{\mathbf{x}}}{2}, 0), \vec{\mathbf{y}}_\star, \overline{\omega} + \tfrac{\theta\widetilde{\omega}}{2}\right)} e^{-\frac{\widetilde{k}^2 D_{f z_\star}}{2} - \frac{\overline{k}^2 D_{p z_\star} |\widetilde{\mathbf{x}}|^2}{6}} \tag{5.62}$$

$$\overline{\widehat{G}_0\left((\overline{\mathbf{x}} - \tfrac{\theta\widetilde{\mathbf{x}}}{2}, 0), \vec{\mathbf{y}}^s, \overline{\omega} - \tfrac{\theta\widetilde{\omega}}{2}\right)} \widehat{G}_0\left((\overline{\mathbf{x}} + \tfrac{\theta\widetilde{\mathbf{x}}}{2}, 0), \vec{\mathbf{y}}^s, \overline{\omega} + \tfrac{\theta\widetilde{\omega}}{2}\right).$$

Using expression (5.60) of $\widehat{G}_0$, we have

$$\widehat{G}_0\left((\overline{\mathbf{x}} - \tfrac{\theta\widetilde{\mathbf{x}}}{2}, 0), \vec{\mathbf{y}}_\star, \overline{\omega} - \tfrac{\theta\widetilde{\omega}}{2}\right) \overline{\widehat{G}_0\left((\overline{\mathbf{x}} + \tfrac{\theta\widetilde{\mathbf{x}}}{2}, 0), \vec{\mathbf{y}}_\star, \overline{\omega} + \tfrac{\theta\widetilde{\omega}}{2}\right)} \sim \tag{5.63}$$

$$\frac{1}{z_\star^2} e^{i\left(\frac{L_z}{L_{\mathbf{x}}}\right)^2 \frac{1}{\theta}\left[\left(\overline{k} - \frac{\theta\widetilde{k}}{2}\right) z_\star - \left(\overline{k} + \frac{\theta\widetilde{k}}{2}\right) z_\star\right]} \times e^{i\left(\overline{k} - \frac{\theta\widetilde{k}}{2}\right)\frac{|\overline{\mathbf{x}} - \mathbf{y}_\star - \frac{\theta}{2}\widetilde{\mathbf{x}}|^2}{2\theta z_\star} - i\left(\overline{k} + \frac{\theta\widetilde{k}}{2}\right)\frac{|\overline{\mathbf{x}} - \mathbf{y}_\star + \frac{\theta}{2}\widetilde{\mathbf{x}}|^2}{2\theta z_\star}}.$$

For $\theta \ll 1$ we can write

$$\frac{|\overline{\mathbf{x}} - \mathbf{y}_\star - \frac{\theta}{2}\widetilde{\mathbf{x}}|^2}{2z_\star} + \frac{|\overline{\mathbf{x}} - \mathbf{y}_\star + \frac{\theta}{2}\widetilde{\mathbf{x}}|^2}{2z_\star} \approx \frac{|\overline{\mathbf{x}} - \mathbf{y}_\star|^2}{z_\star} \tag{5.64}$$

and

$$\begin{aligned}\tfrac{|\overline{\mathbf{x}}-\mathbf{y}_\star-\frac{\theta}{2}\widetilde{\mathbf{x}}|^2}{2\theta z_\star}-\tfrac{|\overline{\mathbf{x}}-\mathbf{y}_\star+\frac{\theta}{2}\widetilde{\mathbf{x}}|^2}{2\theta z_\star} &\approx -\widetilde{\mathbf{x}}\cdot\frac{\nabla_{\overline{\mathbf{x}}}|\overline{\mathbf{x}}-\mathbf{y}_\star|^2}{2z_\star}\\ &\approx -\left(\frac{L_z}{L_{\mathbf{x}}}\right)^2\widetilde{\mathbf{x}}\cdot\nabla_{\overline{\mathbf{x}}}|(\overline{\mathbf{x}},0)-\vec{\mathbf{y}}_\star|,\end{aligned} \tag{5.65}$$

with the last approximation in (5.65) coming from (5.40).

Gathering the results (5.63)-(5.65) and recalling once more (5.40) we get

$$\begin{aligned}&\widehat{G}_0\left((\overline{\mathbf{x}}-\tfrac{\theta\widetilde{\mathbf{x}}}{2},0),\vec{\mathbf{y}}_\star,\overline{\omega}-\tfrac{\theta\widetilde{\omega}}{2}\right)\overline{\widehat{G}_0\left((\overline{\mathbf{x}}+\tfrac{\theta\widetilde{\mathbf{x}}}{2},0),\vec{\mathbf{y}}_\star,\overline{\omega}+\tfrac{\theta\widetilde{\omega}}{2}\right)}\sim\tfrac{1}{z_\star^2}\times\\ &\qquad e^{-i\left(\frac{L_z}{L_{\mathbf{x}}}\right)^2\left[\widetilde{k}\,|(\overline{\mathbf{x}},0)-\vec{\mathbf{y}}_\star|+\overline{k}\,\widetilde{\mathbf{x}}\cdot\nabla_{\overline{\mathbf{x}}}|(\overline{\mathbf{x}},0)-\vec{\mathbf{y}}_\star|\right)}\end{aligned} \tag{5.66}$$

and, similarly,

$$\begin{aligned}&\overline{\widehat{G}_0\left(\overline{\mathbf{x}}-\tfrac{\theta\widetilde{\mathbf{x}}}{2},0),\vec{\mathbf{y}}^s,\overline{\omega}-\tfrac{\theta\widetilde{\omega}}{2}\right)}\widehat{G}_0\left((\overline{\mathbf{x}}+\tfrac{\theta\widetilde{\mathbf{x}}}{2},0),\vec{\mathbf{y}}^s,\overline{\omega}+\tfrac{\theta\widetilde{\omega}}{2}\right)\sim\tfrac{1}{z_s^2}\times\\ &\qquad e^{i\left(\frac{L_z}{L_{\mathbf{x}}}\right)^2\left[\widetilde{k}\,|(\overline{\mathbf{x}},0)-\vec{\mathbf{y}}^s|+\overline{k}\,\widetilde{\mathbf{x}}\cdot\nabla_{\overline{\mathbf{x}}}|(\overline{\mathbf{x}},0)-\vec{\mathbf{y}}^s|\right)}.\end{aligned} \tag{5.67}$$

Equation (5.62) becomes, after approximating the amplitude $1/(z_\star z_s)^2\approx 1/z_\star^4$,

$$\begin{aligned}\mathcal{I}^{\mathrm{CINT}}(\vec{\mathbf{y}}^s) \sim\tfrac{1}{z_\star^4}\int_{\overline{\mathbf{x}}\in A}d\overline{\mathbf{x}}\int_{|\overline{\omega}-1|\in B}d\overline{\omega}\left|\widehat{f}_B(\overline{\omega}-1)\right|^2\int_{\theta|\widetilde{\omega}|\le\Omega_d}d\widetilde{\omega}\int_{\theta|\widetilde{\mathbf{x}}|\le X_d(\overline{\omega})}d\widetilde{\mathbf{x}}\\ e^{-\frac{\overline{k}^2D_pz_\star|\widetilde{\mathbf{x}}|^2}{6}-\frac{\widetilde{k}^2D_fz_\star}{2}}e^{i\left(\frac{L_z}{L_{\mathbf{x}}}\right)^2\left[\widetilde{k}(|(\overline{\mathbf{x}},0)-\vec{\mathbf{y}}^s|-|(\overline{\mathbf{x}},0)-\vec{\mathbf{y}}_\star|)+\overline{k}\widetilde{\mathbf{x}}\cdot(\nabla_{\overline{\mathbf{x}}}|(\overline{\mathbf{x}},0)-\vec{\mathbf{y}}^s|-\nabla_{\overline{\mathbf{x}}}|(\overline{\mathbf{x}},0)-\vec{\mathbf{y}}_\star|)\right]},\end{aligned} \tag{5.68}$$

where we set

$$\widehat{f}_B\left(\overline{\omega}-1\pm\frac{\theta\widetilde{\omega}}{2}\right)\approx\widehat{f}_B\left(\overline{\omega}-1\right), \tag{5.69}$$

assuming that Ω_d is much smaller than the bandwidth B of the pulse. This is precisely the setup in which coherent interferometry is expected to work well, since achieving a stable imaging function requires averaging over $\overline{\omega}$ spanning many decoherence frequencies.

Recalling from Section 5.2 that the domains of integration over $\widetilde{\omega}$ and $\widetilde{\mathbf{x}}$ are chosen as the essential support§ of the Gaussians in (5.68), we can approximate the integrals over $\widetilde{\omega}$ and $\widetilde{\mathbf{x}}$ by extending them to the entire real axis and $\mathbb{R}^2$ plane, respectively. The result is

$$\begin{aligned}\mathcal{I}^{\mathrm{CINT}}(\vec{\mathbf{y}}^s)\sim\tfrac{1}{z_\star^5\sqrt{z_\star}}\int_{|\overline{\omega}-1|\in B}d\overline{\omega}\,\frac{|\widehat{f}_B(\overline{\omega}-1)|^2}{\overline{\omega}^4}\int_{\overline{\mathbf{x}}\in A}d\overline{\mathbf{x}}\;e^{-\left(\frac{L_z}{L_{\mathbf{x}}}\right)^4\frac{|\nabla_{\overline{\mathbf{x}}}|(\overline{\mathbf{x}},0)-\vec{\mathbf{y}}^s|-\nabla_{\overline{\mathbf{x}}}|(\overline{\mathbf{x}},0)-\vec{\mathbf{y}}_\star||^2}{2D_pz_\star/3}}\times\\ e^{-\left(\frac{L_z}{L_{\mathbf{x}}}\right)^4\frac{\left(|(\overline{\mathbf{x}},0)-\vec{\mathbf{y}}^s|-|(\overline{\mathbf{x}},0)-\vec{\mathbf{y}}_\star|\right)^2}{2D_fz_\star}},\end{aligned} \tag{5.70}$$

§ While the Gaussians have infinite support, they are very small outside the essential support defined as three standard deviations.

where the extra factors of $z_\star$ in the amplitude are due to the integration.

We can write (5.70) in a simpler form that makes the resolution of the coherent interferometric point spread function $\mathcal{I}^{\rm CINT}(\vec{\mathbf{y}}^s)$ more transparent. Using the parabolic approximation (5.40) we have

$$\left(\frac{L_z}{L_{\mathbf{x}}}\right)^2 \left(\nabla_{\overline{\mathbf{x}}}|(\overline{\mathbf{x}},0)-\vec{\mathbf{y}}^s| - \nabla_{\overline{\mathbf{x}}}|(\overline{\mathbf{x}},0)-\vec{\mathbf{y}}_\star|\right) \approx \frac{\overline{\mathbf{x}}-\mathbf{y}_s}{z_s} - \frac{\overline{\mathbf{x}}-\mathbf{y}_\star}{z_\star} \tag{5.71}$$

and

$$\left(|(\overline{\mathbf{x}},0)-\vec{\mathbf{y}}^s| - |(\overline{\mathbf{x}},0)-\vec{\mathbf{y}}_\star|\right) \approx z_s - z_\star + \left(\frac{L_{\mathbf{x}}}{L_z}\right)^2 \left(\frac{|\overline{\mathbf{x}}-\mathbf{y}_s|^2}{2z_s} - \frac{|\overline{\mathbf{x}}-\mathbf{y}_\star|^2}{2z_s}\right) \approx z_s - z_\star.$$

Using also (5.55) and (5.57) we can write the approximation to $\mathcal{I}^{\rm CINT}(\vec{\mathbf{y}}^s)$ in the form

$$\mathcal{I}^{\rm CINT}(\vec{\mathbf{y}}^s) \sim \frac{1}{z_\star^5\sqrt{z_\star}} \int_{|\overline{\omega}-1|\in B} d\overline{\omega}\, \frac{|\widehat{f}_B(\overline{\omega}-1)|^2}{\overline{\omega}^4} \int_{\overline{\mathbf{x}}\in A} d\overline{\mathbf{x}}\; e^{-\frac{\left|\mathbf{y}_\star - \frac{z_\star}{z_s}\mathbf{y}_s + \left(\frac{z_\star}{\zeta_s}-1\right)\overline{\mathbf{x}}\right|^2}{2a_e^2} - \frac{(z_\star-z_s)^2}{2r_e^2}}, \tag{5.72}$$

where

$$L_z r_e = \frac{1}{k_0\Omega_d} \tag{5.73}$$

is defined as the range resolution. It is given in terms of scales and dimensionless variables and it is the distance traveled at speed c_0 over the delay spread $1/(\omega_o\Omega_d)$, as discussed in Section 3.4. Thus, in dimensional variables the range resolution is determined by c_0/Ω_d, and the larger the delay spread the poorer estimate of $z_\star$ is. Moreover, assuming that $r_e \ll 1$, we can simplify $\mathcal{I}^{\rm CINT}$ further to obtain

$$\mathcal{I}^{\rm CINT}(\vec{\mathbf{y}}^s) \sim \frac{1}{z_\star^5\sqrt{z_\star}} \int_{|\overline{\omega}-1|\in B} d\overline{\omega}\, \frac{|\widehat{f}_B(\overline{\omega}-1)|^2}{\overline{\omega}^4} \int_{\overline{\mathbf{x}}\in A} d\overline{\mathbf{x}}\; e^{-\frac{|\mathbf{y}_\star-\mathbf{y}_s|^2}{2a_e^2} - \frac{(z_\star-z_s)^2}{2r_e^2}}, \tag{5.74}$$

and note that the cross-range resolution is determined by the effective aperture a_e.

5.5. Summary of the resolution analysis

In order to relate the results we have obtained above, with the discussion of Section 3.4 we write (5.74) in dimensional variables. By the convention of Section 5.1, all variables in (5.74) should carry a prime because they are scaled. Restoring the scales gives

$$\mathcal{I}^{\rm CINT}(\vec{\mathbf{y}}^s) \sim \int_{|\overline{\omega}-\omega_0|\in B} d\overline{\omega}\, \frac{|\widehat{f}_B(\overline{\omega}-\overline{\omega}_0)|^2}{\overline{\omega}^4} \int_{\overline{\mathbf{x}}\in A} d\overline{\mathbf{x}}\; e^{-\frac{|\mathbf{y}_\star-\mathbf{y}_s|^2}{2(L_x a_e)^2} - \frac{(z_\star-z_s)^2}{2(L_z r_e)^2}}. \tag{5.75}$$

As already noted above, the range resolution is

$$L_z r_e = \frac{c_0}{\Omega_d}, \tag{5.76}$$

where Ω_d has been dimensionalized by multiplying (5.55) with ω_0. Since Ω_d is usually much smaller than the bandwidth B, the range resolution in random media can be considerably worse than in a homogeneous medium, where it is given by c_0/B (see Appendix A.1).

The cross-range resolution is given by $L_x a_e$ or, in dimensional variables, by a_e. This agrees with the result obtained in [11] for the cross-range resolution of the matched field functional (3.18). Using (5.58) we also have that

$$L_x a_e = \frac{c_0 L_z}{\omega_0 X_d(\omega_0)}, \tag{5.77}$$

where X_d has been dimensionalized by multiplying (5.56) with L_x. Note that the product $\omega X_d(\omega)$ is independent of the frequency, as seen from (5.58), so we used the carrier frequency ω_0 in (5.77).

The broadband cross-range resolution of Kirchhoff migration is given by $\frac{c_0 L_z}{Ba}$, as reviewed in Appendix A.1. Thus, we see from (5.77) that Ba is replaced by $\omega_0 X_d(\omega_0)$ in coherent interferometry. Since X_d is usually smaller than Ba/ω_0, the cross-range resolution in random media is worse than it is in a homogeneous one. The images that are obtained with the coherent interferometric functional are stable but blurred.

6. Interferometric imaging of extended sources

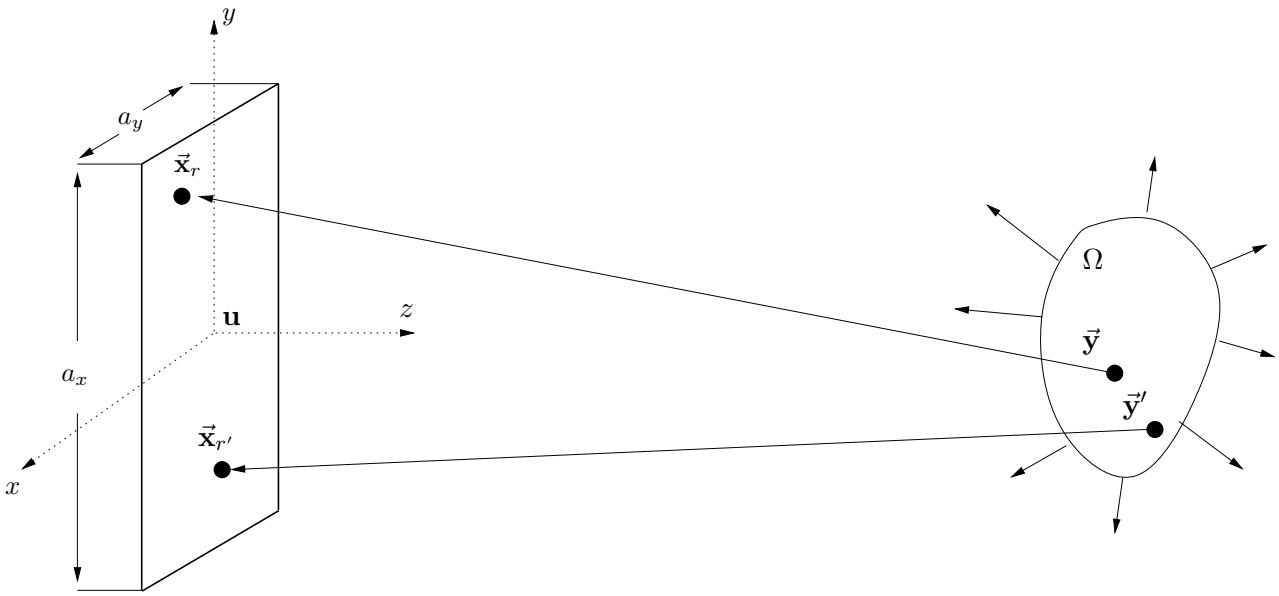

Figure 14. Sources distributed continuously in $\mathcal{D}$ emit simultaneously a pulse which propagates through the medium and is partially captured at an array of transducers shown in the Figure.

In this section we extend the resolution analysis of Section 5 for a point source, to a distributed source. The setup is described in Section 2.1 and the forward model is given by (2.10). We use the assumptions and notation of Section 5.

To fix ideas we suppose that the support $\mathcal{D}$ of the source is much larger than θ, in all directions. If the diameter of $\mathcal{D}$ is $\leq O(\theta)$, then for all practical purposes the source is like a point and the analysis of Section 5 applies. Of course, we can have a

thin domain $\mathcal{D}$ as well, but the analysis presented here extends easily to such particular cases.

We image $\mathcal{D}$ with the coherent interferometric function (5.59), for arbitrary search points $\vec{\mathbf{y}}^s$. Using the forward model (2.10) and the self-averaging of $\mathcal{I}^{\text{CINT}}$, we have

$$\mathcal{I}^{\text{CINT}}(\vec{\mathbf{y}}^s) = \sum_{\mathbf{x}_r \in A} \int_{|\omega-1|\le B} d\omega \int_{\substack{|\omega'-1|\le B \\ |\omega'-\omega|\le \Omega_d}} d\omega' \sum_{\substack{\mathbf{x}_{r'} \in A \\ |\mathbf{x}_r - \mathbf{x}_{r'}| \le X_d(\overline{\omega})}} \widehat{f}_B(\omega-1)\overline{\widehat{f}_B(\omega'-1)} \times \tag{6.1}$$

$$\int_{\mathcal{D}} d\vec{\mathbf{y}} \int_{\mathcal{D}} d\vec{\mathbf{y}}' \rho(\vec{\mathbf{y}})\rho(\vec{\mathbf{y}}') \left\langle G(\vec{\mathbf{x}}_r, \vec{\mathbf{y}}, \omega)\overline{G(\vec{\mathbf{x}}_{r'}, \vec{\mathbf{y}}', \omega')} \right\rangle \overline{G_0(\vec{\mathbf{x}}_r, \vec{\mathbf{y}}^s, \omega)} G_0(\vec{\mathbf{x}}_{r'}, \vec{\mathbf{y}}^s, \omega').$$

We proceed as in Section 5.4 by changing variables as in (5.46) and (5.47) and by replacing the sums over the array with integrals over the aperture. This leads to the replacement of the discrete location $\overline{\mathbf{x}}_r$ and $\widetilde{\mathbf{x}}_r$ in (6.1) with the continuously varying $\overline{\mathbf{x}}$ and $\widetilde{\mathbf{x}}$, respectively. We also define for two arbitrary points $\vec{\mathbf{y}} = (\mathbf{y}, z)$ and $\vec{\mathbf{y}}' = (\mathbf{y}', z')$ in $\mathcal{D}$, new variables

$$\overline{\mathbf{y}} = \frac{\mathbf{y}+\mathbf{y}'}{2}, \quad \overline{z} = \frac{z+z'}{2}, \tag{6.2}$$

$$\widetilde{\mathbf{y}} = \frac{\mathbf{y}'-\mathbf{y}}{\theta}, \quad \widetilde{z} = \frac{z'-z}{\theta}. \tag{6.3}$$

Then, moment formula

$$\begin{aligned} \left\langle \widehat{G}(\vec{\mathbf{x}}, \vec{\mathbf{y}}, \omega)\overline{\widehat{G}(\vec{\mathbf{x}}', \vec{\mathbf{y}}', \omega')} \right\rangle \; &\approx \widehat{G}_0(\vec{\mathbf{x}}, \vec{\mathbf{y}}, \omega)\overline{\widehat{G}_0(\vec{\mathbf{x}}', \vec{\mathbf{y}}', \omega')} \; \exp\{-\tfrac{\overline{k}^2 D_f |z'-z|}{2\theta^2}\} \times \\ &\exp\left\{-\tfrac{\widetilde{k}^2 D_f z\wedge z'}{2} - \tfrac{\overline{k}^2 D_p z\wedge z'}{6}\left(|\widetilde{\mathbf{x}}|^2 + \widetilde{\mathbf{x}}\cdot\widetilde{\mathbf{y}} + |\widetilde{\mathbf{y}}|^2\right)\right\}, \end{aligned} \tag{6.4}$$

derived in Appendix B, and the approximation (5.69) give

$$\begin{aligned} \mathcal{I}^{\text{CINT}}(\vec{\mathbf{y}}^s) \sim \int_{\overline{\mathbf{x}}\in A} d\overline{\mathbf{x}} \int_{|\overline{\omega}-1|\le B} d\overline{\omega} \int_{\theta|\widetilde{\mathbf{x}}|\le X_d(\overline{\omega})} |\widehat{f}_B(\overline{\omega}-1)|^2 d\widetilde{\mathbf{x}} \int_{\theta|\widetilde{\omega}|\le \Omega_d} d\widetilde{\omega} \int_{\mathcal{D}} d\overline{z}\, d\overline{\mathbf{y}} \int d\widetilde{z}\, d\widetilde{\mathbf{y}} \times \\ \rho\left(\overline{\mathbf{y}} - \tfrac{\theta\widetilde{\mathbf{y}}}{2}, \overline{z} - \tfrac{\theta\widetilde{z}}{2}\right) \rho\left(\overline{\mathbf{y}} + \tfrac{\theta\widetilde{\mathbf{y}}}{2}, \overline{z} + \tfrac{\theta\widetilde{z}}{2}\right) G_0\left((\overline{\mathbf{x}} - \tfrac{\theta\widetilde{\mathbf{x}}}{2}, 0), (\overline{\mathbf{y}} - \tfrac{\theta\widetilde{\mathbf{y}}}{2}, \overline{z} - \tfrac{\theta\widetilde{z}}{2}), \overline{\omega} - \tfrac{\theta\widetilde{\omega}}{2}\right) \times \\ \overline{G_0\left((\overline{\mathbf{x}} + \tfrac{\theta\widetilde{\mathbf{x}}}{2}, 0), (\overline{\mathbf{y}} + \tfrac{\theta\widetilde{\mathbf{y}}}{2}, \overline{z} + \tfrac{\theta\widetilde{z}}{2}), \overline{\omega} + \tfrac{\theta\widetilde{\omega}}{2}\right)} \, \overline{G_0\left((\overline{\mathbf{x}} - \tfrac{\theta\widetilde{\mathbf{x}}}{2}, 0), \vec{\mathbf{y}}^s, \overline{\omega} - \tfrac{\theta\widetilde{\omega}}{2}\right)} \times \\ G_0\left((\overline{\mathbf{x}} + \tfrac{\theta\widetilde{\mathbf{x}}}{2}, 0), \vec{\mathbf{y}}^s, \overline{\omega} + \tfrac{\theta\widetilde{\omega}}{2}\right) e^{-\frac{\overline{k}^2 D_f |\widetilde{z}|}{2\theta} - \frac{\widetilde{k}^2 D_f z\wedge z'}{2} - \frac{\overline{k}^2 D_p z\wedge z'}{6}\left(|\widetilde{\mathbf{x}}|^2 + \widetilde{\mathbf{x}}\cdot\widetilde{\mathbf{y}} + |\widetilde{\mathbf{y}}|^2\right)}, \end{aligned} \tag{6.5}$$

where

$$z \wedge z' = \min\{z, z'\}. \tag{6.6}$$

Further, we recall (5.60) and write

$$G_0\left((\overline{\mathbf{x}}-\tfrac{\theta\widetilde{\mathbf{x}}}{2},0),(\overline{\mathbf{y}}-\tfrac{\theta\widetilde{\mathbf{y}}}{2},\overline{z}+\tfrac{\theta\widetilde{z}}{2}),\overline{\omega}-\tfrac{\theta\widetilde{\omega}}{2}\right)\overline{G_0\left((\overline{\mathbf{x}}+\tfrac{\theta\widetilde{\mathbf{x}}}{2},0),(\overline{\mathbf{y}}+\tfrac{\theta\widetilde{\mathbf{y}}}{2},\overline{z}+\tfrac{\theta\widetilde{z}}{2}),\overline{\omega}+\tfrac{\theta\widetilde{\omega}}{2}\right)}\sim$$

$$\tfrac{1}{(\overline{z}-\frac{\theta\widetilde{z}}{2})(\overline{z}+\frac{\theta\widetilde{z}}{2})}\exp\left\{-ik_0L_z\overline{k}\widetilde{z}/\theta-i\theta k_0L_z\widetilde{k}\overline{z}+i(\overline{k}-\tfrac{\theta\widetilde{k}}{2})\tfrac{|\overline{\mathbf{x}}-\overline{\mathbf{y}}-\frac{\theta(\widetilde{\mathbf{x}}-\widetilde{\mathbf{y}})}{2}|^2}{2\theta(\overline{z}-\frac{\theta\widetilde{z}}{2})}-\right.$$

$$\left.i(\overline{k}+\tfrac{\theta\widetilde{k}}{2})\tfrac{|\overline{\mathbf{x}}-\overline{\mathbf{y}}+\frac{\theta(\widetilde{\mathbf{x}}-\widetilde{\mathbf{y}})}{2}|^2}{2\theta(\overline{z}+\frac{\theta\widetilde{z}}{2})}\right\}$$

and

$$\overline{G_0\left((\overline{\mathbf{x}}-\tfrac{\theta\widetilde{\mathbf{x}}}{2},0),\vec{\mathbf{y}}^s,\overline{\omega}-\tfrac{\theta\widetilde{\omega}}{2}\right)}\,G_0\left((\overline{\mathbf{x}}+\tfrac{\theta\widetilde{\mathbf{x}}}{2},0),\vec{\mathbf{y}}^s,\overline{\omega}+\tfrac{\theta\widetilde{\omega}}{2}\right)\sim\tfrac{1}{z_s^2}\times$$

$$\exp\left\{i\theta k_0L_z\widetilde{k}z_s-i(\overline{k}-\tfrac{\theta\widetilde{k}}{2})\tfrac{|\overline{\mathbf{x}}-\mathbf{y}_s-\frac{\theta\widetilde{\mathbf{x}}}{2}|^2}{2\theta z_s}+i(\overline{k}+\tfrac{\theta\widetilde{k}}{2})\tfrac{|\overline{\mathbf{x}}-\mathbf{y}_s+\frac{\theta\widetilde{\mathbf{x}}}{2}|^2}{2\theta z_s}\right\}. \tag{6.7}$$

The first exponential in (6.5) indicates a rapid loss of coherence for $\widetilde{z}>O(\theta)\ll 1$ and, because of our assumptions on ρ, we can set $\widetilde{z}=0$ in all the factors of the integrand in (6.5) except the exponential

$$e^{-\frac{\overline{k}^2D_f|\widetilde{z}|}{2\theta}-ik_0L_z\overline{k}\widetilde{z}/\theta},$$

whose integral over $\widetilde{z}$ is

$$\int d\widetilde{z}e^{-\frac{\overline{k}^2D_f|\widetilde{z}|}{2\theta}-ik_0L_z\overline{k}\widetilde{z}/\theta}\approx\theta\int_{-\infty}^{\infty}ds\,e^{-\frac{\overline{k}^2D_f|s|}{2}-ik_0L_z\overline{k}s}=\frac{4\theta D_f}{\overline{k}^2D_f^2+4k_0^2L_z^2}=C(\overline{\omega}). \tag{6.8}$$

Next, we note that moment formula (6.4) restricts the magnitude of $\theta\widetilde{\mathbf{y}}$ to the decoherence length $X_d(\omega)$, that coincides with the time reversal spot size. Since $X_d(\omega)=O(\theta)$ in our scaling, the assumptions on ρ allow us to write $\rho\left(\overline{\mathbf{y}}\pm\frac{\theta\widetilde{\mathbf{y}}}{2},\overline{z}\right)\approx\rho\left(\overline{\mathbf{y}},\overline{z}\right)$ and obtain

$$\begin{aligned}\mathcal{I}^{\rm CINT}(\vec{\mathbf{y}}^s)\;\sim&\int_{\overline{\mathbf{x}}\in A}d\overline{\mathbf{x}}\int_{|\overline{\omega}-1|\le B}d\overline{\omega}\,C(\overline{\omega})|\widehat{f}_B(\overline{\omega}-1)|^2\int_{\mathcal{D}}d\overline{\mathbf{y}}d\overline{z}\,\frac{\rho^2(\overline{\mathbf{y}},\overline{z})}{\overline{z}^2z_s^2}\int_{\theta|\widetilde{\mathbf{x}}|\le X_d(\overline{\omega})}d\widetilde{\mathbf{x}}\int_{\theta|\widetilde{\mathbf{y}}|\le X_d(\overline{\omega})}d\widetilde{\mathbf{y}}\\&\int_{\theta|\widetilde{\omega}|\le\Omega_d}d\widetilde{\omega}\,\exp\left\{ik_0\theta L_z\widetilde{k}(z_s-\overline{z})-\frac{\widetilde{k}^2D_f\overline{z}}{2}-\frac{\overline{k}^2D_p\overline{z}}{6}\left(|\widetilde{\mathbf{x}}|^2+\widetilde{\mathbf{x}}\cdot\widetilde{\mathbf{y}}+|\widetilde{\mathbf{y}}|^2\right)\right\}\times\\&\exp\left\{i(\overline{k}-\tfrac{\theta\widetilde{k}}{2})\tfrac{|\overline{\mathbf{x}}-\overline{\mathbf{y}}-\frac{\theta(\widetilde{\mathbf{x}}-\widetilde{\mathbf{y}})}{2}|^2}{2\theta\overline{z}}-i(\overline{k}+\tfrac{\theta\widetilde{k}}{2})\tfrac{|\overline{\mathbf{x}}-\overline{\mathbf{y}}+\frac{\theta(\widetilde{\mathbf{x}}-\widetilde{\mathbf{y}})}{2}|^2}{2\theta\overline{z}}\right\}\times\\&\exp\left\{i(\overline{k}-\tfrac{\theta\widetilde{k}}{2})\tfrac{|\overline{\mathbf{x}}-\mathbf{y}_s-\frac{\theta\widetilde{\mathbf{x}}}{2}|^2}{2\theta z_s}+i(\overline{k}+\tfrac{\theta\widetilde{k}}{2})\tfrac{|\overline{\mathbf{x}}-\mathbf{y}_s+\frac{\theta\widetilde{\mathbf{x}}}{2}|^2}{2\theta z_s}\right\}.\end{aligned} \tag{6.9}$$

Now, in the scaling (5.38), we have

$$\begin{aligned}
-\theta k_0 L_z \widetilde{k}\overline{z} \ &+(\overline{k}-\tfrac{\widetilde{\theta k}}{2})\tfrac{|\overline{\mathbf{x}}-\overline{\mathbf{y}}-\frac{\theta(\widetilde{\mathbf{x}}-\widetilde{\mathbf{y}})}{2}|^2}{2\theta\overline{z}} - (\overline{k}+\tfrac{\widetilde{\theta k}}{2})\tfrac{|\overline{\mathbf{x}}-\overline{\mathbf{y}}+\frac{\theta(\widetilde{\mathbf{x}}-\widetilde{\mathbf{y}})}{2}|^2}{2\theta\overline{z}} \approx \\
&-\overline{k}(\widetilde{\mathbf{x}}-\widetilde{\mathbf{y}})\cdot\nabla_{\overline{\mathbf{x}}}\tfrac{|\overline{\mathbf{x}}-\overline{\mathbf{y}}|^2}{2\overline{z}} - \widetilde{k}\tfrac{|\overline{\mathbf{x}}-\overline{\mathbf{y}}|^2}{2\overline{z}} - \theta k_0 L_z\widetilde{k}\overline{z} \approx \\
&-\left(\tfrac{L_z}{L_{\mathbf{x}}}\right)^2\left[\overline{k}(\widetilde{\mathbf{x}}-\widetilde{\mathbf{y}})\cdot\nabla_{\mathbf{x}}|(\overline{\mathbf{x}},0)-(\overline{\mathbf{y}},\overline{z})| - \widetilde{k}|(\overline{\mathbf{x}},0)-(\overline{\mathbf{y}},\overline{z})|\right]
\end{aligned} \tag{6.10}$$

and, similarly,

$$\begin{aligned}
\theta k_0 L_z\widetilde{k}z_s \ &-(\overline{k}-\tfrac{\widetilde{\theta k}}{2})\tfrac{|\overline{\mathbf{x}}-\mathbf{y}_s-\frac{\theta\widetilde{\mathbf{x}}}{2}|^2}{2\theta z_s} + (\overline{k}+\tfrac{\widetilde{\theta k}}{2})\tfrac{|\overline{\mathbf{x}}-\mathbf{y}_s+\frac{\theta\widetilde{\mathbf{x}}}{2}|^2}{2\theta z_s} \approx \\
&\overline{k}\widetilde{\mathbf{x}}\cdot\nabla_{\mathbf{x}}\tfrac{|\overline{\mathbf{x}}-\mathbf{y}_s|^2}{2z_s} + \widetilde{k}\tfrac{|\overline{\mathbf{x}}-\mathbf{y}_s|^2}{2z_s} + \theta k_0 L_z\widetilde{k}z_s \approx \\
&\left(\tfrac{L_z}{L_{\mathbf{x}}}\right)^2\left[\overline{k}\,\widetilde{\mathbf{x}}\cdot\nabla_{\mathbf{x}}|(\overline{\mathbf{x}},0)-\vec{\mathbf{y}}^s| + \widetilde{k}|(\overline{\mathbf{x}},0)-\vec{\mathbf{y}}^s|\right].
\end{aligned} \tag{6.11}$$

Using these expressions, equation (6.9) becomes

$$\begin{aligned}
\mathcal{I}^{\mathrm{CINT}}(\vec{\mathbf{y}}^s) \sim \int_{\overline{\mathbf{x}}\in A} d\overline{\mathbf{x}} \int_{|\overline{\omega}-1|\le B} d\overline{\omega}\, C(\overline{\omega})|\widehat{f}_B(\overline{\omega}-1)|^2 \int_{\mathcal{D}} d\overline{\mathbf{y}}\,\frac{\rho^2(\overline{\mathbf{y}})}{\overline{z}^2 z_s^2} \\
\int_{\theta|\widetilde{\omega}|\le\Omega_d} d\widetilde{\omega}\exp\left\{i\widetilde{k}\left(\frac{L_z}{L}\right)^2\left(|(\overline{\mathbf{x}},0)-\vec{\mathbf{y}}^s| - |(\overline{\mathbf{x}},0)-(\overline{\mathbf{y}},\overline{z})|\right) - \frac{\widetilde{k}^2 D_f\overline{z}}{2}\right\} \\
\int_{\theta|\widetilde{\mathbf{x}}|\le X_d(\overline{\omega})} d\widetilde{\mathbf{x}}\exp\left\{i\overline{k}\left(\frac{L_z}{L}\right)^2\widetilde{\mathbf{x}}\cdot\left(\nabla_{\overline{\mathbf{x}}}|(\overline{\mathbf{x}},0)-\vec{\mathbf{y}}^s| - \nabla_{\overline{\mathbf{x}}}|(\overline{\mathbf{x}},0)-(\overline{\mathbf{y}},\overline{z})|\right) - \frac{\overline{k}^2 D_p\overline{z}|\widetilde{\mathbf{x}}|^2}{6}\right\} \\
\int_{\theta|\widetilde{\mathbf{y}}|\le X_d(\overline{\omega})} d\widetilde{\mathbf{y}}\exp\left\{i\overline{k}\left(\frac{L_z}{L}\right)^2\widetilde{\mathbf{y}}\cdot\nabla_{\overline{\mathbf{x}}}|(\overline{\mathbf{x}},0)-(\overline{\mathbf{y}},\overline{z})| - \frac{\overline{k}^2 D_p\overline{z}}{6}\left(|\widetilde{\mathbf{y}}|^2+\widetilde{\mathbf{y}}\cdot\widetilde{\mathbf{x}}\right)\right\}.
\end{aligned} \tag{6.12}$$

Because the domain of integration in $\widetilde{\mathbf{y}}$ is chosen as the essential support of the Gaussian in (6.12) we can extend the integral over the whole $\mathbb{R}^2$ and obtain

$$\begin{aligned}
&\int_{\theta|\widetilde{\mathbf{y}}|\le X_d(\overline{\omega})} d\widetilde{\mathbf{y}}\exp\left\{i\overline{k}\left(\frac{L_z}{L}\right)^2\widetilde{\mathbf{y}}\cdot\nabla_{\overline{\mathbf{x}}}|(\overline{\mathbf{x}},0)-(\overline{\mathbf{y}},\overline{z})| - \frac{\overline{k}^2 D_p\overline{z}}{6}\left(|\widetilde{\mathbf{y}}|^2+\widetilde{\mathbf{y}}\cdot\widetilde{\mathbf{x}}\right)\right\} \sim \\
&\frac{1}{\overline{k}\overline{z}}\exp\left\{\frac{\overline{k}^2 D_p\overline{z}|\widetilde{\mathbf{x}}|^2}{24} - \frac{i\overline{k}}{2}\left(\frac{L_z}{L}\right)^2\widetilde{\mathbf{x}}\cdot\nabla_{\overline{\mathbf{x}}}|(\overline{\mathbf{x}},0)-(\overline{\mathbf{y}},\overline{z})| - \frac{3}{2}\left(\frac{L_z}{L_{\mathbf{x}}}\right)^4\frac{|\nabla_{\overline{\mathbf{x}}}|(\overline{\mathbf{x}},0)-(\overline{\mathbf{y}},\overline{z})||^2}{D_p\overline{z}}\right\}.
\end{aligned}$$

Similarly, the integral over $\widetilde{\omega}$ is evaluated by extending it to the entire real line and the result is

$$\begin{aligned}
&\int_{\theta|\widetilde{\omega}|\le\Omega_d} d\widetilde{\omega}\ \ \exp\left\{i\widetilde{k}\left(\tfrac{L_z}{L}\right)^2\left(|(\overline{\mathbf{x}},0)-\vec{\mathbf{y}}^s| - |(\overline{\mathbf{x}},0)-(\overline{\mathbf{y}},\overline{z})|\right) - \tfrac{\widetilde{k}^2 D_f\overline{z}}{2}\right\} \sim \\
&\tfrac{1}{\sqrt{\overline{z}}}\exp\left\{-\left(\tfrac{L_z}{L_{\mathbf{x}}}\right)^4\tfrac{||(\overline{\mathbf{x}},0)-\vec{\mathbf{y}}^s|-|(\overline{\mathbf{x}},0)-(\overline{\mathbf{y}},\overline{z})||^2}{2D_f\overline{z}}\right\}.
\end{aligned}$$

Finally, we calculate the integral over $\widetilde{\mathbf{x}}$

$$\int_{\theta|\widetilde{\mathbf{x}}|\le X_d(\overline{\omega})} d\widetilde{\mathbf{x}} \quad \exp\left\{ i\overline{k}\left(\frac{L_z}{L_{\mathbf{x}}}\right)^2 \widetilde{\mathbf{x}}\cdot\left(\nabla_{\overline{\mathbf{x}}}|(\overline{\mathbf{x}},0)-\vec{\mathbf{y}}^s| - \tfrac{3}{2}\nabla_{\overline{\mathbf{x}}}|(\overline{\mathbf{x}},0)-(\overline{\mathbf{y}},\overline{z})|\right) - \frac{\overline{k}^2 D_p \overline{z}|\widetilde{\mathbf{x}}|^2}{8}\right\} \sim$$

$$\tfrac{1}{\overline{z}} \exp\left\{ -2\left(\frac{L_z}{L_{\mathbf{x}}}\right)^4 \frac{\left|\nabla_{\overline{\mathbf{x}}}|(\overline{\mathbf{x}},0)-\vec{\mathbf{y}}^s| - \frac{3}{2}\nabla_{\overline{\mathbf{x}}}|(\overline{\mathbf{x}},0)-(\overline{\mathbf{y}},\overline{z})|\right|^2}{D_p\overline{z}}\right\}.$$

Gathering all the results, we have

$$\mathcal{I}^{\rm CINT}(\vec{\mathbf{y}}^s) \sim \int_{\overline{\mathbf{x}}\in A} d\overline{\mathbf{x}} \int_{|\overline{\omega}-1|\le B} d\overline{\omega}\, \frac{C(\overline{\omega})}{\overline{\omega}}\, |\widehat{f}_B(\overline{\omega}-1)|^2 \int_{\mathcal{D}} d\overline{\mathbf{y}}\, d\overline{z} \rho^2(\overline{\mathbf{y}},\overline{z})\, \frac{1}{\overline{z}^{4+1/2} z_s^2} \times$$

$$\exp\left\{ -\tfrac{3}{2}\left(\frac{L_z}{L_{\mathbf{x}}}\right)^4 \frac{|\nabla_{\overline{\mathbf{x}}}|(\overline{\mathbf{x}},0)-(\overline{\mathbf{y}},\overline{z})||^2}{D_p\overline{z}} - \left(\frac{L_z}{L_{\mathbf{x}}}\right)^4 \frac{||(\overline{\mathbf{x}},0)-\vec{\mathbf{y}}^s|-|(\overline{\mathbf{x}},0)-(\overline{\mathbf{y}},\overline{z})||^2}{2D_f\overline{z}} - \right. \tag{6.13}$$

$$\left. 2\left(\frac{L_z}{L_{\mathbf{x}}}\right)^4 \frac{\left|\nabla_{\overline{\mathbf{x}}}|(\overline{\mathbf{x}},0)-\vec{\mathbf{y}}^s| - \frac{3}{2}\nabla_{\overline{\mathbf{x}}}|(\overline{\mathbf{x}},0)-(\overline{\mathbf{y}},\overline{z})|\right|^2}{D_p\overline{z}}\right\}.$$

Let us rewrite (6.13) in a simpler form that shows explicitly the resolution of the imaging functional. The parabolic approximation (5.40) gives

$$|(\overline{\mathbf{x}},0)-\vec{\mathbf{y}}^s| - |(\overline{\mathbf{x}},0)-(\overline{\mathbf{y}},\overline{z})| \approx z_s - \overline{z} \tag{6.14}$$

and

$$\left(\frac{L_z}{L_{\mathbf{x}}}\right)^2 \nabla_{\overline{\mathbf{x}}}|(\overline{\mathbf{x}},0)-(\overline{\mathbf{y}},\overline{z})| \approx \frac{\overline{\mathbf{x}}-\overline{\mathbf{y}}}{\overline{z}}; \qquad \left(\frac{L_z}{L_{\mathbf{x}}}\right)^2 \nabla_{\overline{\mathbf{x}}}|(\overline{\mathbf{x}},0)-\vec{\mathbf{y}}^s| \approx \frac{\overline{\mathbf{x}}-\overline{\mathbf{y}}_s}{\overline{z}_s}, \tag{6.15}$$

so (6.13) becomes

$$\mathcal{I}^{\rm CINT}(\vec{\mathbf{y}}^s) \sim \int_{\overline{\mathbf{x}}\in A} d\overline{\mathbf{x}} \int_{|\overline{\omega}-1|\le B} d\overline{\omega}\, \frac{C(\overline{\omega})}{\overline{\omega}}\, |\widehat{f}_B(\overline{\omega}-1)|^2 \int_{\mathcal{D}} d\overline{\mathbf{y}}\, d\overline{z} \rho^2(\overline{\mathbf{y}},\overline{z})\, \frac{1}{\overline{z}^{4+1/2} z_s^2} \times$$

$$\exp\left\{ -\frac{3|\overline{\mathbf{x}}-\overline{\mathbf{y}}|^2}{2\overline{a_e}^2} - \frac{(z_s-\overline{z})^2}{2r_e^2} - \frac{2\left|\frac{\overline{z}}{z_s}(\overline{\mathbf{x}}-\mathbf{y}_s) - \frac{3}{2}(\overline{\mathbf{x}}-\overline{\mathbf{y}})\right|^2}{3\overline{a_e}^2}\right\}. \tag{6.16}$$

Here r_e is given by (5.73) and

$$\overline{a_e} = \sqrt{\frac{D_p\overline{z}^3}{3}} \tag{6.17}$$

is the effective aperture in the random medium for scaled distance $\overline{z}$.

6.1. Summary of the resolution analysis

As we have seen in Section 5, the range resolution is determined by r_e, the distance traveled at speed c_0 over the delay spread. Assuming that $r_e \ll 1$, we can simplify (6.16) further and obtain

$$\mathcal{I}^{\rm CINT}(\vec{\mathbf{y}}^s) \sim \tfrac{1}{z_s^{6+1/2}} \int_{\overline{\mathbf{x}}\in A} d\overline{\mathbf{x}} \int_{|\overline{\omega}-1|\le B} d\overline{\omega}\, \frac{C(\overline{\omega})}{\overline{\omega}}\, |\widehat{f}_B(\overline{\omega}-1)|^2 \int_{\mathcal{D}} d\overline{\mathbf{y}}\, d\overline{z} \rho^2(\overline{\mathbf{y}},\overline{z}) \times$$

$$\exp\left\{ -\frac{2|\overline{\mathbf{y}}_s-\overline{\mathbf{y}}|^2}{3\overline{a_e}^2} - \frac{(z_s-\overline{z})^2}{2r_e^2} - \frac{5|\overline{\mathbf{x}}-\overline{\mathbf{y}}|^2}{3\overline{a_e}^2} - \frac{2(\overline{\mathbf{y}}-\overline{\mathbf{x}})\cdot(\overline{\mathbf{y}}-\mathbf{y}_s)}{3\overline{a_e}^2}\right\}. \tag{6.18}$$

This result is similar to the point spread function derived in Section 5, in the sense that the cross-range resolution is given by the effective aperture (6.17). Instead of recovering the point value of ρ at $\vec{\mathbf{y}}^s$ we get an averaged ρ over a vicinity of the search point, of size r_e in the range and $\overline{a_e}$ in the cross-range.

The biggest influence on the imaging functional comes from the array locations $\overline{\mathbf{x}}$ in an $O(\overline{a_e})$ vicinity of $\mathbf{y}$ and therefore of $\mathbf{y}_s$. The integral over the array takes a simple form when $\mathbf{y}_s \in A$ and the aperture A is larger than $\overline{a_e}$. In this case the imaging functional simplifies further

$$\mathcal{I}^{\text{CINT}}(\vec{\mathbf{y}}^s) \;\sim \frac{1}{z_s^{6+1/2}} \int_{|\overline{\omega}-1|\le B} d\overline{\omega}\; \frac{C(\overline{\omega})}{\overline{\omega}}\, |\widehat{f}_B(\overline{\omega}-1)|^2 \int_{\mathcal{D}} d\overline{\mathbf{y}}\, d\overline{z} \rho^2(\overline{\mathbf{y}},\overline{z}) e^{-\frac{3|\overline{\mathbf{y}}_s-\overline{\mathbf{y}}|^2}{5\overline{a_e}^2} - \frac{(z_s-\overline{z})^2}{2r_e^2}}.$$

We end with the final note that the blurring kernel in (6.18) is not the same as that in (5.74). This comes from the forward model (2.10) and the moment formula that depends on the scaled difference $\widetilde{\mathbf{y}}$ of two points in $\mathcal{D}$. More precisely, the difference in the kernel originates from the $\widetilde{\mathbf{y}}$ integral in (6.12), which assumes that the size of $\mathcal{D}$ is larger than the time reversal spot size $X_d(\overline{\omega})$, for all frequencies $\overline{\omega}$ in the bandwidth of the pulse. In the case of small, point-like sources considered in Section 5, the domain of the $\widetilde{\mathbf{y}}$ integral collapses to $\widetilde{\mathbf{y}} = 0$, the moment formula (6.4) reduces to (5.53) and the point spread function is given by (5.74).

7. Summary and conclusions

We have introduced the coherent interferometric functional (3.21) as an effective way to image in clutter with array data, and we have compared it to Kirchhoff migration and to matched field imaging. This functional depends on two parameters, the decoherence length X_d and the decoherence frequency Ω_d, that are not known and must be estimated from the array data by the imaging process itself.

We have given three different and interrelated interpretations of these parameters. First, they are smoothing or regularization parameters for the Kirchhoff migration functional that produces unstable images in clutter. Second, they are decoherence or decorrelation scales associated with the array data, although they cannot be readily estimated directly from the data without the imaging process. Third, they characterize the range and cross range resolution limits of the coherent interferometric imaging functional. The resolution theory is obtained first in a phenomenological, model independent, way in Section 3.4 and then, from first principles, in a particular asymptotic regime, in Section 5.5.

We find that the range resolution is proportional to c_0/Ω_d, where c_0 is the background propagation speed, and it is worse than the corresponding one in a homogeneous medium, c_0/B, because Ω_d is typically much smaller than B. The cross-range resolution is proportional to L/X_d and is typically worse than $c_0 L/(Ba)$, the

cross-range resolution in a homogeneous medium, since $X_d < a$. The decoherence length can also be identified with the focal spot size in time reversal, $X_d = \lambda_0 L/a_e$, where a_e is the effective apperture in the clutter. This makes the cross-range resolution of (3.21) proportional to a_e, as obtained in [11] for matched field functionals.

We have shown with numerical simulations, in Section 4, that the coherent interferometric functional (3.21) does produce statistically stable but blurred images, provided that the parameters X_d and Ω_d are chosen adaptively in an optimal way. The adaptive estimation of these parameters and the deblurring of the images is presented in a companion paper [12].

Appendix

Appendix A. Kirchhoff migration

We review briefly the analysis of the Kirchhoff migration functional (1.1), [21, 41, 9, 7, 49]. It is very successful in imaging the support of sources or scatterers in *smooth* and *known* backgrounds. For brevity, we focus attention on the inverse source problem where we wish to determine the support $\mathcal{D}$ of an extended source, given the recorded array data.

The Kirchhoff imaging functional for variable backgrounds is

$$\mathcal{I}^{\mathrm{KM}}(\vec{\mathbf{y}}^s) = \sum_{\vec{\mathbf{x}}_r \in A} P\left(\vec{\mathbf{x}}_r, \tau(\vec{\mathbf{x}}_r, \vec{\mathbf{y}}^s)\right), \tag{A.1}$$

where A denotes the array and $\vec{\mathbf{y}}^s$ is a search point to which we back propagate (migrate) $P(\vec{\mathbf{x}}_r, t)$ by evaluating it at the travel time

$$\tau(\vec{\mathbf{x}}_r, \vec{\mathbf{y}}^s) = \int_{\Gamma(\vec{\mathbf{x}}_r, \vec{\mathbf{y}}^s)} \frac{ds}{c(\vec{\mathbf{x}}(s))}. \tag{A.2}$$

This is the integral of the slowness $c^{-1}(\vec{\mathbf{x}})$ along the characteristic curve $\Gamma(\vec{\mathbf{x}}_r, \vec{\mathbf{y}}^s)$, connecting $\vec{\mathbf{x}}_r$ to $\vec{\mathbf{y}}^s$. The underlying assumption in (A.1) is that the background medium is smooth and known, so geometrical optics applies and travel times (A.2) can be calculated. In our setup the background velocity c_0 is a constant, and (A.2) simplifies to

$$\tau(\vec{\mathbf{x}}_r, \vec{\mathbf{y}}^s) = c_0^{-1} |\vec{\mathbf{x}}_r - \vec{\mathbf{y}}^s|. \tag{A.3}$$

In this case, we can redefine the migration function as

$$\begin{aligned} \mathcal{I}^{\mathrm{KM}}(\vec{\mathbf{y}}^s) &= \sum_{\vec{\mathbf{x}}_r \in A} \frac{1}{2\pi} \int_{|\omega - \omega_0| \le B} d\omega\, \widehat{P}(\vec{\mathbf{x}}_r, \omega) e^{-i\omega\tau(\vec{\mathbf{x}}_r, \vec{\mathbf{y}}^s)} \\ &\sim \sum_{\vec{\mathbf{x}}_r \in A} \int_{|\omega - \omega_0| \le B} d\omega\, \widehat{P}(\vec{\mathbf{x}}_r, \omega) \overline{\widehat{G}_0(\vec{\mathbf{x}}_r, \vec{\mathbf{y}}^s, \omega)}, \end{aligned} \tag{A.4}$$

where $\sim$ stands for approximate equality up to an amplitude factor in the integrand that plays essentially no role in imaging, and $\widehat{G}_0$ is the Green's function in the homogeneous medium, at frequency ω,

$$G_0(\vec{\mathbf{x}}_r, \vec{\mathbf{y}}^s) = \frac{1}{4\pi|\vec{\mathbf{x}}_r - \vec{\mathbf{y}}^s|} e^{ik|\vec{\mathbf{x}}_r - \vec{\mathbf{y}}^s|} \quad , \; k = \frac{\omega}{c_0}. \tag{A.5}$$

Let us suppose for now that there are no fluctuations in the medium so that the forward model (2.10) is

$$P(\vec{\mathbf{x}}_r, t) = \int_{\mathcal{D}} \rho(\vec{\mathbf{y}}) e^{-i\omega_0 t} f_B(t) \star G_0(\vec{\mathbf{x}}_r, \vec{\mathbf{y}}, t) d\vec{\mathbf{y}}. \tag{A.6}$$

Assume further that the receivers are closely spaced on the array, which lies on a surface $\mathcal{S}_A$ parameterized by $\mathbf{u} \in \mathbb{R}^2$. Using (A.6) in (A.4) we obtain the following theoretical form of the Kirchhoff imaging functional

$$\begin{aligned} \mathcal{I}^{\rm KM}(\vec{\mathbf{y}}^s) \; &\sim \int_{\mathcal{D}} \rho(\vec{\mathbf{y}}) \int_{\mathcal{S}_A} d\mathbf{u} \int_{|\omega-\omega_0|\le B} d\omega \, \widehat{f}_B(\omega-\omega_0) \widehat{G}_0(\vec{\mathbf{x}}(\mathbf{u}), \vec{\mathbf{y}}, \omega) \overline{\widehat{G}_0(\vec{\mathbf{x}}(\mathbf{u}), \vec{\mathbf{y}}^s, \omega)}, \\ &\sim \int_{\mathcal{D}} \rho(\vec{\mathbf{y}}) \int_{\mathcal{S}_A} \frac{d\mathbf{u}}{|\vec{\mathbf{x}}(\mathbf{u}) - \vec{\mathbf{y}}||\vec{\mathbf{x}}(\mathbf{u}) - \vec{\mathbf{y}}^s|} \int_{|\omega-\omega_0|\le B} d\omega \, \widehat{f}_B(\omega-\omega_0) e^{ik(|\vec{\mathbf{x}}(\mathbf{u})-\vec{\mathbf{y}}| - |\vec{\mathbf{x}}(\mathbf{u})-\vec{\mathbf{y}}^s|)}. \end{aligned} \tag{A.7}$$

We will analyze this functional using the method of stationary phase [6]. It is a high frequency asymptotic analysis that is justified physically by a scale separation assumption [9, 49]. This means that the background medium is slowly varying (it is constant in our case) relative to a typical wavelength, whereas $\rho(\vec{\mathbf{y}})$ is "rough", due to its discontinuity at $\partial\mathcal{D}$. The reference wavelength is $\lambda_0 = 2\pi c_0/\omega_0$.

¿From the method of stationary phase, the leading order term of the ω and $\mathbf{u}$ integrals in $\mathcal{I}^{\rm KM}(\vec{\mathbf{y}}^s)$ comes from the vicinity of the stationary points satisfying

$$\begin{aligned} |\vec{\mathbf{x}}(\mathbf{u}) - \vec{\mathbf{y}}| - |\vec{\mathbf{x}}(\mathbf{u}) - \vec{\mathbf{y}}^s| \quad &= 0, \\ \nabla_{\mathbf{u}}(|\vec{\mathbf{x}}(\mathbf{u}) - \vec{\mathbf{y}}| - |\vec{\mathbf{x}}(\mathbf{u}) - \vec{\mathbf{y}}^s|) \; &= \mathbf{0}. \end{aligned}$$

These equations hold, without any restriction on $\mathbf{u}$, if $\vec{\mathbf{y}} = \vec{\mathbf{y}}^s$, so only the vicinity of the search point $\vec{\mathbf{y}}^s$ counts. The amplitudes in $\mathcal{I}^{\rm KM}(\vec{\mathbf{y}}^s)$ play a negligible role in this argument, so we can modify $\mathcal{I}^{\rm KM}(\vec{\mathbf{y}}^s)$ with amplitude weight factors

$$\begin{aligned} \widetilde{\mathcal{I}^{\rm KM}}(\vec{\mathbf{y}}^s) &= \int_{\mathcal{S}_A} d\mathbf{u} \, \mathcal{M}(\mathbf{u}, \vec{\mathbf{y}}^s) \int_{|\omega-\omega_0|\le B} \widehat{P}(\vec{\mathbf{x}}(\mathbf{u}), \omega) \overline{\widehat{G}_0(\vec{\mathbf{x}}(\mathbf{u}), \vec{\mathbf{y}}^s, \omega)} \\ &\sim \int_{\mathcal{D}} \rho(\vec{\mathbf{y}}) \int_{\mathcal{S}_A} d\mathbf{u} \frac{\mathcal{M}(\mathbf{u}, \vec{\mathbf{y}}^s)}{|\vec{\mathbf{x}}(\mathbf{u}) - \vec{\mathbf{y}}||\vec{\mathbf{x}}(\mathbf{u}) - \vec{\mathbf{y}}^s|} \int_{|\omega-\omega_0|\le B} d\omega \, \widehat{f}_B(\omega-\omega_0) e^{ik(|\vec{\mathbf{x}}(\mathbf{u})-\vec{\mathbf{y}}| - |\vec{\mathbf{x}}(\mathbf{u})-\vec{\mathbf{y}}^s|)}. \end{aligned} \tag{A.8}$$

The factor $\mathcal{M}$ will be defined later to simplify the asymptotic form of the functional.

By the stationary phase approximation the phase in (A.8) is given by

$$k\left(|\vec{\mathbf{x}}(\mathbf{u}) - \vec{\mathbf{y}}| - |\vec{\mathbf{x}}(\mathbf{u}) - \vec{\mathbf{y}}^s|\right) \approx \vec{\boldsymbol{\zeta}} \cdot (\vec{\mathbf{y}} - \vec{\mathbf{y}}^s), \quad \text{where } \vec{\boldsymbol{\zeta}} = \omega \nabla_{\vec{\mathbf{y}}} \tau(\vec{\mathbf{x}}(\mathbf{u}), \vec{\mathbf{y}}^s),$$

where τ is given by (A.3). We can also let $\vec{\mathbf{y}} \rightsquigarrow \vec{\mathbf{y}}^s$ in the amplitude of (A.8) and then change variables from $(\mathbf{u}, \omega) \rightsquigarrow \vec{\boldsymbol{\zeta}}$. The Jacobian of the transformation is $J(\mathbf{u}, \vec{\mathbf{y}}^s, \omega) = \nabla_{\mathbf{u},\omega}\vec{\boldsymbol{\zeta}}$ and

$$|\det J(\mathbf{u}, \vec{\mathbf{y}}^s, \omega)| = \omega^2 \mathcal{J}(\mathbf{u}, \vec{\mathbf{y}}^s) \neq 0, \tag{A.9}$$

which is called the Beylkin determinant [7, 9], specialized to this calculation. If we let

$$\mathcal{M}(\mathbf{u}, \vec{\mathbf{y}}^s) = |\vec{\mathbf{x}}(\mathbf{u}) - \vec{\mathbf{y}}^s|^2 \mathcal{J}(\mathbf{u}, \vec{\mathbf{y}}^s), \tag{A.10}$$

we obtain from (A.8)

$$\widetilde{\mathcal{I}^{\mathrm{KM}}}(\vec{\mathbf{y}}^s) \sim \int_{\mathcal{D}} \rho(\vec{\mathbf{y}}) \mathcal{P}^{\mathrm{KM}}(\vec{\mathbf{y}} - \vec{\mathbf{y}}^s) d\vec{\mathbf{y}}, \tag{A.11}$$

where the point spread function $\mathcal{P}^{\mathrm{KM}}$ is

$$\mathcal{P}^{\mathrm{KM}}(\vec{\mathbf{y}} - \vec{\mathbf{y}}^s) = \int \frac{\widehat{f}_B(\omega(\vec{\boldsymbol{\zeta}}) - \omega_0)}{\omega^2(\vec{\boldsymbol{\zeta}})} e^{i\vec{\boldsymbol{\zeta}}\cdot(\vec{\mathbf{y}} - \vec{\mathbf{y}}^s)} d\vec{\boldsymbol{\zeta}} \tag{A.12}$$

with

$$\omega(\vec{\boldsymbol{\zeta}}) = \frac{\vec{\boldsymbol{\zeta}} \cdot \nabla_{\vec{\mathbf{y}}} \tau(\vec{\mathbf{x}}(\mathbf{u}), \vec{\mathbf{y}}^s)}{|\nabla_{\vec{\mathbf{y}}} \tau(\vec{\mathbf{x}}(\mathbf{u}), \vec{\mathbf{y}}^s)|^2}. \tag{A.13}$$

Appendix A.1. Resolution of Kirchhoff migration images

It is clear from (A.12) that the Kirchhoff migration point spread function is determined by the domain of integration in $\vec{\boldsymbol{\zeta}}$ or, equivalently, by the bandwidth B of the pulse and the aperture of the array. In the ideal situation, the aperture and B are infinite (i.e. $\widehat{f}_B/\omega^2 = 1$ for all $\omega \in \mathbb{R}$) so $\vec{\boldsymbol{\zeta}}$ spans the whole $\mathbb{R}^3$, the point spread function is $\mathcal{P}^{\mathrm{KM}}(\vec{\mathbf{y}} - \vec{\mathbf{y}}^s) \sim \delta(\vec{\mathbf{y}} - \vec{\mathbf{y}}^s)$ and $\widetilde{\mathcal{I}^{\mathrm{KM}}}(\vec{\mathbf{y}}^s) \sim \rho(\vec{\mathbf{y}}^s)$. This is never the case in practice, however, so we do not have a precise estimate of $\rho(\vec{\mathbf{y}}^s)$ but rather a blurrier version, given by an average of ρ over a vicinity of $\vec{\mathbf{y}}^s$. The size of this vicinity depends on the aperture and the bandwidth and it is usually different in the range and cross-range directions. To see this more clearly, consider a simpler set-up in which the array aperture a is small compared to the range of the extended source, as in Figure 14, and the search point is in front of the array. Using the notation $\vec{\mathbf{y}} = (\mathbf{y}, z)$ that distinguishes between the range and cross-range coordinates z and $\mathbf{y}$, respectively, and approximating the array by a planar, square one, with $\vec{\mathbf{x}}(u) = (\mathbf{x}(u), 0)$, we have

$$\begin{aligned} \vec{\boldsymbol{\zeta}} \cdot (\vec{\mathbf{y}} - \vec{\mathbf{y}}^s) &= k \left(\tfrac{\mathbf{x}(\mathbf{u}) - \mathbf{y}^s}{|\vec{\mathbf{x}}(\mathbf{u}) - \vec{\mathbf{y}}^s|}, \tfrac{z^s}{|\vec{\mathbf{x}}(\mathbf{u}) - \vec{\mathbf{y}}^s|} \right) \cdot (\mathbf{y} - \mathbf{y}^s, z - z^s) \\ &\approx k \tfrac{(\mathbf{x}(\mathbf{u}) - \mathbf{y}^s)}{z^s} \cdot (\mathbf{y} - \mathbf{y}^s) + k(z - z^s). \end{aligned} \tag{A.14}$$

Thus, the component of $\vec{\boldsymbol{\zeta}}$ pointing in the range direction, is essentially k, and its variation is restricted to the interval $\left(k_0 - \frac{B}{c_0}, k_0 + \frac{B}{c_0}\right)$. Consequently, the range resolution of $\widetilde{\mathcal{I}^{\mathrm{KM}}}$ is proportional to $\frac{c_0}{B}$.

To estimate the cross-range resolution let us suppose that $z^s = z$, so the right hand-side in (A.14) reduces to

$$\frac{k}{z}(\mathbf{x}(\mathbf{u}) - \mathbf{y}^s)\cdot(\mathbf{y} - \mathbf{y}^s) = \frac{\omega}{c_0 z^s}(\mathbf{x}_c - \mathbf{y}^s)\cdot(\mathbf{y} - \mathbf{y}^s) + \frac{\omega}{c_0 z^s}(\mathbf{x}(\mathbf{u}) - \mathbf{x}_c)\cdot(\mathbf{y} - \mathbf{y}^s), \quad \text{(A.15)}$$

where $\omega \in (\omega_0 - B, \omega_0 + B)$, $\mathbf{x}_c$ is the center point in the array and $\mathbf{x}(\mathbf{u})$ varies over the array aperture a. Let us also integrate over the array aperture to obtain

$$\begin{aligned}\mathcal{P}^{\rm KM}(\mathbf{y} - \mathbf{y}^s, 0) \;\sim \int_{\omega_0 - B}^{\omega_0 + B} d\omega \frac{\widehat{f}(\omega)}{\omega^2} e^{i\frac{\omega}{c_0 z}(\mathbf{x}_c - \mathbf{y}^s)\cdot(\mathbf{y} - \mathbf{y}^s)} \times \\ \frac{\sin\left[\frac{\omega a}{2c_0 z}(y - y^s)_1\right]}{(y - y^s)_1} \frac{\sin\left[\frac{\omega a}{2c_0 z}(y - y^s)_2\right]}{(y - y^s)_2},\end{aligned} \quad \text{(A.16)}$$

where $(y - y^s)_i$, $i = 1, 2$ denote the components of $\mathbf{y} - \mathbf{y}^s$ (see Figure 14).

The expression (A.16) is rather complicated, but we can simplify it by taking $(y - y^s)_2 = 0$ and assuming that $|\widehat{f}(\omega)|/\omega$ is constant over the bandwidth. Equation (A.16) becomes

$$\begin{aligned}\mathcal{P}^{\rm KM}((y - y^s)_1, 0, 0) \sim \; \frac{\sin\left\{\frac{B}{c_0 z}\left[(x_c - y^s)_1 + \frac{a}{2}\right](y - y^s)_1\right\}}{\left[(x_c - y^s)_1 + \frac{a}{2}\right](y - y^s)_1^2} e^{i\frac{k_0}{z}\left[(x_c - y^s)_1 + \frac{a}{2}\right](y - y^s)_1} - \\ \frac{\sin\left\{\frac{B}{c_0 z}\left[(x_c - y^s)_1 - \frac{a}{2}\right](y - y^s)_1\right\}}{\left[(x_c - y^s)_1 - \frac{a}{2}\right](y - y^s)_1^2} e^{i\frac{k_0}{z}\left[(x_c - y^s)_1 - \frac{a}{2}\right](y - y^s)_1},\end{aligned} \quad \text{(A.17)}$$

and we observe that

$$\mathcal{P}^{\rm KM}((y - y^s)_1, 0, 0) = O\left(\frac{1}{(y - y^s)_1}\right) \to \infty, \quad \text{as } (y - y^s)_1 \to 0.$$

Moreover, the point spread function is large only in an interval of length $O\left(\frac{c_0 z}{B(2|(x_c - y^s)_1| + a)}\right)$, centered at $(y^s)_1$. Clearly, the same result applies to $\mathcal{P}^{\rm KM}(0, (y - y^s)_2, 0)$ so the cross-range resolution is $\frac{c_0 z}{B(2|\mathbf{x}_c - \mathbf{y}^s| + a)}$. In particular, if $|\mathbf{x}_c - \mathbf{y}^s| \ll a$, this becomes $\frac{c_0 z}{Ba}$.

We summarize our results with the following statement. Assuming a small array of aperture a and a target at range $z \sim L_z$, the resolution of the Kirchhoff migration image in a homogeneous medium with constant wave speed c_0 is given by c_0/B in the range direction and by $\frac{c_0 L_z}{Ba}$ in cross-range direction.

Appendix B. Derivation of the moment formula

We calculate here the expectation

$$\left\langle \widehat{G}(\vec{\mathbf{x}}_1, \vec{\mathbf{y}}_1, \omega_1)\overline{\widehat{G}(\vec{\mathbf{x}}_2, \vec{\mathbf{y}}_2, \omega_2)} \right\rangle, \quad \text{(B.1)}$$

for points $\vec{\mathbf{x}}_i = (\mathbf{x}_i, 0)$ in the array and $\vec{\mathbf{y}}_i = (\mathbf{y}_i, z_i)$ in the random medium. We use the parabolic approximation (5.34) of the Green's function and the scaling defined in Section 5.1. We also assume that

$$|\mathbf{x}_1 - \mathbf{x}_2| = O(\theta), \quad |\mathbf{y}_1 - \mathbf{y}_2| = O(\theta) \quad \text{and} \quad |\omega_1 - \omega_2| = O(\theta). \quad \text{(B.2)}$$

When imaging a point source at $\vec{\mathbf{y}}_\star$ we take $\vec{\mathbf{y}}_1 = \vec{\mathbf{y}}_2 = \vec{\mathbf{y}}_\star$, as in Section 5, whereas for the distributed sources considered in Section 6, we let $\vec{\mathbf{y}}_1$ and $\vec{\mathbf{y}}_2$ be two arbitrary points in $\mathcal{D}$, the support of the source. Two-frequency moment calculations like the ones given here have been done before [45] in special cases. We present the calculations in detail for completeness.

Although in the context of Sections 5 and 6 we think of $\vec{\mathbf{y}}_j$ in (B.1) as source locations, we may use reciprocity and assume that the Green's function originates from the array, that is, from $\vec{\mathbf{x}}_j$, for $j = 1, 2$. This makes the notation of this appendix more convenient and it gives for arbitrary $\vec{\mathbf{x}} = (\mathbf{x}, z)$ the parabolic approximation of the Green's function

$$\widehat{G}(\vec{\mathbf{x}}, \vec{\boldsymbol{\xi}}, \omega) = e^{ik_0 L_z k z} \psi(\vec{\mathbf{x}}, \vec{\boldsymbol{\xi}}, \omega), \tag{B.3}$$

with amplitude ψ satisfying

$$\begin{aligned} 2ik\psi_z + \theta \Delta_{\mathbf{x}} \psi + \frac{\sigma\delta}{\theta\sqrt{\epsilon}} k^2 \mu\left(\frac{\mathbf{x}}{\delta}, \frac{z}{\epsilon}\right)\psi = 0, \quad z > 0, \\ \psi = \delta(\mathbf{x} - \boldsymbol{\xi}), \quad z = 0. \end{aligned} \tag{B.4}$$

Here $\vec{\boldsymbol{\xi}} = (\boldsymbol{\xi}, 0)$ and it will be set equal to either $\vec{\mathbf{x}}_1$ or $\vec{\mathbf{x}}_2$ later.

Our derivation of the moment formulas (5.49) and (6.4) is based on the scale ordering

$$\epsilon \ll \theta \ll \delta \ll 1, \tag{B.5}$$

and it involves two limits: the *white noise limit* $\epsilon \to 0$ and then, the *high frequency limit* $\theta \to 0$. The *broad beam limit* $\delta \to 0$ is not needed here, but it plays a key role in the statistical stability of the imaging functional [40].

Let us change the notation in (B.4) by setting $\psi \rightsquigarrow \psi^{\epsilon,\theta}$, to remind us that the amplitude depends on the two parameters ϵ and θ that tend to zero. In the white noise limit $\epsilon \to 0$, $\psi^{\epsilon,\theta}$ converges weakly, in law [36, 40], to solution ψ^θ of the Ito-Schrödinger equation

$$\begin{aligned} d\psi^\theta = \left(\frac{i\theta}{2k}\Delta_{\mathbf{x}}\psi^\theta - \frac{k^2\sigma^2\delta^2}{8\theta^2} R_0(0)\psi^\theta\right) dz + \frac{ik\sigma\delta}{2\theta}\psi^\theta dB\left(\frac{\mathbf{x}}{\delta}, z\right), \quad z > 0, \\ \psi^\theta = \delta(\mathbf{x} - \boldsymbol{\xi}), \quad z = 0. \end{aligned} \tag{B.6}$$

Here $B(\mathbf{x}, z)$ is a Brownian motion field in z that is smooth in the transverse variable $\mathbf{x}$. The covariance of the Gaussian process B is

$$\langle B(\mathbf{x}_1, z_1) B(\mathbf{x}_2, z_2)\rangle = z_1 \wedge z_2 R_0(|\mathbf{x}_1 - \mathbf{x}_2|), \tag{B.7}$$

where $z_1 \wedge z_2$ denotes the minimum of z_1, z_2 and $R_0(\mathbf{x})$ is a smooth function of $\mathbf{x}$, defined in terms of the compactly supported covariance (2.9) of the fluctuations as

$$R_0(|\mathbf{x}|) = \int_{-\infty}^{\infty} R(|\mathbf{x}|, z) dz. \tag{B.8}$$

The expectation of ψ^θ follows immediately from (B.6), but we are interested in

$$\left\langle \psi^\theta(\vec{\mathbf{y}}_1,\vec{\mathbf{x}}_1,\omega_1)\overline{\psi^\theta(\vec{\mathbf{y}}_2,\vec{\mathbf{x}}_2,\omega_2)}\right\rangle \quad \text{or} \quad \left\langle \psi_1^\theta\overline{\psi_2^\theta}\right\rangle, \tag{B.9}$$

for points $\vec{\mathbf{x}}_i$, $\vec{\mathbf{y}}_i$ and frequencies $\omega_i = k_i c_0$, $i = 1, 2$, satisfying (B.2).

Appendix B.1. The moment formula for a fixed range

First, we derive the moment formula for the same range $z_1 = z_2 = z$. Then, we extend the result to the general case, in Section Appendix B.2. By Ito's formula [36], we have

$$\begin{aligned} d\left(\psi_1^\theta\overline{\psi_2^\theta}\right) = {} & \tfrac{i\theta}{2k_1}\Delta_{\mathbf{x}_1}\psi_1^\theta\overline{\psi_2^\theta}dz - \tfrac{i\theta}{2k_2}\Delta_{\mathbf{x}_2}\psi_1^\theta\overline{\psi_2^\theta}dz + \tfrac{k_1k_2\sigma^2\delta^2}{4\theta^2}R_0\left(\tfrac{|\mathbf{x}_1-\mathbf{x}_2|}{\delta}\right)\psi_1^\theta\overline{\psi_2^\theta}dz - \\ & \tfrac{(k_1^2+k_2^2)\sigma^2\delta^2}{8\theta^2}R_0(0)\psi_1^\theta\overline{\psi_2^\theta}dz + \tfrac{ik_1\sigma\delta}{2\theta}\psi_1^\theta\overline{\psi_2^\theta}dB(\mathbf{x}_1,z) - \tfrac{ik_2\sigma\delta}{2\theta}\psi_1^\theta\overline{\psi_2^\theta}dB(\mathbf{x}_2,z), \end{aligned} \tag{B.10}$$

with initial condition

$$\psi_1^\theta\overline{\psi_2^\theta} = \delta(\mathbf{y}_1-\mathbf{x}_1)\delta(\mathbf{y}_2-\mathbf{x}_2) \quad \text{at} \quad z = 0. \tag{B.11}$$

Equivalently, in terms of new variables

$$\overline{k} = \frac{k_1+k_2}{2}, \quad \widetilde{k} = \frac{k_2-k_1}{\theta}, \tag{B.12}$$

$$\overline{\mathbf{x}} = \frac{\mathbf{x}_1+\mathbf{x}_2}{2}, \quad \widetilde{\mathbf{x}} = \frac{\mathbf{x}_2-\mathbf{x}_1}{\theta}, \tag{B.13}$$

$$\overline{\mathbf{y}} = \frac{\mathbf{y}_1+\mathbf{y}_2}{2}, \quad \widetilde{\mathbf{y}} = \frac{\mathbf{y}_2-\mathbf{y}_1}{\theta}, \tag{B.14}$$

equation (B.10) becomes

$$\begin{aligned} d\left(\psi_1^\theta\psi_2^\theta\right) = {} & \tfrac{i\theta}{2\overline{k}-\theta k}\left(\tfrac{1}{4}\Delta_{\overline{\mathbf{x}}} - \tfrac{1}{\theta}\nabla_{\overline{\mathbf{x}}}\cdot\nabla_{\widetilde{\mathbf{x}}} + \tfrac{1}{\theta^2}\Delta_{\widetilde{\mathbf{x}}}\right)\psi_1^\theta\psi_2^\theta dz - \tfrac{i\theta}{2\overline{k}+\theta k}\left(\tfrac{1}{4}\Delta_{\overline{\mathbf{x}}} + \tfrac{1}{\theta}\nabla_{\overline{\mathbf{x}}}\cdot\nabla_{\widetilde{\mathbf{x}}} + \right. \\ & \left.\tfrac{1}{\theta^2}\Delta_{\widetilde{\mathbf{x}}}\right)\psi_1^\theta\psi_2^\theta dz + \left[\tfrac{\left(\overline{k}^2-\frac{\theta^2}{4}\widetilde{k}^2\right)\sigma^2\delta^2}{4\theta^2}R_0\left(\tfrac{\theta|\widetilde{\mathbf{x}}|}{\delta}\right) - \tfrac{\left(\overline{k}^2+\frac{\theta^2}{4}\widetilde{k}^2\right)\sigma^2\delta^2}{4\theta^2}R_0(0)\right]\psi_1^\theta\psi_2^\theta dz \\ & + \tfrac{i\sigma\delta}{2\theta}\left[\left(\overline{k}-\tfrac{\theta}{2}\widetilde{k}\right)dB\left(\tfrac{\overline{\mathbf{x}}}{\delta}-\tfrac{\theta\widetilde{\mathbf{x}}}{2\delta},z\right) - \left(\overline{k}+\tfrac{\theta}{2}\widetilde{k}\right)dB\left(\tfrac{\overline{\mathbf{x}}}{\delta}+\tfrac{\theta\widetilde{\mathbf{x}}}{2\delta},z\right)\right]. \end{aligned}$$

In this form we can pass to the high frequency limit $\theta \to 0$. In principle, this means having $\theta \ll 1$, but, because we seek a simple moment formula, we ask that $\theta/\delta \ll 1$ and we expand R_0 and B (which are smooth functions of $\mathbf{x}$) around $\mathbf{0}$. Note that $\theta/\delta \ll 1$ means

$$\frac{\lambda_0}{l} \ll \frac{\epsilon}{\delta} \ll 1,$$

so this is a regime with very short wavelengths, typical of optical or infrared applications. The limit amplitude ψ satisfies

$$\begin{aligned} d\left(\psi_1\overline{\psi_2}\right) = {} & -\tfrac{i}{\overline{k}}\nabla_{\overline{\mathbf{x}}}\cdot\nabla_{\widetilde{\mathbf{x}}}\psi_1\overline{\psi_2}dz + \tfrac{i\widetilde{k}}{2\overline{k}^2}\Delta_{\widetilde{\mathbf{x}}}\psi_1\overline{\psi_2}dz - \left(\tfrac{\overline{k}^2D_p}{2}|\widetilde{\mathbf{x}}|^2 + \tfrac{\widetilde{k}^2D_f}{2}\right)\psi_1\overline{\psi_2}dz - \\ & \tfrac{i\widetilde{k}\sigma\delta}{2}\psi_1\overline{\psi_2}dB\left(\tfrac{\overline{\mathbf{x}}}{\delta},z\right) - \tfrac{i\overline{k}\sigma}{2}\psi_1\overline{\psi_2}d\left[\widetilde{\mathbf{x}}\cdot\nabla_{\overline{\mathbf{x}}}B\left(\tfrac{\overline{\mathbf{x}}}{\delta},z\right)\right], \end{aligned} \tag{B.15}$$

where we set $\nabla_{\mathbf{x}} R_0(0) = \mathbf{0}$, because R_0 is an even function of $\mathbf{x}$, and we define the random medium parameters

$$D_p = -\frac{\sigma^2 R_0''(0)}{4}, \quad D_f = \frac{\sigma^2 \delta^2}{4} R_0(0). \tag{B.16}$$

Next, Fourier transform over $\widetilde{\mathbf{x}}$

$$W = \int e^{i\mathbf{p}\cdot\widetilde{\mathbf{x}}} \psi_1 \overline{\psi_2} d\widetilde{\mathbf{x}} \tag{B.17}$$

and obtain from (B.15) the Ito-Liouville equation

$$\begin{aligned} dW + \tfrac{\mathbf{p}}{\overline{k}} \cdot \nabla_{\overline{\mathbf{x}}} W dz + \tfrac{i\widetilde{k}|\mathbf{p}|^2}{2\overline{k}^2} W dz = \; & \tfrac{\overline{k}^2 D_p}{2} \Delta_{\mathbf{p}} W dz - \tfrac{\widetilde{k}^2 D_f}{2} W dz - \tfrac{i\widetilde{k}\sigma\delta}{2} W dB\left(\tfrac{\overline{\mathbf{x}}}{\delta}, z\right) \\ & - \tfrac{\sigma\overline{k}}{2} d\nabla_{\overline{\mathbf{x}}} B\left(\tfrac{\overline{\mathbf{x}}}{\delta}, z\right) \cdot \nabla_{\mathbf{p}} W, \quad z > 0, \end{aligned} \tag{B.18}$$

with initial condition

$$\begin{aligned} W \; &= \int e^{i\mathbf{p}\cdot\widetilde{\mathbf{x}}} \delta\left(\overline{\mathbf{x}} - \overline{\mathbf{y}} - \frac{\theta}{2}(\widetilde{\mathbf{x}} - \widetilde{\mathbf{y}})\right) \delta\left(\overline{\mathbf{x}} - \overline{\mathbf{y}} + \frac{\theta}{2}(\widetilde{\mathbf{x}} - \widetilde{\mathbf{y}})\right) d\widetilde{\mathbf{x}} \\ &\sim e^{i\mathbf{p}\cdot\widetilde{\mathbf{y}}} \delta\left(\overline{\mathbf{x}} - \overline{\mathbf{y}}\right) \quad \text{at} \;\; z = 0, \end{aligned} \tag{B.19}$$

up to a multiplicative constant that we neglect. We take expectations in (B.18) and Fourier transform with respect to $\overline{\mathbf{x}}$ to get

$$\int e^{i\overline{\mathbf{x}}\cdot\mathbf{q}} < W > d\overline{\mathbf{x}} = e^{-\frac{\widetilde{k}^2 D_f z}{2}} V. \tag{B.20}$$

The new dependent variable V satisfies the partial differential equation

$$\begin{aligned} & \frac{\partial V}{\partial z} - \frac{i\mathbf{p}\cdot\mathbf{q}}{\overline{k}} V + \frac{i\widetilde{k}|\mathbf{p}^2|}{2\overline{k}^2} V = \frac{\overline{k}^2 D_p}{2} \Delta_{\mathbf{p}} V, \quad z > 0, \\ & V = e^{i(\mathbf{p}\cdot\widetilde{\mathbf{y}} + \mathbf{q}\cdot\overline{\mathbf{y}})}, \quad z = 0. \end{aligned} \tag{B.21}$$

We can solve (B.21) in the form

$$V = A(z, \mathbf{q}, \overline{\mathbf{y}}, \widetilde{\mathbf{y}}) e^{\frac{F(z)|\mathbf{p}|^2}{2} + \mathbf{C}(z,\mathbf{q},\widetilde{\mathbf{y}})\cdot\mathbf{p}}, \tag{B.22}$$

where, for $z > 0$,

$$\frac{\partial \ln A}{\partial z} = \frac{\overline{k}^2 D_p}{2}(F + |\mathbf{C}|^2), \tag{B.23}$$

$$\frac{\partial \mathbf{C}}{\partial z} = \frac{i\mathbf{q}}{\overline{k}} + \overline{k}^2 D_p F \mathbf{C}, \tag{B.24}$$

$$\frac{\partial F}{\partial z} = -\frac{i\widetilde{k}}{\overline{k}^2} + \overline{k}^2 D_p F^2, \tag{B.25}$$

and, at $z = 0$. This leads to the ordinary differential equations

$$A = e^{i\mathbf{q}\cdot\overline{\mathbf{y}}}, \quad \mathbf{C} = i\widetilde{\mathbf{y}}, \quad F = 0. \tag{B.26}$$

A straightforward integration of (B.23)-(B.26) gives

$$A(z,\mathbf{q},\overline{\mathbf{y}},\widetilde{\mathbf{y}}) \;= \cosh^{-\frac{1}{2}}(z\sqrt{i\widetilde{k}D_p})\exp\left\{i\mathbf{q}\cdot\overline{\mathbf{y}} - \frac{\overline{k}^2 D_p|\widetilde{\mathbf{y}}|^2}{2}\frac{\tanh(z\sqrt{i\widetilde{k}D_p})}{\sqrt{i\widetilde{k}D_p}} - \frac{i\overline{k}\mathbf{q}\cdot\widetilde{\mathbf{y}}}{\widetilde{k}}\times\right.$$
$$\left.\left[\cosh^{-1}(z\sqrt{i\widetilde{k}D_p})-1\right] + \frac{i|\mathbf{q}|^2}{2\widetilde{k}}\left[z - \frac{\tanh(z\sqrt{i\widetilde{k}D_p})}{\sqrt{i\widetilde{k}D_p}}\right]\right\}, \tag{B.27}$$

$$\mathbf{C} = i\widetilde{\mathbf{y}}\cosh^{-1}(z\sqrt{i\widetilde{k}D_p}) + \frac{i\mathbf{q}}{\overline{k}}\frac{\tanh(z\sqrt{i\widetilde{k}D_p})}{\sqrt{i\widetilde{k}D_p}} \tag{B.28}$$

and

$$F(z) = -\frac{\sqrt{i\widetilde{k}D_p}\tanh(z\sqrt{i\widetilde{k}D_p})}{\overline{k}^2 D_p}. \tag{B.29}$$

The moment formula follows from the inverse Fourier transform

$$\left\langle\psi_1\overline{\psi}_2\right\rangle = e^{-\frac{\widetilde{k}^2 D_f z}{2}}\int\frac{d\mathbf{p}}{(2\pi)^2}\int\frac{d\mathbf{q}}{(2\pi)^2}A(z,\mathbf{q},\overline{\mathbf{y}},\widetilde{\mathbf{y}})e^{\frac{F(z)|\mathbf{p}|^2}{2}+\mathbf{C}(z,\mathbf{q},\widetilde{\mathbf{y}})\cdot\mathbf{p}-i\mathbf{p}\cdot\widetilde{\mathbf{x}}-i\mathbf{q}\overline{\mathbf{x}}}.$$

We have

$$\left\langle\psi_1\overline{\psi}_2\right\rangle \;= -\frac{\overline{k}^2}{4\pi^2 z^2}\phi_1(z)\exp\left\{-\frac{i\widetilde{k}}{2z}|\overline{\mathbf{x}}-\overline{\mathbf{y}}|^2 - \frac{i\overline{k}}{z}(\widetilde{\mathbf{x}}-\widetilde{\mathbf{y}})\cdot(\overline{\mathbf{x}}-\overline{\mathbf{y}}) - \frac{\widetilde{k}^2 D_f z}{2}\right.$$
$$-\frac{\overline{k}^2 D_p z}{6}\phi_2(z)\left[|\widetilde{\mathbf{x}}|^2 + \frac{\widetilde{\mathbf{x}}\cdot\widetilde{\mathbf{y}}}{\cosh(z\sqrt{i\widetilde{k}D_p})} + \frac{|\widetilde{\mathbf{y}}|^2}{\cosh^2(z\sqrt{i\widetilde{k}D_p})}\right] \tag{B.30}$$
$$\left.+\overline{k}^2 z D_p\phi_3(z)\widetilde{\mathbf{x}}\cdot\widetilde{\mathbf{y}} - \overline{k}^2 z D_p\phi_4(z)|\widetilde{\mathbf{y}}|^2\right\},$$

where

$$\phi_1(z) = \cosh^{\frac{1}{2}}(z\sqrt{i\widetilde{k}D_p})\;\frac{z\sqrt{i\widetilde{k}D_p}}{\sinh(z\sqrt{i\widetilde{k}D_p})}, \tag{B.31}$$

$$\phi_2(z) = \frac{3}{i\widetilde{k}D_p z}\left(\frac{\sqrt{i\widetilde{k}D_p}}{\tanh(z\sqrt{i\widetilde{k}D_p})} - \frac{1}{z}\right), \tag{B.32}$$

$$\phi_3(z) = \frac{1}{2i\widetilde{k}D_p z^2}\left[\frac{3z\sqrt{i\widetilde{k}D_p}}{\sinh(z\sqrt{i\widetilde{k}D_p})} - \frac{1}{\cosh(z\sqrt{i\widetilde{k}D_p})} - 2\right], \tag{B.33}$$

$$\phi_4(z) = \frac{\tanh(z\sqrt{i\widetilde{k}D_p})}{2z\sqrt{i\widetilde{k}D_p}}\left[1 - \frac{\tanh(z\sqrt{i\widetilde{k}D_p})}{z\sqrt{i\widetilde{k}D_p}}\right]. \tag{B.34}$$

Equivalently, letting

$$\left(\psi_1\overline{\psi}_2\right)_0 = -\frac{\overline{k}^2}{4\pi^2 z^2}e^{-\frac{i\widetilde{k}}{2z}|\overline{\mathbf{x}}-\overline{\mathbf{y}}|^2-\frac{i\overline{k}}{z}(\widetilde{\mathbf{x}}-\widetilde{\mathbf{y}})\cdot(\overline{\mathbf{x}}-\overline{\mathbf{y}})} \tag{B.35}$$

be the right hand side of (B.30) for $D_p = D_f = 0$, we can rewrite our result as

$$\left\langle \psi_1 \overline{\psi}_2 \right\rangle = \left(\psi_1 \overline{\psi}_2\right)_0 \phi_1(z) \exp\left\{ -\frac{\widetilde{k}^2 D_f z}{2} - \frac{\overline{k}^2 D_p z}{6}\phi_2(z)\left[|\widetilde{\mathbf{x}}|^2 + \frac{\widetilde{\mathbf{x}}\cdot\widetilde{\mathbf{y}}}{\cosh(z\sqrt{i\widetilde{k}D_p})} + \frac{|\widetilde{\mathbf{y}}|^2}{\cosh^2(z\sqrt{i\widetilde{k}D_p})}\right] + \right.$$

$$\left. \overline{k}^2 z D_p \phi_3(z)\widetilde{\mathbf{x}}\cdot\widetilde{\mathbf{y}} - \overline{k}^2 z D_p \phi_4(z)|\widetilde{\mathbf{y}}|^2 \right\}.$$

We note that

$$\begin{aligned}
\left(\psi_1 \overline{\psi}_2\right)_0 &= -\lim_{\theta\to 0} \frac{\left(\overline{k} - \frac{\theta}{2}\widetilde{k}\right)\left(\overline{k} + \frac{\theta}{2}\widetilde{k}\right)}{4\pi^2 z^2} \exp\left[\frac{i}{2z\theta}\left(\overline{k} - \frac{\theta}{2}\widetilde{k}\right)\left|\overline{\mathbf{x}} - \overline{\mathbf{y}} - \frac{\theta}{2}\left(\widetilde{\mathbf{x}} - \widetilde{\mathbf{y}}\right)\right|^2 \right. \\
&\qquad \left. -\tfrac{i}{2z\theta}\left(\overline{k} + \tfrac{\theta}{2}\widetilde{k}\right)\left|\overline{\mathbf{x}} - \overline{\mathbf{y}} + \tfrac{\theta}{2}\left(\widetilde{\mathbf{x}} - \widetilde{\mathbf{y}}\right)\right|^2 \right] \\
&= \lim_{\theta\to 0} \psi_0^\theta\left((\overline{\mathbf{y}} - \frac{\theta}{2}\widetilde{\mathbf{y}}, z), (\overline{\mathbf{x}} - \frac{\theta}{2}\widetilde{\mathbf{x}}, 0), \overline{\omega} - \frac{\theta}{2}\widetilde{\omega}\right) \times \\
&\qquad \overline{\psi_0^\theta\left((\overline{\mathbf{y}} + \frac{\theta}{2}\widetilde{\mathbf{y}}, z), (\overline{\mathbf{x}} + \frac{\theta}{2}\widetilde{\mathbf{x}}, 0), \overline{\omega} + \frac{\theta}{2}\widetilde{\omega}\right)} \\
&= (\psi_1)_0 \overline{(\psi_2)_0}
\end{aligned} \tag{B.36}$$

so (B.35) is precisely the result in a homogeneous medium. Therefore, recalling the parabolic approximation (B.3) and the change of variables (B.12)-(B.14), we have

$$\left\langle \widehat{G}(\vec{\mathbf{y}}_1, \vec{\mathbf{x}}_1, \omega_1)\overline{\widehat{G}(\vec{\mathbf{x}}_2, \vec{\mathbf{y}}_2, \omega_2)} \right\rangle = \widehat{G}_0(\vec{\mathbf{y}}_1, \vec{\mathbf{x}}_1, \omega_1)\overline{\widehat{G}_0(\vec{\mathbf{x}}_2, \vec{\mathbf{y}}_2, \omega_2)}\phi_1(z)\times$$

$$\exp\left\{ -\frac{\widetilde{k}^2 D_f z}{2} - \frac{\overline{k}^2 D_p z}{6}\phi_2(z)\left[|\widetilde{\mathbf{x}}|^2 + \frac{\widetilde{\mathbf{x}}\cdot\widetilde{\mathbf{y}}}{\cosh(z\sqrt{i\widetilde{k}D_p})} + \frac{|\widetilde{\mathbf{y}}|^2}{\cosh^2(z\sqrt{i\widetilde{k}D_p})}\right] \right. \tag{B.37}$$

$$\left. + \overline{k}^2 z D_p \phi_3(z)\widetilde{\mathbf{x}}\cdot\widetilde{\mathbf{y}} - \overline{k}^2 z D_p \phi_4(z)|\widetilde{\mathbf{y}}|^2 \right\}.$$

Finally in the asymptotic regime of small fluctuations $\sigma \ll \delta$,

$$\cosh(z\sqrt{i\widetilde{k}D_p}) = 1 + O(\widetilde{k}D_p z^2) = 1 + O(\sigma^2), \tag{B.38}$$

$$\phi_i(z) = 1 + O(\widetilde{k}D_p z^2) = 1 + O(\sigma^2), \quad i = 1, 2, \tag{B.39}$$

$$\phi_i(z) = O(\widetilde{k}D_p z^2) = O(\sigma^2), \quad i = 3, 4 \tag{B.40}$$

so (B.37) reduces to

$$\begin{aligned}
\left\langle \widehat{G}(\vec{\mathbf{y}}_1, \vec{\mathbf{x}}_1, \omega_1)\overline{\widehat{G}(\vec{\mathbf{x}}_2, \vec{\mathbf{y}}_2, \omega_2)} \right\rangle &\approx \widehat{G}_0(\vec{\mathbf{y}}_1, \vec{\mathbf{x}}_1, \omega_1)\overline{\widehat{G}_0(\vec{\mathbf{y}}_2, \vec{\mathbf{x}}_2, \omega_2)}\times \\
&\qquad e^{-\frac{\widetilde{k}^2 D_f z}{2} - \frac{\overline{k}^2 D_p z}{6}\left(|\widetilde{\mathbf{x}}|^2 + \widetilde{\mathbf{x}}\cdot\widetilde{\mathbf{y}} + |\widetilde{\mathbf{y}}|^2\right)}.
\end{aligned} \tag{B.41}$$

Using the reciprocity of the Green's function, we obtain moment formula (5.49) and its simplification, given by (B.37) and (B.41), respectively, for $\widetilde{\mathbf{y}} = \mathbf{0}$ and $z = z_\star$.

Appendix B.2. The general moment formula

Let us address the general case $z_1 \neq z_2$. To fix ideas, suppose that $z_2 > z_1$ and return to the second moment (B.9). Using conditional expectations, we have

$$\left\langle \psi^\theta(\vec{\mathbf{y}}_1, \vec{\mathbf{x}}_1, \omega_1)\overline{\psi^\theta(\vec{\mathbf{y}}_2, \vec{\mathbf{x}}_2, \omega_2)} \right\rangle = \left\langle \psi^\theta(\vec{\mathbf{y}}_1, \vec{\mathbf{x}}_1, \omega_1)\overline{\langle \psi^\theta(\vec{\mathbf{y}}_2, \vec{\mathbf{x}}_2, \omega_2)|\mathcal{F}_{z_1}\rangle} \right\rangle, \tag{B.42}$$

where $\vec{\mathbf{y}}_i = (\mathbf{y}_i, z_i)$, $\vec{\mathbf{x}}_i = (\mathbf{x}_i, 0)$, for $i = 1, 2$ and $\{\mathcal{F}_z\}_{z\geq 0}$ denotes the Brownian σ-field up to z. For arbitrary points $\vec{\mathbf{x}} = (\mathbf{x}, z)$, $\vec{\boldsymbol{\xi}} = (\boldsymbol{\xi}, 0)$ we see from (B.6) and (B.16) that $\psi^\theta(\vec{\mathbf{x}}, \vec{\boldsymbol{\xi}}, \omega)$ satisfies

$$d\psi^\theta = \left(\frac{i\theta}{2k}\Delta_{\mathbf{x}}\psi^\theta - \frac{k^2 D_f}{2\theta^2}\psi^\theta \right) dz + \frac{ik\sigma\delta}{2\theta}\psi^\theta dB\left(\frac{\mathbf{x}}{\delta}, z\right) \quad \text{for } z > 0. \tag{B.43}$$

Next, take expectations and obtain, for $z > z_1$,

$$\begin{aligned} \tfrac{\partial}{\partial z}\left\langle \psi^\theta((\mathbf{x}, z), \vec{\boldsymbol{\xi}}, \omega)|\mathcal{F}_{z_1}\right\rangle &= \frac{i\theta}{2k}\Delta_{\mathbf{x}}\left\langle \psi^\theta((\mathbf{x}, z), \vec{\boldsymbol{\xi}}, \omega)|\mathcal{F}_{z_1}\right\rangle \\ &\quad - \frac{k^2 D_f}{2\theta^2}\left\langle \psi^\theta((\mathbf{x}, z), \vec{\boldsymbol{\xi}}, \omega)|\mathcal{F}_{z_1}\right\rangle, \end{aligned} \tag{B.44}$$

whereas at $z = z_1$,

$$\left\langle \psi^\theta((\mathbf{x}, z_1), \vec{\boldsymbol{\xi}}, \omega)|\mathcal{F}_{z_1}\right\rangle = \psi^\theta((\mathbf{x}, z_1), \vec{\boldsymbol{\xi}}, \omega). \tag{B.45}$$

The conditional expectation can be calculated by substituting

$$\left\langle \psi^\theta((\mathbf{x}, z), \vec{\boldsymbol{\xi}}, \omega)|\mathcal{F}_{z_1}\right\rangle = e^{-\frac{k^2 D_f (z-z_1)}{2\theta^2}}\phi((\mathbf{x}, z), \vec{\boldsymbol{\xi}}, \omega) \tag{B.46}$$

in (B.44) and Fourier transforming in $\mathbf{x}$. This gives

$$\widehat{\phi} = e^{-\frac{i\theta}{2k}(z-z_1)|\mathbf{p}|^2}\int \psi((\mathbf{u}, z_1), \vec{\boldsymbol{\xi}}, \omega)\, e^{i\mathbf{p}\cdot\mathbf{u}} d\mathbf{u} \tag{B.47}$$

and therefore

$$\begin{aligned} \left\langle \psi^\theta((\mathbf{x}, z), \vec{\boldsymbol{\xi}})|\mathcal{F}_{z_1}\right\rangle &= e^{-\frac{k^2 D_f}{2\theta^2}(z-z_1)}\tfrac{1}{4\pi^2}\int d\mathbf{p}\int d\mathbf{u} e^{-i\mathbf{p}\cdot(\mathbf{x}-\mathbf{u})-\frac{i\theta}{2k}(z-z_1)|\mathbf{p}|^2}\psi((\mathbf{u}, z_1), \vec{\boldsymbol{\xi}}, \omega) \\ &= -\tfrac{ik}{2\pi\theta(z-z_1)}e^{-\frac{k^2 D_f (z-z_1)}{2\theta^2}}\int \psi((\mathbf{u}, z_1), \vec{\boldsymbol{\xi}}, \omega) e^{\frac{ik|\mathbf{x}-\mathbf{u}|^2}{2\theta(z-z_1)}} d\mathbf{u}. \end{aligned}$$

We are interested in the high frequency regime $\theta \ll 1$, when the integrand in (B.47) is highly oscillatory and we can use a stationary phase argument [6] to get the main contribution to (B.47) from $\mathbf{u}$ satisfying

$$\nabla_{\mathbf{u}}|\mathbf{x} - \mathbf{u}|^2 = \mathbf{0} \Longrightarrow \mathbf{x} = \mathbf{u}.$$

Then,

$$\begin{aligned} \left\langle \psi^\theta((\mathbf{x}, z), \vec{\boldsymbol{\xi}}, \omega)|\mathcal{F}_{z_1}\right\rangle &\approx -\tfrac{ik}{2\pi\theta(z-z_1)}e^{-\frac{k^2 D_f (z-z_1)}{2\theta^2}}\psi((\mathbf{x}, z_1), \vec{\boldsymbol{\xi}}, \omega)\int e^{\frac{ik|\mathbf{x}-\mathbf{u}|^2}{2\theta(z-z_1)}} d\mathbf{u} \\ &= e^{-\frac{k^2 D_f (z-z_1)}{2\theta^2}}\psi((\mathbf{x}, z_1), \vec{\boldsymbol{\xi}}, \omega) \end{aligned} \tag{B.48}$$

and, setting $z = z_2$, $\mathbf{x} = \mathbf{y}_2$, $\vec{\boldsymbol{\xi}} = \vec{\mathbf{x}}_2$ and $\omega = \omega_2$, we get from (B.42) and (B.48) that

$$\left\langle \psi^\theta((\mathbf{y}_1, z_1), \vec{\mathbf{x}}_1, \omega_1)\overline{\psi^\theta((\mathbf{y}_2, z_2), \vec{\mathbf{x}}_2, \omega_2)}\right\rangle \approx e^{-\frac{k_2^2 D_f(z_2-z_1)}{2\theta^2}} \times \left\langle \psi^\theta((\mathbf{y}_1, z_1), \vec{\mathbf{x}}_1, \omega_1)\overline{\psi^\theta((\mathbf{y}_2, z_1), \vec{\mathbf{x}}_2, \omega_2)}\right\rangle,$$

for $z_2 > z_1$.

Obviously, the same argument applies to the case $z_1 > z_2$, so we can write directly the general result

$$\left\langle \psi^\theta((\mathbf{y}_1, z_1), \vec{\mathbf{x}}_1, \omega_1)\overline{\psi^\theta((\mathbf{y}_2, z-2), \vec{\mathbf{x}}_2, \omega_2)}\right\rangle \approx e^{-\frac{\overline{k}^2 D_f|z_2-z_1|}{2\theta^2}} \times \left\langle \psi^\theta\left((\mathbf{y}_1, z_1 \wedge z_2), \vec{\mathbf{x}}_1, \omega_1\right)\overline{\psi^\theta\left((\mathbf{y}_2, z_1 \wedge z_2), \vec{\mathbf{x}}_2, \omega_2\right)}\right\rangle, \tag{B.49}$$

where we approximated the wavenumber k_1 or k_2 in the exponential, given by $\overline{k} \mp \theta\widetilde{k}/2$, by $\overline{k}$. Thus, the general moment formula is given by the simpler one, at fixed range, and an exponential factor that indicates a rapid loss of coherence at different ranges. The fixed range moment formula is given by (B.36) and, in the asymptotic regime of small fluctuations, (B.49) simplifies to

$$\left\langle \widehat{G}\left((\mathbf{y}_1, z_1), \vec{\mathbf{x}}_1, \omega_1\right)\overline{\widehat{G}\left((\mathbf{y}_2, z_2), \vec{\mathbf{x}}_2, \omega_2\right)}\right\rangle \approx \widehat{G}_0\left((\mathbf{y}_1, z_1), \vec{\mathbf{x}}_1, \omega_1\right)\overline{\widehat{G}_0\left((\mathbf{y}_2, z_2), \vec{\mathbf{x}}_2, \omega_2\right)} \times \exp\left\{-\frac{\overline{k}^2 D_f|z_2-z_1|}{2\theta^2} - \frac{\widetilde{k}^2 D_f z_1\wedge z_2}{2} - \frac{\overline{k}^2 D_p z_1\wedge z_2}{6}\left(|\widetilde{\mathbf{x}}|^2 + \widetilde{\mathbf{x}}\cdot\widetilde{\mathbf{y}} + |\widetilde{\mathbf{y}}|^2\right)\right\}, \tag{B.50}$$

with the notation (B.12)-(B.14). Finally, using reciprocity of the Green's functions, we get the moment formula (6.4).

Acknowledgments

The work of L. Borcea was partially supported by the Office of Naval Research, under grant N00014-02-1-0088 and by the National Science Foundation, grants DMS-0305056, DMS-0354658. The work of G. Papanicolaou was supported by grants AFOSR F49620-01-1-0465, ONR N00014-02-1-0088 and 02-SC-ARO-1067-MOD 1. The work of C. Tsogka was partially supported by the Office of Naval Research, under grant N00014-02-1-0088 and by 02-SC-ARO-1067-MOD 1.

[1] A. B. Baggeroer, W. A. Kuperman, and P. N. Mikhalevsky. An overview of matched field methods in ocean acoustics. *IEEE J. Ocean Eng.*, 18:401–424, 1993.

[2] G. Bal, G. Papanicolaou, and L. Ryzhik. Self-averaging in time reversal for the parabolic wave equation. *Stochastics and Dynamics*, 2:507–531, 2002.

[3] G. Bal and L. Ryzhik. Time reversal and refocusing in random media. *SIAM J. Appl. Math.*, 63(5):1475–1498, 2003.

[4] E. Bécache, P. Joly, and C. Tsogka. Etude d'un nouvel élément fini mixte permettant la condensation de masse. *C. R. Acad. Sci. Paris Sér. I Math.*, 324:1281–1286, 1997.

[5] E. Bécache, P. Joly, and C. Tsogka. An analysis of new mixed finite elements for the approximation of wave propagation problems. *SIAM J. Numer. Anal.*, 37:1053–1084, 2000.

[6] C. M. Bender and S. A. Orszag. *Advanced mathematical methods for scientists and engineers.* McGraw-Hill, New York, 1978.

[7] G. Beylkin. Imaging of discontinuities in the inverse scattering problem by inversion of a causal generalized Radon transform. *J. Math. Phys.*, 26(1):99–108, 1985.

[8] G. Beylkin and R. Burridge. Linearized inverse scattering problems in acoustics and elasticity. *Wave Motion*, 12(1):15–52, 1990.

[9] N. Bleistein, J.K. Cohen, and J.W. Stockwell Jr. *Mathematics of multidimensional seismic imaging, migration, and inversion.* Springer, New York, 2001.

[10] P. Blomgren, G. Papanicolaou, and H. Zhao. Super-resolution in time-reversal acoustics. *Journal of the Acoustical Society of America*, 111:238–248, 2002.

[11] L. Borcea, G. Papanicolaou, and C. Tsogka. Theory and applications of time reversal and interferometric imaging. *Inverse Problems*, 19:S134–164, 2003.

[12] L. Borcea, G. Papanicolaou, and C. Tsogka. Adaptive interferometric imaging in random media. preprint, 2004.

[13] L. Borcea, G. Papanicolaou, C. Tsogka, and J. Berryman. Imaging and time reversal in random media. *Inverse Problems*, 18:1247–1279, 2002.

[14] L. Borcea, G. Papanicolaou, C. Tsogka, and J. Berryman. Statistically stable ultrasonic imaging in random media. *JASA*, 112:1509–1522, 2002.

[15] B. Borden. Mathematical problems in radar inverse scattering. *Inverse Problems*, 19:R1–R28, 2002.

[16] M. Born and E. Wolf. *Principles of optics.* Academic Press, New York, 1970.

[17] D. E. Bray and D. McBride. *Nondestructive testing techniques.* Wiley, New York, 1992.

[18] H. P. Bucker. Use of calculated sound field and matched-field detection to locate sound sources in shallow water. *J. Acoust. Soc. Am.*, 59:368–373, 1976.

[19] J. Carazzone and W. Symes. Velocity inversion by differential semblance optimization. *Geophysics*, 56:654–663, 1991.

[20] T. K. Chan, Y. Kuga, and A. Ishimaru. Experimental studies on circular sar imaging in clutter using angular correlation function technique. *IEEE Trans. Geoscience and Remote Sensing*, 37:2192–2197, 1999.

[21] J. F. Claerbout. *Fundamentals of geophysical data processing : with applications to petroleum prospecting.* CA : Blackwell Scientific Publications, Palo Alto, 1985.

[22] J. F. Clouet and J. P. Fouque. A time reversal method for an acoustical pulse propagating in randomly layered media. *Wave Motion*, 25:361–368, 1997.

[23] D. Colton and R. Cress. *Inverse acoustic and electromagnetic scattering theory*, volume 93 of *Applied Math. Sc.* Springer Verlag, Berlin, Heidelberg, second edition edition, 1998.

[24] J.C. Curlander and R.N. McDonough. *Synthetic Aperture Radar.* Wiley, New York, 1991.

[25] A. Derode, P. Roux, and M. Fink. Robust acoustic time reversal with high-order multiple scattering. *Physical Review Letters*, 75:4206–4209, 1995.

[26] D. R. Dowling and D. R. Jackson. Phase conjugation in underwater acoustics. *J. Acoust. Soc. Am.*, 89:171–181, 1990.

[27] D. R. Dowling and D. R. Jackson. Narrow band performance of phase conjugate arrays in dynamic random media. *J. Acoust. Soc. Am.*, 91:3257–3277, 1992.

[28] G. L. D'Spain, J. J. Murray, W. S. Hodkiss, N. O. Booth, and P. W. Schey. Mirages in shallow water matched field processing. *J. Acoust. Soc. Am.*, 105:3245–3265, 1999.

[29] C. Elachi. *Spaceborne Radar Remote Sensing: Applications and Techniques.* IEEE, New York, 1987.

[30] M. Fink. Time reversal mirrors. *J. Phys. D*, 26:1330–1350, 1993.

[31] M. Fink. Time reversed acoustics. *Phys. Today*, 50:34–40, 1997.

[32] M. Fink, D. Cassereau, A. Derode, C. Prada, P. Roux, and M. Tanter. Time-reversed acoustics.

Rep. Prog. Phys., 63:1933–1994, 2000.

[33] J. P. Fouque, J. Garnier, A. Nachbin, and K. Solna. Time reversal refocusing for a point source in randomly layered media. *Wave Motion*, 42:238–260, 2005.

[34] A. Ishimaru. *Waves propagation and scattering in random media*. Academic Press, 1978.

[35] J. L. Krolik. Matched field minimum-variance beamforming in random ocean channel. *J. Acoust. Soc. Am.*, 92:1408–1419, 1992.

[36] H. Kunita. *Stochastic flows and stochastic differential equations*, volume 24 of *Cambridge Studies in Mathematics*. Cambridge University Press, Cambridge, UK, 1997.

[37] W. A. Kuperman, W. S. Hodgkiss, H. C. Song, T. Akal, C. Ferla, and D. R. Jackson. Phase conjugation in the ocean : Experimental demonstration of an acoustic time reversal mirror. *J. Acoust. Soc. Am.*, 103:25–40, 1998.

[38] R. Marklein, K. Mayer, R. Hannemann, T. Krylow, K. Balasubramanian, K. J. Langenberg, and V. Schmitz. Linear and nonlinear inversion algorithms applied in nondestructive evaluation. *Inverse Problems*, 18:1733–1759, 2002.

[39] C. Nolan and M. Cheney. Synthetic aperture inversion. *Inverse Problems*, 18(1):221–235, 2002.

[40] G. Papanicolaou, L. Ryzhik, and K. Solna. Statistical stability in time reversal. *SIAM J. Applied Mathematics*, 64(4):1133–1155, 2004.

[41] W. A. Schneider. Integral formulation for migration in two and three dimensions. *Geophysics*, 43:49–76, 1978.

[42] R. Snieder, A. Gret, H. Douma, and J. Scales. Coda wave interferometry for estimating nonlinear behavior in seismic velocity. *Science*, 295:2253–2255, 2002.

[43] K. Solna. Focusing of time-reversed reflections. *Waves Random Media*, 12(3):365–385, 2002.

[44] H. C. Song, W. A. Kuperman, and W. S. Hodgkiss. Iterative time reversal in the ocean. *J. Acoust. Soc. Am.*, 105:3176–3184, 1999.

[45] I. Sreenivasiah, A. Ishimaru, and S. T. Hong. Two-frequency mutual coherence function and pulse propagation in a random medium: An analytic solution to the plane wave case. *Radio Science*, 11:775–778, 1976.

[46] G. T. Sschuster, J. Yu, J. Sheng, and J. Rickett. Interferometric daylight seismic imaging. *Geophysics Journal International*, 157:838–852, 2004.

[47] C.C. Stolk and W. Symes. Smooth objective functionals for seismic velocity inversion. *Inverse Problems*, 19(1):73–89, 2003.

[48] W. Symes. A differential semblance criterion for inversion of multioffset seismic reflection data. *J. Geophys. Res.*, 88:2061–2074, 1993.

[49] W. Symes. Lecture notes in seismic imaging. Mathematical Geophysics Summer School, Stanford, available at www.trip.caam.rice.edu, 1998.